Growth of InAsSb and GaAsSb Nanowires

Catalysed by Au, AgAu and Ag Nanoparticles on (001) Oriented Substrates

Robin Sjökvist

Supervisors: Kimberly Dick Thelander, Hanna Kindlund & Erik Mårtensson

Lund University

Faculty of Engineering

Division of Solid State Physics

A Master's Thesis in Physics

LUND UNIVERSITY

2018-09-06

Abstract

The ability to tailor the properties of nanowires exactly to fit a specific application is important if nanowires are to be useful and incorporated into the electronics industry. The bandgap is one such property, which, for ternary III-V semiconductors, can be altered by the presence of ordering. In this sense, ordering is referred to as a spontaneous modulation of the ingoing components along certain crystallographic directions. A step towards achieving ordering is to make nanowires to grow in the [001] direction, which has been shown to promote it. In this project, the possibility to grow InAsSb and GaAsSb nanowires in the [001] direction on InAs (001) and GaAs (001) substrates, respectively, is investigated. The nanowires are grown from Au, AgAu and Ag particles with the final goal of achieving ordering. Transmission electron microscopy is used to determine the crystal structure, growth direction and presence of ordering in the final nanowires. Ultimately, growth of Au and AgAu seeded InAsSb wires in the [001] direction was achieved, but no ordering was observed.

Svensk sammanfattning

Att kunna ändra egenskaperna hos nanotrådar till specifika applikationer är viktigt om nanotrådar ska kunna inkorporeras i elektronikindustrin. Bandgapet är en sådan egenskap som för ternära III-V halvledare kan ändras om ”ordning” uppstår i materialet. Med ordning menas här att de ingående komponenterna spontant lägger sig periodiskt längs med en kristallografisk riktning. Ett steg mot att uppnå ordning är att få nanotrådarna att växa i den kristallografiska riktningen [001], som har setts vara fördelaktig för ordning. I det här projektet har förmågan av InAsSb och GaAsSb nanotrådar att växa i [001] på InAs (001) respektive GaAs (001) substrat, utforskats. Nanotrådarna har växts från Au, AgAu och Ag partiklar med det slutgiltiga målet att uppnå ordning. Transmissionselektronmikroskopi har använts för att bestämma kristallstruktur, växtriktning och för att se om någon ordning har uppstått i de färdiga trådarna. Vertikal växt uppnåddes för InAsSb trådar från både Au och AgAu partiklar, men ordning observerades inte.

Acknowledgements

First and foremost I would like to thank my main supervisor, Kimberly, and my co-supervisors, Erik and Hanna, for all their help and ideas that have pushed this project forward whenever I got stuck, and their continuous help and support throughout the whole project. This involves both theory, where all have helped me, and lab work, where Erik has been a huge support. I would also like to thank Sebastian, Marcus, Robert and Luna for help with specific questions and problems that needed attention, and of course also the rest of the group for valuable input and discussion during our meetings. I would like to thank my examiner, Carina, for her help during the different steps of the examination process, and also my opponent Oskar, for great questions during my presentation. I would like to thank everyone who I have had the pleasure of sharing offices with during my time at FTF. Not only have you helped me with scientific problems, but you have also been an important stress relief and great company during our walks around the building (which I will try to continue to take). Of course, I would never have made it through this project without my friends and family there to support me and take my mind away from work. I would especially like to thank my girlfriend, who has always supported me and believed in me when things were rough and I was stressed out. You bring forth the best in me, so thank you Linnea.

This thesis was written as the final step towards my Master of Science degree in Engineering Nanoscience, at Lund University Faculty of Engineering. It was written at the Division of Solid State Physics, with funding from NanoLund, where the experiments were carried out in Lund Nano Lab. I would like to thank all these organisation for giving me this opportunity.

Contents

Abstract i

Svensk sammanfattning i

Acknowledgements ii

List of Figures v

List of Tables vii

List of Abbreviations viii

1 Introduction 1
1.1 Motivation 2

2 Theoretical background 3
2.1 Semiconductors 3
2.2 Nanowires 4
2.3 Crystal structure 5
2.4 Vegard's Law and Bowing Parameter 5
2.5 Metal Organic Vapor Phase Epitaxy 5
2.6 Thermodynamics and kinetics 7
2.7 Nucleation 8
2.7.1 3D Homonucleation 9
2.7.2 3D Heteronucleation 10
2.7.3 Nanowire nucleation and growth 11
2.8 Theories of Nanowire Growth 14
2.9 Phase Diagrams 15
2.10 Growth from Different Seed Particles 16
2.11 Crystallographic Planes and Directions 17
2.12 Growth on (001) 17
2.13 Ordering 19
2.14 Properties of III-Antimonides 21
2.15 Characterisation 22
2.15.1 Scanning Electron Microscopy 22
2.15.2 Transmission Electron Microscopy 23
2.15.3 X-ray Energy Dispersive Spectroscopy 24

3 Experimental Procedure 25
3.1 General Procedure 25
3.2 Growth runs performed 26

4 Results 28
4.1 Types of wires observed 28
4.2 InAsSb 30
4.2.1 Au seeded InAsSb 30
4.2.2 AgAu seeded InAsSb 33

4.2.3 Ag seeded InAsSb 36
4.3 GaAsSb 38
4.3.1 Au seeded GaAsSb 39
4.3.2 AgAu seeded GaAsSb 41
4.3.3 Ag seeded GaAsSb 43
4.4 InAs nanowires 45
4.5 InAs stem and InAsSb wire 46
4.6 Reproduce the best sample 47
4.7 Annealing tests 49

5 Discussion **52**
5.1 General growth characteristics of the particle types 52
5.1.1 InAsSb samples 52
5.1.2 GaAsSb samples 53
5.2 The Good Samples 53
5.2.1 [001] Nanowire Morphology 56
5.2.2 Growth initiation 58
5.3 The Planar wires 62
5.4 High order [11x] wires 63
5.5 InAs samples 65
5.6 TEM Analysis 67

6 Conclusions **71**

7 References **72**

List of Figures

2.1 Semiconductor bandgap . . . 3
2.2 MOVPE setup . . . 6
2.3 Critical nucleus Size and energy . . . 10
2.4 Nucleus and wetting angle . . . 11
2.5 Nucleation in wires . . . 12
2.6 Diffusion and incorporation . . . 13
2.7 Area of uptake . . . 14
2.8 Ag-In binary phase diagram . . . 15
2.9 Ag-In-As ternary phase diagram . . . 16
2.10 Crystallographic directions . . . 18
2.11 CuPt ordering . . . 20
4.1 Observed wire-types . . . 29
4.2 Temperature series for Au seeded InAsSb wires . . . 30
4.3 As/In ratio series for Au seeded InAsSb wires . . . 31
4.4 Sb/In ratio series for Au seeded InAsSb wires . . . 32
4.5 Temperature series for AgAu seeded InAsSb wires . . . 33
4.6 As/In ratio series for AgAu seeded InAsSb wires . . . 34
4.7 Sb/In ratio series for AgAu seeded InAsSb wires . . . 35
4.8 Temperature series for Ag seeded InAsSb wires . . . 36
4.9 As/In ratio series for Ag seeded InAsSb wires . . . 37
4.10 Sb/In ratio series for Ag seeded InAsSb wires . . . 38
4.11 Temperature series for Au seeded GaAsSb wires . . . 39
4.12 As/Ga ratio series for Au seeded GaAsSb wires . . . 40
4.13 Temperature series for AgAu seeded GaAsSb wires . . . 41
4.14 As/Ga ratio series for AgAu seeded GaAsSb wires . . . 42
4.15 Temperature series for Ag seeded GaAsSb wires . . . 43
4.16 As/Ga ratio series for Ag seeded GaAsSb wires . . . 44
4.17 As/In ratio series for Au seeded InAs wires . . . 45
4.18 Au seeded InAsSb wires on InAs stems . . . 46
4.19 Attempts to recreate Sample 4.2(b) . . . 48
4.20 Particles after annealing . . . 49
4.21 Wires without annealing . . . 50
5.1 More images of sample 4.2(b) . . . 54
5.2 More images of sample 4.19(d) . . . 55
5.3 More images of sample 4.21(d) . . . 56
5.4 Hexagonal nanowire cross section . . . 57
5.5 Nanowire facets . . . 57
5.6 Square nanowire cross section . . . 58
5.7 Trench . . . 59
5.8 Growth from a trench . . . 60
5.9 Particles before and after annealing . . . 61
5.10 "Christmas tree" wire growth . . . 63
5.11 The 11x higher order inclined nanowires . . . 64
5.12 The InAs stems . . . 66
5.13 TEM images and diffraction patterns/FFTs . . . 68

5.14 TEM image of ZB strucutre 69

List of Tables

2.1 Material properties 21
3.1 Standard growth parameters 26
3.2 InAsSb initial growth values 26

List of Abbreviations

NW - Nanowire

IR - Infrared Radiation

VB - Valence Band

CB - Conduction Band

ZB - Zincblende

WZ - Wurtzite

CCP - Cubic Close Packed

HCP - Hexagonal Close Packed

FCC - Face Centered Cubic

MOVPE - Metal Organic Vapor Phase Epitaxy

TMIn - TriMethylIndium

TMGa - TriMethylGallium

TMSb - TriMethylAntimony

VLS - Vapor-Liquid-Solid

VSS - Vapor-Solid-Solid

SEM - Scanning Electron Microscope(y)

SE - Secondary Electron

BSE - Backscattered Electron

TEM - Transmission Electron Microscope(y)

STEM - Scanning Transmission Electron Microscope(y)

CCD - Charge-Coupled Device

FFT - Fast Fourier Transform

XEDS, EDX - X-ray Energy Dispersive Spectroscopy

CCS - Close Coupled Showerhead

SCCM - Standard Cubic Centimeters

1 Introduction

Over the last few decades, the growth of nanowires (NWs), has been the subject of much research due to their unique, finely tunable electrical and optical properties. The original nanowires were grown from Si and other group IV semiconductor elements [1], but it was later discovered that nanowires can be grown from other materials as well. By combining elements from group III and group V, semiconductors with very specific properties like direct bandgaps, high carrier mobilities and good absorption for certain wavelengths of light can be produced.

Nanowires containing antimony are sought after for exactly these specific reasons. Most III-Sbs have small, direct bandgaps, the smallest of all binary III-V semiconductors, and the carrier mobility is high, meaning that good conductivity can be achieved for low carrier concentrations [2]. Due to the small bandgap, the wavelengths of light that can be detected (or emitted) by III-Sbs are in the Infrared Radiation (IR) regime, which means that III-Sb nanowires could be used as infrared detectors, detecting for example CO, CO_2 and CH_4, or as lasers [3][4][5]. III-Sbs are also difficult to grow as epitaxial layers due to a large lattice parameter which gives a big mismatch to most substrates. Due to their geometry, NWs have inherent strain relaxing properties, which therefore helps when growing lattice mismatched materials [2].

Systems that have been explored more thoroughly than III-Sbs are III-As materials, where a group III element is combined with arsenic to get semiconductors. These materials also tend to have high carrier mobilities and direct bandgaps. By growing NWs using both of the group V materials (Sb and As) at the same time, the composition can be tailored, which will determine the bandgap and the lattice parameters in the final crystal. These materials are called ternary III-V semiconductors. When combining semiconductor materials this way, a composition dependent offset will be added to the band structure. This will in some cases lead to even smaller bandgaps than predicted by a linear combination of the ingoing bandgaps, making ternaries very interesting to explore [2].

When growing III-V semiconductors, pairs of the ingoing group III and group V elements are formed in the crystal lattice. If a ternary material with two group V elements is grown, every pair will contain one of these two elements, at random. However, when growing regular epitaxial layers of ternary III-V semiconductor materials, ordering is sometimes observed. In this case, ordering refers to the periodicity of the incorporation of the two different group V elements, which in effect means that layers in certain crystallographic directions only contain one of the two group V elements. These layers are formed in a periodic pattern so that for example every other layer contains one of the group V elements, while the other group V element is found in the layers in between. Ordering is interesting, since it affects the electrical and optical properties, and enables the bandgap, for example, to be even more tailored. Ordered III-V semiconductors are common when grown as thin films, and one of the most common types of ordering is observed along a <111> direction when the layers are grown in the [001] direction [6].

Ordering has never been observed in the axial segments of growing nanowires. It has however been observed in the lateral overgrowth in InAs-InAsSb heterostructure nanowires [7]. This means that InAsSb grown on InAs is a potential nanowire system where ordering can be observed. InAsSb also has the smallest bandgap of the ternary III-V semiconductors, and InSb has the highest electron mobility, making the material attractive for industrial applications. Since Ga is also very common and important in nanowire growth, and the fact that GaSb has the highest hole mobility, GaAsSb also has several applications where its properties would benefit from ordering.

To facilitate growth of nanowires, seed particles are often used. The most commonly used is Au, which mainly promotes growth in the <111> directions [8]. If growth in <100> is to be achieved, other seed particles may prove more useful. Ag, for example, is one of the particles that seem to promote growth in <100> [9]. One reason for using other particles than Au, is that (001) substrates are the most widely used substrates for device growth [10]. Another reason to try out new seed particles is that Au forms deep level traps in the Si bandgap. So if nanowires made out of other materials should be incorporated into the (Si dominated) integrated circuit industry, one needs to get rid of the gold [11]. Silver might not be the best option, since it also forms deep level traps in the Si bandgap, but it is at least a step away from Au, towards the exploration of new seed particle materials [12].

1.1 Motivation

The final goal of the project is to achieve some type of ordered structure in the axially grown part of ternary III-V nanowires containing Sb, since they already have a small bandgap and high carrier mobility. The reason for this is because it enables a tailoring of the bandgap of the nanowire materials, which could give access to a larger part of the IR spectrum, and open up for new possible applications. InAs and GaAs substrates, with (001) orientation will be used, since ordering has been mostly observed for epitaxial III-V semiconductor layers grown in the [001] direction. Upon these substrates, InAsSb (on InAs) and GaAsSb (on GaAs) wires will be grown, with the hope to achieve growth in the [001] direction. Growth of high yield, sufficiently long, (001) oriented wires will therefore be the first goal of the project. Ag is tested as a seed particle since it has been shown to promote growth in [001], Au is used since it is the most common seed particle, and AgAu (50/50) is used since it is largely unexplored and could potentially be useful. The exploration of the material/orientation combinations used is in itself worthwhile, since these systems have not been explored thoroughly. Therefore, another motivation for this project is to contribute with more data to the nanowire community, and potentially enable further exploration and experiments.

2 Theoretical background

In this section, basic underlying concepts and theories required for the understanding of the experimental methods and the results presented in this thesis, are introduced. The basic properties of semiconductors, nanowires and the specific materials used are introduced firstly. After that, the concepts of epitaxial growth, with a description of the actual process in the machine, are presented. Then specific aspects and difficulties of nanowires, related to the results in this thesis, are discussed. Finally, the methods with which the samples are analysed are presented.

2.1 Semiconductors

Semiconductors are a class of materials with important electrical properties that are used in many applications, e.g. in transistors used in integrated circuits. Their main characteristic is that they have a gap in their band structure, with a specific bandgap energy, E_g, that acts as a barrier for conduction. The gap creates what is defined as the valence band (VB), where all states are occupied by electrons at 0 K, and the conduction band (CB), that is empty at 0 K. Contrary to the large gap in insulators, the gap in the semiconductors can, relatively easily, be overcome for the electrons, provided the temperature or voltage applied is high enough. Elevating electrons to the CB makes the semiconductor conducting, and the conduction will increase with increasing temperature, since more electrons will be elevated. This is shown schematically in Figure 2.1. By doping the semiconductor with other materials the semiconductor can be tailored to conduct more easily [13].

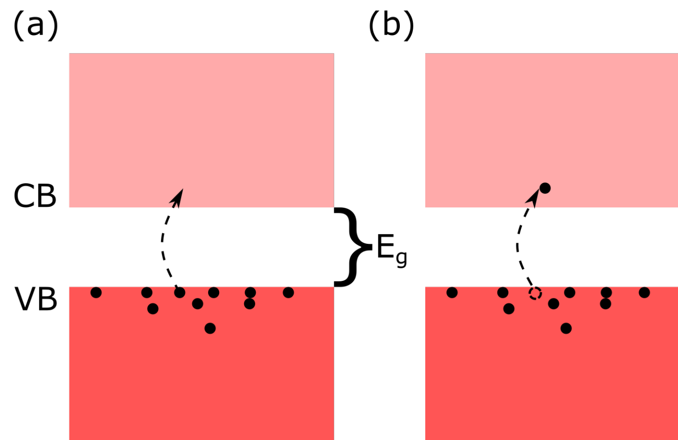

Figure 2.1: A schematic showing the gap between the VB and the CB of a semiconductor. The bandgap energy is shown as E_g. In (a) an arrow indicating an electron jumping from the VB to the CB is shown. In (b) the electron has arrived to the CB, and left behind an empty state called a hole. Both of these contribute to the total conduction in the semiconductor.

In group IV of the periodic table there are a couple of naturally occurring semiconductors. The most common ones are of course Si (dominating the industry for decades) and Ge.

Semiconducting materials may also be created by combining elements from group III and group V, or from group II and group VI, in the periodic table. III-V semiconductors are often studied due to their flexibility in bandgap energy and because they very often have direct bandgaps, which is desired for optical applications. This is because the absorption or emission of a photon then does not need to be accompanied by a phonon/lattice vibration. Common examples are InAs, InSb, GaAs, GaSb and InP. By combining two group V and one group III material (or the other way around), ternary semiconductor alloys can be made. An example is $InAs_{1-x}Sb_x$, where x determines the amount of the two group V species. The properties of ternary semiconductors will depend on the ratio between the two elements from the same group, so the bandgap of ternaries can be more finely tuned [13][14][15]. This effect is not linear, however, since band bowing arises when different III-V semiconductors are combined. This gives rise to the bowing parameter, as discussed in Section 2.4, and can effectively decrease the bandgap of the ternary alloy [2].

2.2 Nanowires

A typical nanowire is rod-shaped, i.e. elongated in one dimension and restricted in the other two, with clear facets. The length of a nanowire can reach several µm, while the radius typically is some tens of nm. Therefore, one of the main properties of nanowires is that they are able to confine electrons, restricting their movement in two of the three dimensions. If structures are created in the nanowire, by changing the growth properties to switch between crystal structures or materials, the confinement effect can be used to create novel nanoscale electrical and optical devices. One example is the creation of thin segments of another material, or the same material with another crystal structure (discussed in Section 2.3), than the rest of the wire, where the segments will act as barriers for the electrons. This way, quantum dots can be made [16]. Core-shell structures, where the initial wire is coated by another material have also been made [11]. This has been directed, by growing segments in the wire that promotes radial growth. That way, radial growth of the nanowire can be localised, which enables even more complex structures [17]. Conical, tapered, nanowires can be produced by allowing material to radially grow on the whole wire. Branched wires have also been made, where new wires grow from the original wires [18]. A big advantage of growing nanowires is that many small, rather complex structures can be made in a reproducible way, without many processing steps [10].

There are a few extraordinary effects that arise when growing crystals in the form of nanowires. One thing is that the growth of lattice mismatched materials, i.e. the grown material does not fit on the substrate, is easier, since the morphology of the nanowires relieves strain [11]. Nanowires have also been observed to grow in crystal structures never observed for the material's bulk counterpart. Most bulk III-V semiconductors normally grow in the zincblende crystal structure, but the shape of nanowires can facilitate the formation of wurtzite crystal structure instead, see Section 2.3 [19].

2.3 Crystal structure

Crystals can grow in many different crystal structures with different fundamental properties. In III-V nanowire growth there are specifically two relevant crystal structures that are observed: the zincblende (ZB) structure and the wurtzite (WZ) structure. The difference between these crystal structures is that ZB can be seen as two interpenetrating cubic close packed (CCP) structures, while in WZ the ingoing elements form interpenetrating hexagonal close packed (HCP) structures. In this sense, "interpenetrating" means that one of the elements forms a crystal structure and the other element forms the same structure shifted some fraction of a lattice parameter. In ZB, for example, the group III atoms will form a Face Centered Cubic (FCC) structure, while the group V atoms will form FCC but shifted by $(\frac{1}{4},\frac{1}{4},\frac{1}{4})$ relative to the group III atoms. This way pairs of group III and V elements are formed [20].

2.4 Vegard's Law and Bowing Parameter

When forming a ternary III-V semiconductor, the final crystal structure will have a lattice parameter that is a combination of the ingoing lattice parameters. If $InAs_{1-x}Sb_x$ is used as an example, the ingoing lattice parameters a_{InAs} and a_{InSb} (in this discussion, a Zincblende crystal structure is assumed) will result in an overall lattice parameter according to Vegard's Law:

$$a_{InAs_{1-x}Sb_x} = (1-x) \cdot a_{InAs} + x \cdot a_{InSb} \tag{1}$$

The lattice parameter is close to linearly related to the bandgap of ternary semiconductors. The simplified equation for the bandgap energies, E_g, looks similar to Vegard's Law:

$$E_{g,InAs_{1-x}Sb_x} = (1-x) \cdot E_{g,InAs} + x \cdot E_{g,InSb} \tag{2}$$

Since the correlation is not completely linear, another term is often added, giving the final equation:

$$E_{g,InAs_{1-x}Sb_x} = (1-x) \cdot E_{g,InAs} + x \cdot E_{g,InSb} - b \cdot x \cdot (1-x) \tag{3}$$

Here, b is called the bowing parameter, which basically corrects for the bowing the band structure experiences when ternary alloys are created. The bowing parameter changes value depending on the temperature, and the degree of ordering (discussed in Section 2.13) in the structure [14][21]. A higher degree of ordering will increase the bowing parameter, giving a smaller bandgap. For InAsSb the band bowing and the bowing parameter affects the lowest possible bandgap a lot: the bandgap of the ingoing III-V compounds are $E_{g,InAs} = 0.36$ eV and $E_{g,InSb} = 0.17$ eV, while some of the lowest bandgaps reported for $InAs_{1-x}Sb_x$ are $E_{g,InAs_{1-x}Sb_x} < 0.1$ eV [22][2].

2.5 Metal Organic Vapor Phase Epitaxy

Metal Organic Vapor Phase Epitaxy (MOVPE) is a method commonly used for growing crystals, most often semiconductors. Epitaxy is defined as the ordering of material into a growing crystal structure on top of another crystalline material, in this case from the vapor phase. It can be further divided depending on whether the grown material is the

same as the substrate (homoepitaxy) or different (heteroepitaxy) [11]. One of the main points of epitaxy is that, when growing heteroepitaxial crystals, the grown material will adopt certain properties from the substrate crystal. For example can crystal structure and growth direction be directed to some extent.

The "Metal Organic" in the name refers to a class of precursor molecules used, that are injected into the chamber as a vapor. Growth is enabled by allowing the precursor molecules, that consist of the element desired for incorporation bound to ligands, to flow into the reactor, where they crack at the surface of the substrate. This frees the atomic species the precursors hold, so they can be incorporated into the growing crystal, while the ligands are released as by-products. Common examples are TMIn, TMGa and TMSb ("TriMethyl"-). The metal-organic precursors are stored as liquids or solid powders in bubblers and have to be fed into the growth chamber with the help of a carrier gas, commonly H_2, see Figure 2.2. Hydride precursors are used as well, and they are also supplied as a vapor, as shown in Figure 2.2. They are stored as gases, for example AsH_3 [15]. Common for all precursors is that they need to have a low stability, so that decomposition to free the atomic specie of interest is easy. The stability can, however, not be so low that long term storage is impossible. Even so, precursors will crack at different temperatures, and for a set temperatures one can estimate the amount of precursors that will be cracked. This will affect the amount of precursors of a certain type that one wants to inject to get sufficient incorporation of the specie. Another aspect that might affect is the vapor pressure, or the tendency to remain in the gas phase, of the elements to be incorporated. The metallic elements, among others, often have low vapor pressures and tend to remain on the surface or get incorporated after cracking. On the other hand, As has a very high vapor pressure, and its precursor therefore has to be supplied in larger amounts to get incorporation [14].

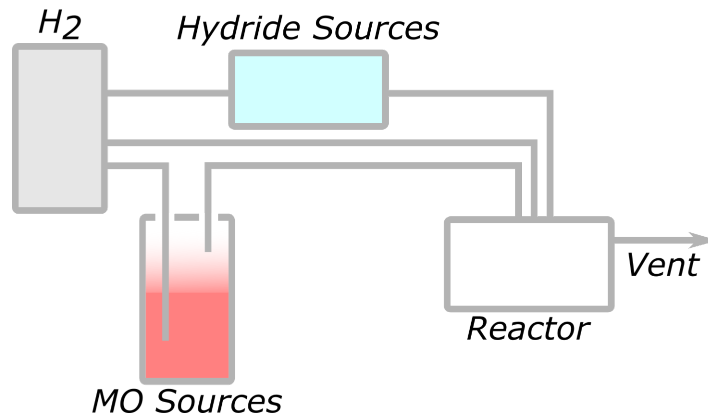

Figure 2.2: A simplified schematic of the precursor and carrier gas lines of a MOVPE setup.

If a regular, flat and crystalline substrate is put into the reactor chamber, the material provided from the vapour will usually form islands that grow together to form layers on

the surface. The growth can, however, be directed in various ways, usually by structuring the surface. The most common way of growing nanowires by MOVPE is by using seed particles as nucleation sites for the nanowires. When growing nanowires using seed particles, the theory of growth describing the system is either Vapor-liquid-solid (VLS) or vapor-solid-solid (VSS) depending on the state of the seed particle. The precursors are always supplied as a vapor, while the growing crystal is obviously solid, so the only thing separating the two theories is the state of the particle (liquid or solid). These theories are described in Section 2.8 [23].

Prior to any growth in the MOVPE reactor, after the substrate has been inserted, an annealing step is performed. This is to ensure an oxide free substrate upon which the new material will be grown. Depending on what material the substrate is made of, the oxides formed are more or less stable, so different temperatures (always above the actual growth temperature) need to be used. If nanowires are to be grown, this may affect the deposited particles, which may split and form smaller particles under certain conditions. This is not desired, so appropriate annealing procedures are carefully investigated [24].

Growth, and most importantly, nucleation, in MOVPE is accomplished through a combination of thermodynamic and kinetic effects. Thermodynamics determine the driving forces in the growth process, where parameters are considered on a global scale. Kinetics treat atomistic effects on the "single molecule"-level, which limits the rates of the growth steps. Evidently, certain parameters, such as temperature, affects both the thermodynamics and kinetics. The systems are also heterogeneous (at least two phases) and often multicomponent (several independent species) making full calculations and predictions difficult [15][25].

2.6 Thermodynamics and kinetics

Thermodynamics considers mainly the energy of a system, where the driving force for growth comes from differences in chemical potential, μ. The chemical potential for a certain component in a phase, μ_k, is defined as the partial derivative of Gibb's free energy, G, with respect to the amount of the component, n_k, at a specific temperature, T, pressure, P, and constant amount of the other components, $n_{j\neq k}$:

$$\mu_k = \left(\frac{\partial G}{\partial n_k}\right)_{T,P,n_{j\neq k}} \tag{4}$$

The chemical potential of a component may differ between different phases in a system. The system will strive to even out these differences by allowing transitions between the different phases. If the chemical potential for a component is the same in two different phases, there will be no driving force for the material to change. If this is true for all components, the free energy will be at a minimum, no driving force is present and the system is said to be in equilibrium. This also means that if a phase available in a system is associated with a low free energy for the current parameters, thermodynamics will present a driving force for the material available to form this phase. In MOVPE a steady

supply of precursors is fed into the growth chamber during growth, which implies that a steady-state non-equilibrium condition is established. For a one-component system the difference in chemical potential between the vapour and solid phase can be described by:

$$\Delta\mu = \mu_v - \mu_s = \mathrm{R}T\ln(P/P_0) \tag{5}$$

Here, the subscripts v and s refer to the vapor and solid phases, respectively, R is the ideal gas constant, P is the partial pressure of the material in the gas phase, while P_0 is the equilibrium partial pressure of the same component. What is described in Equation 5 is a state of supersaturation, where the vapor phase contains more of the component than it would at equilibrium conditions. Depending on the supersaturation, the system will be pushed further from equilibrium, and the driving force for crystallisation will be greater. The same effect can be achieved by cooling the system below the point where the two phases would be in equilibrium, giving a supercooled (undercooled) system. What phases are stable for a certain temperature and pressure (most often atmospheric by convention) is shown in phase diagrams, discussed in Section 2.9. When growing III-V semiconductors, Equation 5 gets a lot more complicated, since there are many components involved [11][14].

By calculating thermodynamic properties, the driving forces and actual numbers in the system, an understanding of how the system should behave under typically ideal, steady-state conditions is formed. The system is never ideal, however, and there are many kinetic factors affecting what is actually observed [14].

The kinetics of a system considers the actual redistribution and movement of species, incorporation and probabilities of various processes. This involves nucleation, where atoms have to diffuse and find preferential sites where they can stick together to form a stable nucleus (discussed in Section 2.7), the cracking of precursor molecules and the actual mass transport to, and diffusion on (discussed in Section 2.8), the surface [11]. All these processes limit and alter the boundaries and driving forces set by thermodynamics, and makes many growth related processes unpredictable in nature. This is mostly due to the limit kinetics put on the steady-state material supply to the growth interface, and different temperature regimes exist. For example, at low temperatures, the precursors may not crack very easily, and the growth will typically be referred to as kinetically limited. At higher temperatures, on the other hand, the precursors may readily crack at the surface, but the replenishing of new precursors is slow. The growth is then referred to as transport limited. There is also a high temperature regime where growth is limited by desorption and parasitic deposition on the reactor walls [14].

2.7 Nucleation

Since the growth of nanowires is facilitated by metallic particles, the actual details of growth differ from regular epitaxial growth. But the general steps and concepts are the same, which is why those mechanisms will be described firstly.

When growing regular epitaxial layers, there always needs to form a stable cluster of atoms, called a nucleus, from where the growth can proceed. Depending on the system, different limiting energetic barriers need to be overcome, but the process steps and mechanisms involved are similar. Common for all nucleation processes is that certain sites are more favourable for incorporation than other. This is especially crucial at the early stages of nucleus formation, when there are few atoms present. The general rule is that an atom is less likely to leave a site where it has many neighbouring atoms, so sites like these are good for incorporation. This is due to the amount of dangling bonds that naturally needs to exist whenever there is a surface, since the atoms lack neighbours and bonding is incomplete. This also means that it is difficult to start forming a nucleus on a completely flat surface, and whenever irregularities are present they can facilitate nucleation. There are a few different types of nucleation depending on the shape of the nucleus and if the phase it is grown from is homogeneous or if there exists more phases in the system. These cases are described below [14].

2.7.1 3D Homonucleation

As was discussed in Section 2.6, thermodynamics can provide driving forces for the transition from one phase to another, when parameters are changed to make the new phase stable. It is however not sufficient to merely set the parameters to where the phase transformation should occur, but a certain driving force is needed to start the transformation. This is done via supersaturation or supercooling. This means that the original phase will stay in a metastable state before the transition begins. The reason for this is the energy required when creating the interface between the new and the old phase. The energy required is related to the standardised surface free energy of the phases, γ, or the work to form a unit area of surface at equilibrium, if the number of components and the volume is constant. The energy required to form the surface is lowered whenever a disturbance is present, which will be discussed more in Section 2.7.2, about Heteronucleation. Homonucleation on the other hand refers to nucleation from a homogeneous phase, in the absence of any surfaces or defects that can act as nucleation sites and facilitate the nucleation. The energy required to form stable nuclei in this type of system is therefore high, and the change in Gibb's free energy, ΔG_N, associated with the formation of the nucleus is given by

$$\Delta G_N = \Delta G_S + \Delta G_V \tag{6}$$

Here ΔG_V is the energy released when a volume of the original phase is transformed into the new phase, while ΔG_S is the energy required when the surface between the two phases is formed. This means that the ΔG_S is positive, while ΔG_V is negative. For a very small nucleus, the surface-related term will be much larger than the volume-related term. This means that a certain size needs to be achieved, after which ΔG_N starts to decrease with size. This point defines the critical volume, V_N*, and the critical work for nucleus formation ΔG_N*, see Figure 2.3. From this point, the nucleus may either shrink or grow, since both paths will decrease ΔG_N. If it passes the maximum, the nucleus is considered stable.

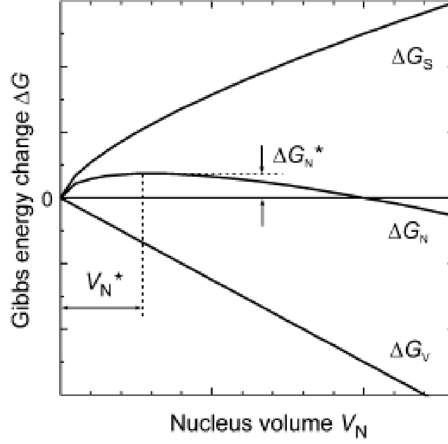

Figure 2.3: The change in Gibb's free energy versus nucleus size shows the critical point where the nucleus can lower the energy by either shrinking or growing, indicated by ΔG_N* and V_N*. Figure taken from [14].

2.7.2 3D Heteronucleation

In most realistic cases, there exists a defect, substrate surface or reactor wall that can act as a nucleation site for the growing material. The nucleation will then be termed heteronucleation. The substrates placed in the MOVPE reactor will be preferred as nucleation sites over nucleation in the vapour. The lowering of the energy required to form the nucleus comes from the interfaces and surfaces that need to be formed, and their related surface free energies, introduced in Section 2.7.1. The nucleus is assumed to form as a spherical cap, with a set contact-angle called the wetting angle, θ, determined by the surface free energies according to Young's equation:

$$cos(\theta) = \frac{\gamma_{vs} - \gamma_{ns}}{\gamma_{vn}} \tag{7}$$

Here the subscripts show what interface the surface free energies are related to; v stands for vapor, n for nucleus and s for substrate. This is shown in Figure 2.4 [14].

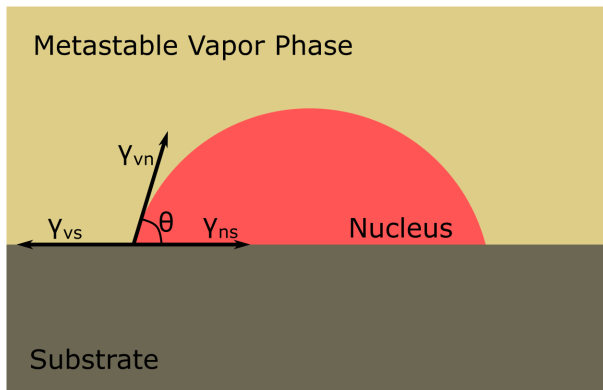

Figure 2.4: A 3D nucleus formed on a substrate surface. The surface free energies related to each interface are shown, as well as the wetting angle.

The energy required for a nucleus to form an interface with a solid substrate is much less than for an interface with the vapor phase. The pre-existing interface between the substrate and the vapor is also removed, freeing some energy. This results in an overall decrease in $\Delta G_N{*}$, making heteronucleation easier than homonucleation. This of course also depends on γ_{ns}, or how the substrate and nucleus material interact, since this will affect the wetting angle. The wetting angle can attain values between the two extremes 0° and 180°, where 0° means complete coverage, where the material wets the whole surface without forming droplets, while 180° implies that the droplets will remain as spheres on top of the surface. An angle closer to 0° is therefore sought after in epitaxial layer growth, since this produces an atomically flat surface. This occurs naturally if the material grown is the same as the substrate, since $\gamma_{ns} = 0$ and $\gamma_{vs} = \gamma_{vn}$ [14][25].

2.7.3 Nanowire nucleation and growth

One of the common ways to facilitate growth of one dimensional structures, nanowires, is by allowing liquid, or solid, particles to facilitate the growth. The state of the particle will be discussed further in Section 2.8, but for now it is assumed to be liquid. A particle on the surface of the substrate will act as a material sink, enabling a supersaturation of growth material to form in the particle with respect to the crystalline phase. When the particle is supersaturated enough to overcome the energy barriers of nucleation, an atomically flat (one monolayer of III-V pairs high) nucleus will form in the particle. It has been proposed that the most energetically favourable way for the nucleus to form is to originate at the triple phase line at the edge of the particle-substrate interface. This is because calculations have shown that it is more energetically favourable to replace parts of the particle-vapour interface with nucleus-vapour interface, instead of keeping the interface and forming more nucleus-particle interface. This is shown in Figure 2.5. After nucleation, the incorporation of more atoms will be facilitated and a full layer will form. The particle will continue to rest on the topmost layer, and eventually the supersaturation will build up again and initiate a new nucleation event [19][23].

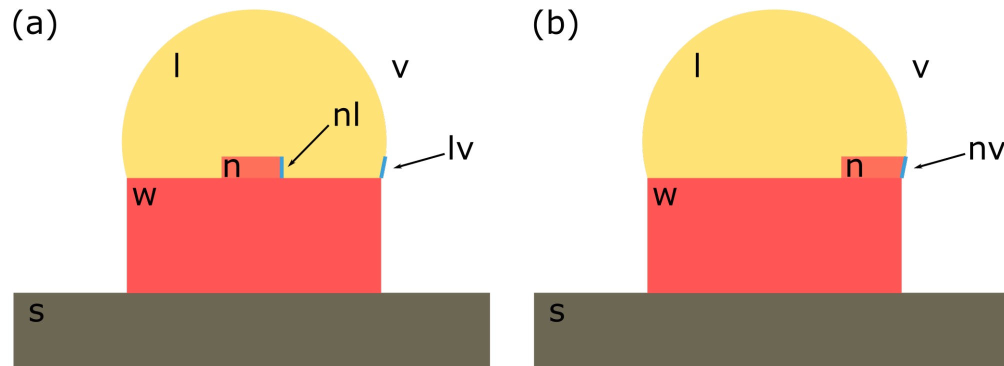

Figure 2.5: Two ways the nucleation could theoretically be initiated. Indicated in both (a) and (b) are s-substrate, w-wire, l-liquid, v-vapour and n-nucleus. In (a) the nucleus forms in the particle, forming new interfaces between nucleus and liquid particle, nl, while the interface between particle and vapour, lv, remains the same. In (b) the nucleus forms at the edge of the particle-wire interface, forming less interface between nucleus and particle, while replacing parts of the lv interface in (a) with nucleus-vapour, nv, interface. The situation in (b) has been proposed as a more energetically preferred way of nucleation in nanowire growth.

For the actual nucleation to take place, material firstly has to be delivered to the particle. Since precursors may crack at different sites on the heated substrate or wire, there are many different pathways available for the atoms that are supposed to be incorporated. Some atoms will arrive directly at the particle at the tip of the growing nanowire, where they will be absorbed. At the particle surface, a portion of the atoms will also desorb and return to the vapor phase. Atoms may also adsorb to the surface of the wire, where they may diffuse to the particle and be incorporated, desorb from the wire, diffuse to the substrate or get incorporated into the wire as radial growth. Atoms impinging at the substrate might diffuse up the wire, desorb or get incorporated into the growing surface layer. All of these effects are shown in Figure 2.6 [23].

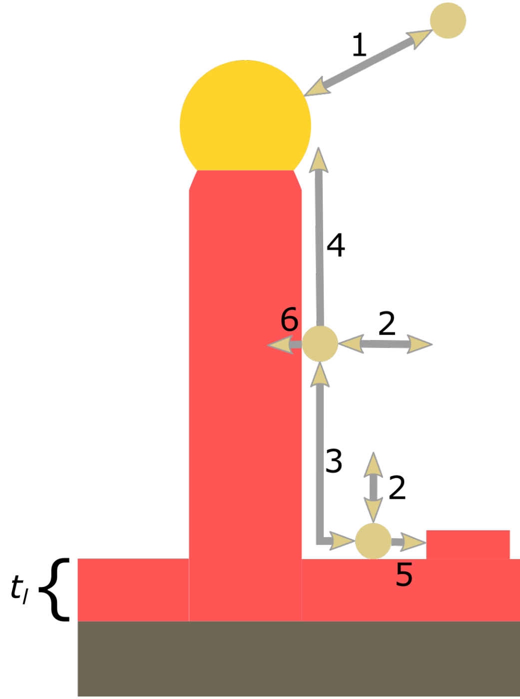

Figure 2.6: Several different pathways are indicated by numbers. 1. The direct impingement of atoms into the particle, as well as the desorption of atoms from the particle to the vapour. 2. Adsorption/desorption of atoms to/from either the side of the wire or the substrate. 3. Diffusion along the wire to/from the substrate. 4. Diffusion on the side of the wire to the particle for incorporation. 5. Diffusion on the substrate surface can lead to incorporation in the growing surface layer. The thickness, t_l of the surface layer is indicated. 6. Material incorporation in the radially grown layer on the side of the wire.

There is a statistical limit to how far from a wire, on the substrate, an atom can adsorb and still be incorporated. This will be represented as a circular area around the wire. The radius depends on the diffusion length, λ, of the species, i.e. how far it will diffuse on the surface before desorbing. For a longer wire, the area from which atoms may originate and still be incorporated will be smaller, as shown in Figure 2.7. There may as well be competition between wires if these areas overlap. Atomic species that do not get incorporated may instead contribute to the surface growth of the substrate, making wires appear shorter They could also simply desorb and leave the reactor with the flowing vapours, or get incorporated into the sides of the wire as parts of the radial overgrowth. The radial overgrowth is more pronounced if the diffusion length of the atoms is insufficient for them to reach the particle (i.e. λ is similar to the length of the wire) [11][25][23].

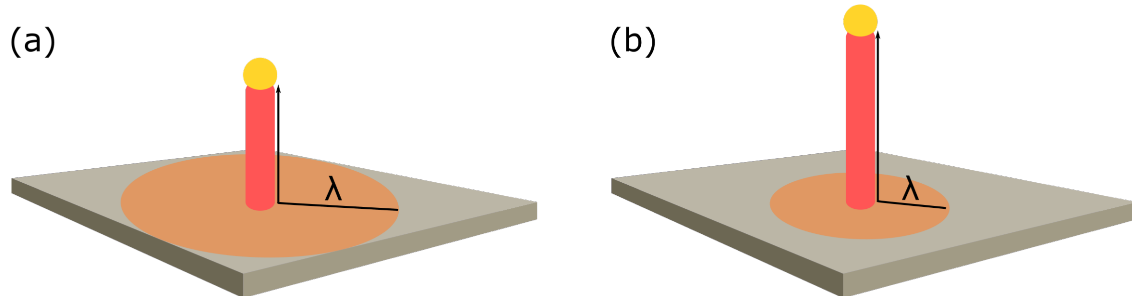

Figure 2.7: A schematic showing the difference in uptake of material from the surface for a short (a) and a long (b) nanowire. The brown circle indicates the area where precursors may crack and still be within one diffusion length, λ, from the particle, so that incorporation is statistically favoured.

2.8 Theories of Nanowire Growth

In the previous discussions, the particles used when growing nanowires have been presented as liquid during growth. The theory of liquid nanoparticles is the basis of the vapor-liquid-solid (VLS) growth model. This model was first described in 1964 by Ellis and Wagner [1]. The parts of the name corresponds to the states of the components in the system: the precursors, that are provided as a vapor, crack to release the growth species, whose incorporation into the growing solid crystal is facilitated by the liquid seed particle. The particle facilitates the reaction by alloying with the ingoing elements to varying extents depending on their respective vapor pressure. When growing III-V semiconductors, the group III elements are typically solved more easily than the group V elements. The group III and V elements are then incorporated into the growing crystal as pairs, through nucleation at the interface between the particle and the substrate, as discussed in Section 2.7.3 [23]. For the material to follow this path, the vapor must be supersaturated in relation to the particle, while the particle must be supersaturated in relation to the substrate. The reason this does not induce only direct growth of material on the surface, since the supersaturation of the vapor with respect to the substrate is even larger, is, as was stated in Section 2.7, that the particle also lowers the critical nucleus size, so it is easier to form stable nuclei [25][23].

Sometimes, growth has been reported in systems where the particle, with solved group III and group V elements, is solid instead of liquid. The growth model employed is then vapor-solid-solid (VSS) growth. This has been suggested as a probable route in some cases of nanowire growth using Ag seed particles [26]. VSS has been suggested as a route for nucleation of GaAs [27] and InAs [28] nanowires from Au particles. The mechanisms surrounding the actual nucleation from particles that are solid are expected to be different compared to nucleation from liquid particles, since the diffusivity of the alloyed species is smaller in a solid particle [27].

2.9 Phase Diagrams

Most elements have a certain solubility of other specific elements, while still being considered the same phase. Phase diagrams can be used to predict what phases and what temperatures will be relevant for the growth systems, and to determine if the growth is better described by VLS or VSS, for example. Preferably, phase diagrams showing all the ingoing elements should be used, but they are not always available. The general idea and predictions can, however, be drawn from binary or ternary phase diagrams.

The binary phase diagram of Ag and In is shown in Figure 2.8. As can be seen, Ag can accommodate up to 20% of In up to about 700 °C and still remain in the same phase. For nanowire growth, this is typically what is expected: some amount of group III material solved in the particle. The solubility of group V materials is typically lower, but they are still present in the particle. This depends on the vapor pressures of the elements, or the tendency for elements to stay in the vapor, where the general case is that group III elements have a low vapor pressure and therefore want to stick to the surface rather than being in the vapor. With the exception of Sb, the group V elements have a high vapor pressure, meaning that much material needs to be provided to get incorporation [2].

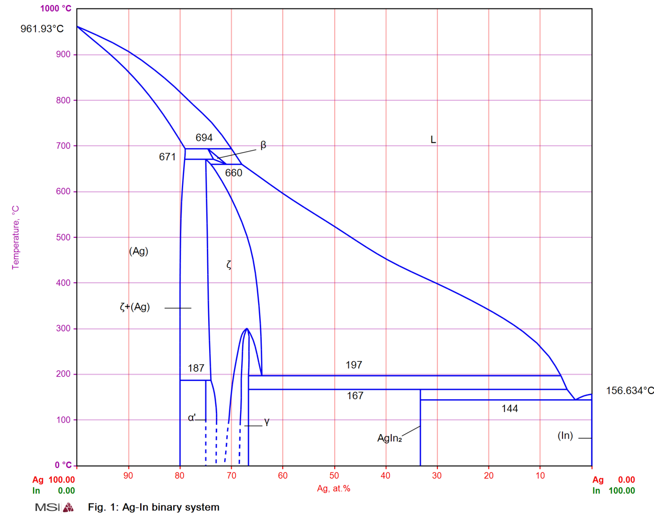

Figure 2.8: The binary phase diagram of the Ag-In system. Figure taken from [29].

For ternary phase diagrams, containing three separate components, different representations are available. Isotherms are common, where the phases existing for different compositions at a set temperature (and pressure, of course), are shown. One such phase diagram is shown in Figure 2.9. Some ternary phase diagrams instead show the liquidus projections, i.e. what compositions are liquid for certain temperatures. Ternary phase

diagrams can also be projected down to pseudo binaries, where the ratio between two of the components is set to a specific value.

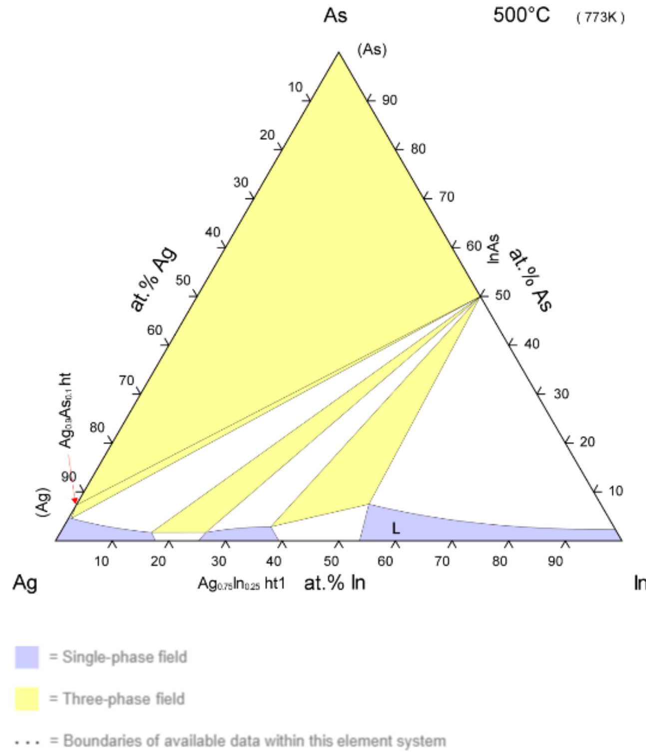

Figure 2.9: An isotherm at 500°C of the Ag-In-As system. Figure taken from [30].

2.10 Growth from Different Seed Particles

Growth from many different seed particles has been demonstrated, even though Au is the seed used to the greatest extent. Au is used since it is easy to work with and generally gives much growth, especially in the <111> directions [8]. A problem with this is that the integrated circuit industry, as of now, mainly works with Si, where the structures are placed on the (001) plane of substrates. Au is also forbidden to be used in the Si industry, since the deep level traps they form in the Si bandgap can destroy the electric effects of the semiconductor even at low levels [11].

Examples of other particles currently being explored are Sn, Pd, Ag and self-seeded among others. Self-seeded means that the actual particle is of the same material as the group III element used in the growth. Growing from other particles of course means that most parameters need to change. The solubility of different elements, melting temperature, response to annealing and even crystal structure may differ between the systems. Therefore, evidently, two different particles are not expected to give growth under the same

conditions, and the two systems need to be optimised separately.

Ag particles also have the problem with deep traps in the Si bandgap [12]. However, Ag has a diffusion length in Si that is 2 orders of magnitude lower than Au, which makes Ag better for integration. Ag has also been shown to promote growth in the [001] direction. This is therefore one of the most promising particles to be explored further, if ordering, discussed in Section 2.13, should be observed. The yield of and control of properties for wires grown from Ag particles has shown varied results, and a further exploration is therefore needed [9].

It has been shown that group IV nanowires can be grown using AgAu particles, which opens up new possibilities to tailor the growth, by varying the composition [31].

2.11 Crystallographic Planes and Directions

The different planes of crystals will present different conditions for heteroepitaxial growth. In zincblende, the (111) plane is the close-packed plane, meaning that the atoms are the most densely packed there. The (111) plane can also be terminated by either the group III or the group V element, giving rise to what is called polarity, since termination presents different conditions for the surface. This has created the distinction between group III terminated, (111)A, and group V terminated, (111)B, surfaces. This can be seen in Figure 2.10 for a generic III-V semiconductor. Due to the different nature of these surfaces, preferred growth directions will also emerge when growing nanowires. The [111]B growth direction is preferred over [111]A in many growth systems. This has to do with the energies required to form interfaces with these specific surfaces [2]. Nanowires grown from a substrate do not necessarily have to grow perpendicular to the surface. So for a specific surface orientation many possible growth directions are typically available for the nanowires, and the differences in energy are sometimes too small to give an exclusive yield of only one growth direction.

2.12 Growth on (001)

One reason to explore nanowire growth on (001) substrates instead of {111} is that (001) is more common in device processing in the electronics industry. Therefore, efficient growth on (001) would help with the integration of nanowires and other nanostructures [9]. When growing on the (001) crystal plane, the nanowires will, as was stated above, choose between many different directions to grow in, depending on the growth conditions. A few directions available will be discussed in relation to the (001) surface. These are also shown in Figure 2.10.

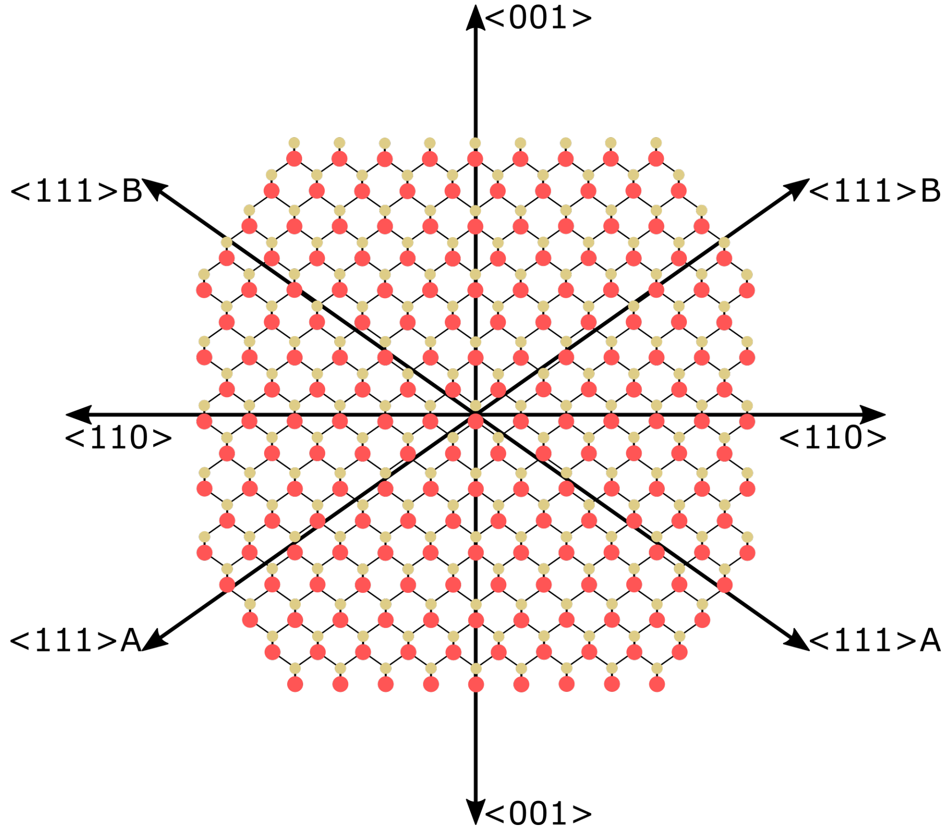

Figure 2.10: A schematic III-V semiconductor viewed along a <110> direction. Indicated are several directions, along with the atomic species. The red circles represent group III elements while the beige circles represent group V elements. Note that the <111>B directions are terminated by group V elements, while the <111>A directions are terminated by group III elements.

Both of the [111] directions, [111]A and [111]B, discussed in Section 2.11, are available, manifested as inclined directions at an angle of 35.3°from the surface. Other low index directions are the <110> directions in the (001) plane, which are non polar and perpendicular [10].

These growth directions, along with the vertical [001] direction, are the most common, but there exists of course other higher order directions. Sometimes the growth is disturbed by the formation of twin planes and other dislocations, creating nanowires with no single growth direction. Wires growing in different directions will be discussed further in Section 4.1.

Even though the wires tend to grow in the <111> directions, i.e. 35.3° angle to the (001) plane, if growth in [001] is initiated they tend to keep this direction. Annealing of Au particles has been shown to promote growth in <111> while the absence of annealing

can promote growth in [001]. This is likely due to trench formation in the substrate underneath the particle, as the particle alloys with the substrate material. In the trenches facets are formed, which will then promote the growth in <111> [32]. On GaAs (100) it has been shown that particles often diffuse exclusively along two parallel <110> directions of the surface, and not the two perpendicular ones. These directions correlates with the trenches that could be observed after annealing of the particles. The reason for the anisotropic behaviour is amounted to energy barrier differences [24].

The side facets of wires grown in the [001] direction on (001) substrates have been observed to be mainly {110} facets, but also {100} facets. The most common cross sectional shape is quadratic, with {110} facets, but more octagonal shapes consisting of both {110} and {100} facets have been observed [9][33].

2.13 Ordering

Ordering is a phenomenon that is sometimes observed in ternary alloy semiconductors. What it means is that during growth, the ingoing elements spontaneously place themselves in a periodic pattern. Recall the discussion in Section 2.3, where it was stated that, for III-V semiconductors, pairs of elements from the two groups are formed when for example a ZB crystal is grown. Now if there are two different group V elements present during growth, each incorporated pair will contain one or the other. The most intuitive prediction would be that this incorporation is completely random, depending on how much material is present and such. Under certain conditions, however, the two group V elements are incorporated in a periodic pattern along a specific growth direction. This means that, for example, every other layer of III-V dimers could contain only one of the two group V elements, while the layers in between would contain only the other. This ordering has primarily been observed when growing thin epitaxial layers, and is named differently depending on along which direction the ordering is observed and what material system it was firstly found in [6][34]. Even though ordering has never been observed in the regular axially grown part of nanowires, it has been observed when lateral core-shell overgrowth of the nanowires is present [7].

The most reported type of ordering is CuPt ordering, where the group V elements form alternating layers in one of the [111] directions. This has been observed when growing epitaxial layers in the [001] direction, for both GaAsSb and InAsSb [34]. An example of CuPt ordering is shown in Figure 2.11.

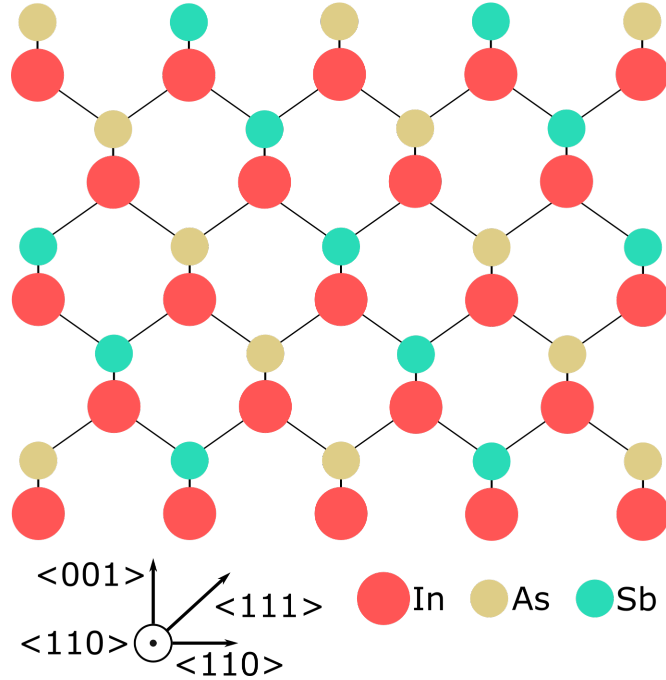

Figure 2.11: An example of CuPt ordering, here for the ternary III-V semiconductor InAsSb. The crystal is here viewed along a <110> direction. Notice the alternating layers formed along <111> for the group V elements.

When a crystal grows, there will be a competition between the surface ordering and the bulk disordering, where bulk diffusion can destroy the ordering after it is formed. Therefore, ordering is also very temperature dependent, needing a high enough T for the atoms to be incorporated in the right sites, but low enough so that bulk diffusion is not a problem. This also implies that ordering will never be perfect, and the layers will in reality of course contain some atoms of the other element [6].

As was mentioned in Section 2.4, ordering can increase the bowing parameter, and therefore also decrease the energy of the bandgap, see Equation 3. According to Svensson et. al. [21], the main driving force for ordering is to relieve strain in the growing crystal. Strain can also be relieved by growing buffer layers, and this will also lower the bandgap energy. This method makes the structure more complex, which is why induced ordering would be a much simpler route for achieving smaller bandgaps [21].

To detect ordering, the diffraction pattern of the material is analysed (discussed in Section 2.15.2). The presence of ordering will manifest itself as extra diffraction spots in between the regular spots. This is due to the periodic nature of ordering [34].

2.14 Properties of III-Antimonides

As was stated earlier, the III-antimonides (III-Sb), and ternaries containing Sb, are suitable for many applications due to their small, direct bandgap and high electron and hole mobilities. Table 2.1 summarises some of the properties of III-Sbs, compared to III-As relevant to this project.

Table 2.1: Some material properties relevant to this project. The properties are derived from bulk materials at T = 300 K [35].

Material	**Lattice parameter [Å]**	**Bandgap [eV]**	**Electron mobility [$\mathbf{cm^2V^{-1}s^{-1}}$]**	**Hole mobility [$\mathbf{cm^2V^{-1}s^{-1}}$]**
InAs	6.06	0.36	$3.3 \cdot 10^4$	450
InSb	6.48	0.17	$7.7 \cdot 10^4$	$1.1 \cdot 10^3$
GaAs	5.65	1.43	$9.3 \cdot 10^3$	450
GaSb	6.10	0.72	$1.2 \cdot 10^4$	$1.6 \cdot 10^3$

Note that InSb has the highest electron mobility, while GaSb has the highest hole mobility, which also holds true when compared to other III-V materials and not only InAs and GaAs. The small bandgap makes III-Sbs suitable for usage in optoelectronic devices operating in the IR-region, both as emitters and as detectors [3][2].

For nanowires containing Sb, under the relevant conditions, zincblende is the crystal structure typically observed, but it is not exclusive [20]. But since ZB is more common and the crystal structure we expect to find, the values presented are for ZB.

One problem with Sb is the surfactant effect it has on the substrate surface. Sb has a tendency to adsorb to the surface, but not get incorporated, and can lower the surface- or interfacial energy between the surface and other phases. This effect can lower the wetting angle of particles on the substrate. If the wetting angle is reduced too much, the particles may spread on the surface and take a flat shape, from which directed growth will prove difficult. This can lead to more surface growth, or enhanced growth in certain directions, for example in the plane of the substrate [25].

The tendency of Sb to stay on the surface of the substrate is due to its low vapor pressure, meaning that it prefers to be adsorbed rather than to be in the vapor. All group III elements also have a low vapor pressure, but they on the other hand get more easily incorporated into the growing structure, or solved in the particles. The other group V elements desorb if they are not incorporated, since their vapor pressure is high. Sb might even precipitate to form crystallites due to the vapor pressure and the reluctance to get incorporated [36].

Another problem encountered when growing with Sb is that the precursor commonly used, TMSb, does not decompose significantly until around 500 °C in vapor (the substrate may however make the TMSb decompose at lower temperatures). This becomes a problem

when growing for example InSb, that has a melting temperature of about 525 °C. This makes the temperature window usable for growth very narrow [36].

2.15 Characterisation

In the following sections, the different techniques used to analyse and characterise the wires are presented.

2.15.1 Scanning Electron Microscopy

SEM stands for Scanning Electron Microscope, and is a type of microscope that uses electrons to create virtual images of mainly the surface of specimens. An advantage of using electrons for the imaging is that a much higher resolution is attainable when compared to regular light microscopy. This is due to the much shorter wavelength of electrons, with which smaller objects can be resolved. Another advantage is the good depth of field attainable in SEMs, which makes objects at different heights stay in focus when a micrograph is recorded.[37]

The electrons are generated by the electron gun at the very top of the column of the SEM. There are different types of sources available depending on the instrument, but the most common are LaB_6 filaments or tungsten wire, and there are different methods for the extraction of electrons depending on the desired resolution. High electric field strengths are used to extract and accelerate the electrons through the column, typically on the order of 10 kV. The acceleration voltage used plays a large role in the final resolution, depending on what imaging mode is used (discussed below). In order to not disrupt the electrons or contaminate the source, a high vacuum is required in the whole column, and most often the sample is also in high vacuum (although there are environmental SEMs that can hold the sample in specific gas environments). In the column there are magnetic lenses used to focus the electrons into an as small spot as possible on the sample surface. A small spot is desired, since if electrons are generated from a smaller volume, the resolution of the detection will be better. The electrons are more easily focused when the acceleration voltage is higher, which is why higher acceleration voltages are preferred in this situation. The lenses exhibit aberrations that limits their functionality. The most important ones are:

- **Spherical aberration:** Electrons farther out from the center of the lens are bent more than those that pass close to the center of the lens.
- **Chromatic aberration:** Electrons of different energies (different velocities) are bent differently when passing the lens. Slower electrons are bent more since they remain in the magnetic field for a longer time and are therefore affected more. There is always a spread in energy of the electrons, which depends mostly on the source and extraction method used.

The different aberration effects also limit the final attainable resolution, but are not very important in SEM. In the column there are also apertures, small holes, that allow passage of parts of the beam and block others. They are there to remove the electrons that have diverged the most from the center. This gives a smaller spot size, at the "cost" of lowering

the beam current, which is sometimes desired. Spot size and beam current are always related to one another, and it is difficult to obtain a small spot size with a high beam current, for example. When imaging, a high resolution is wanted, so a smaller spot size is desired. In the column there are also scan coils that are used to deflect the beam in a scanning manner. This is where the "Scanning" part of SEM comes from; the electron beam is scanned across the surface of the sample and a signal is detected from every point [37][38].

When using the SEM as a tool for imaging, there are many different signals that can be detected and used to form the image. One signal that can be detected is Secondary Electrons, or SEs. These electrons are generated as the incoming electrons from the beam are interacting with the sample, forcing electrons of the sample to be ejected. There are three types of SE signals, called primary SEs, SEII and SEIII.

- Primary SEs are generated throughout the whole volume the beam electrons penetrate into (called the interaction volume), but due to their small energy (about 50 eV) they can only escape the sample if they are generated close to the surface.
- The SEII signal is generated as the electrons in the beam are scattered in the sample to another part of the sample surface, where they knock out a secondary electron.
- SEIIIs are secondary electrons generated as the electrons of the beam are backscattered (discussed below), and hit the walls of the sample chamber, where secondary electrons are ejected.

Due to the fact that these electrons only can escape and be detected if they are generated close to the surface, they are mainly used to get topographical information. Wherever the signal gets blocked due to the surface topography, the image will appear darker, so this type of imaging gives a very natural look of the images. Edges will be very bright due to the amount of surface compared to flat areas. SEs are detected by a detector that has a bias that pulls the electrons to it. This is required due to the low energy of the electrons, but it has the effect that some surface features are seen even though they should not be. Electrons generated at the back of an outcropping is a common example, where the electrons are sucked into the detector and still give a signal [37].

The other primary type of signal is Backscattered Electrons or BSEs. This signal comes from electrons in the primary beam penetrating into the sample, getting elastically backscattered (no loss in energy) out of the sample and then detected by a detector. Since the contrast when using BSEs mainly comes from differences in atomic number, and we are more interested in the topography, BSEs will not be discussed further.

2.15.2 Transmission Electron Microscopy

Transmission Electron Microscopy (TEM) is, as the name suggests, a method of microscopy where electrons are sent through the material being investigated, giving information about the material depending on the electron-material interactions. In general, the TEM and the SEM are quite similar, at least the part above the sample. The big difference is that the TEM handles much higher voltages on the order of 100 kV. This is one of the reasons that a much higher resolution is attainable in the TEM. This also

means that aberrations are much more important in TEM and are sometimes corrected for to get higher resolution. Another big difference is that the sample needs to be very thin for the beam to be transmitted properly through the sample. Nanowires are typically scraped off from the substrate they are grown on, and placed on a carbon grid that is put inside the TEM. As the beam passes through the sample, many signals are generated, and depending on what information is wanted, different detectors can be used. The signals discussed for the SEM are present, and other common detected signals are x-rays for spectroscopy (discussed in Section 2.15.3) and of course the transmitted electrons. In normal operating mode, the TEM shines a parallel beam of electrons through the sample. Most TEMs also have some flexibility in their operation, where the beam can be condensed into a small spot and scanned across the sample like the beam of an SEM. This is called Scanning Transmission Electron Microscopy, STEM [39].

When the electrons pass through the sample, they are diffracted depending on the periodicities in the material. This produces a diffraction pattern that can show the crystallinity of the sample and what the crystal structure is, for example. The image of this diffraction pattern consists, for crystalline materials, of bright spots at certain distances from the central direct beam, depending on how the material is aligned, the lattice parameters and spacing between atomic planes. The pattern shows what is called the reciprocal space, where long distances in real space are represented by short distances in reciprocal space, and the other way around. For amorphous materials, diffuse halos are instead formed around the central spot. The information attained in this diffraction pattern can be used to construct an image of the sample. By only selecting the electrons in the direct beam, for example, a bright field image can be made. This image will be bright in areas where the density in the material is low, and dark where the density is high. This is done by adding an aperture in the column of the microscope that blocks all the unwanted electrons. The remaining electrons are then recorded on a CCD (Charge-Coupled Device) camera [39]. Creating a diffraction pattern is very similar to making a Fourier Transform of the sample, which also presents spots in reciprocal space and in theory contains the same information as a diffraction pattern. Therefore, Fast Fourier Transform (FFT) is often used in post-processing of TEM images, instead of recording a (less noisy but more time consuming) diffraction pattern.

2.15.3 X-ray Energy Dispersive Spectroscopy

As the electrons from the beam pass through the sample, electrons from the sample are sometimes knocked out. Often these electrons were tightly bound to their atom. This will leave an atom with an unoccupied energy state. This state can then be filled again, by another electron that comes from a higher energy state in the atom. The excess energy difference between these two states has to be emitted, which may result in the emission of an x-ray. These x-rays are therefore of a certain energy depending on the difference between the energy levels in the atom. In X-ray Energy Dispersive Spectroscopy (XEDS or EDX, other abbreviations exist) this is used to determine what atoms are present in certain parts of the sample. This is done by operating the TEM in STEM mode, and detect the x-ray emission as the beam is scanned across the sample [39].

3 Experimental Procedure

3.1 General Procedure

The experimental procedure followed a systematic approach, where base parameters were chosen based on earlier experiments and then varied individually, keeping the other parameters constant between growth runs. This procedure was chosen due to the sensitivity of Sb-based systems (antimonides are difficult to grow for several reasons discussed in Section 2.14, and tiny changes in the parameters can disrupt the growth) and the necessity to perform a rigorous and thorough investigation of the effects of the different growth parameters on the system. The parameters that were mainly investigated were the temperature and the flows of the AsH_3 and TMSb precursors, effectively changing their respective V/III ratios independently. This means that, for example, growth time and TMIn (TMGa) flow were kept constant throughout the experiments in order to limit the number of parameters that would be optimised, which facilitated the study.

The substrates were cleaved by hand into pieces of about 4 by 4 mm^2. By scraping the surface with a diamond tipped pen, the InAs(001) and GaAs(001) substrates could be cracked along the flats, i.e. in the <110> directions. Ag and AgAu particles with a diameter of 30 nm were generated and deposited by using a spark discharge generator. This gave a particle density of about 4 μm^{-2}. The same density was acquired for the Au particles as well, which were deposited as an aerosol. The densities were verified in the SEM, a Hitachi SU8010.

The growth was performed using an Aixtron CCS (close-coupled showerhead) MOVPE reactor. In this type of reactor, the gas is supplied from above the susceptor, where the substrates are placed. The gas passes through a holey quartz shield that spreads the gas evenly across the susceptor. When a growth run was completed, the samples were imaged via SEM. This was done to record the results of the growth and to some extent plan for what parameters should be changed for subsequent runs.

Before each growth run, an etch and cover procedure was performed in the growth chamber. The etching, using HCl, would remove any remaining material that could affect the growth. The "cover" process refers to a growth of a surface layer in the growth chamber, consisting of the same material as the substrates upon which the nanowires would be grown on. This was an attempt to increase the reproducibility of the growth, making sure that any material originating from the actual chamber would be the same as what was grown. Thorough cleaning was especially required due to the sensitivity of Sb systems, since residual Sb could change the growth drastically. After the etch and cover, the substrates were placed in the growth chamber. Three samples, each containing one of the three different seed particles, were used in each run. This would show the difference in growth for the different seed particles under truly identical growth conditions.

As was mentioned earlier, some growth parameters were set to a standard value and not changed when creating the growth series. These values were based on the experiences of other people in the group, and are summarised in Table 3.1.

Table 3.1: The standard growth parameters that were chosen at the beginning of the experiment, and not changed during subsequent growths. Values in parentheses are for the GaAsSb samples. SCCM stands for standard cubic centimeters.

Parameter	**Value**
Growth Time	1200 s
TMIn (TMGa) Source Flow	12 (3) sccm
Total Flow	8 l/min
Base Pressure	100 mbar
Anneal Temperature	550 (630)°C
Anneal Time	420 s
Anneal AsH_3 Flow	20 sccm

Annealing under As was performed at the start of each growth run, to deoxidise the surface of the substrates. Different materials require different temperatures, depending on the stability of their oxides. The total flow is achieved by diluting the precursor flows with H_2, see Section 2.5. After the growth was completed, the source flows where switched back to H_2 flows and the samples were cooled to room temperature under H_2, so that they could be extracted for further analysis.

The initial values of the parameters that were to be optimised are shown in Table 3.2. These were also based on other experiments performed by people in my group at FTF, and were just meant to send me off in the right direction for my particular material system.

Table 3.2: The initial values used for the first growth run, where the values in parentheses were used for the first GaAsSb sample.

Parameter	**Value**
Growth Temperature	400°C
As/In (As/Ga) ratio	137 (13)
Sb/In (Sb/Ga) ratio	24.5 (2)

3.2 Growth runs performed

From the initial values shown in Table 3.2, the parameters were varied one by one to see if suitable growth conditions could be found. For the InAsSb samples, the first parameter to be optimised was the temperature, where values between 350°C and 450°C were tested. Then a suitable new starting temperature for the analysis of the next parameter was selected. Growth runs were performed for As/In ratios between 6.9 and 1100. After choosing a suitable As/In ratio, the Sb/In ratio was varied between 12 and 49. Finally, the best, and most interesting, samples were selected for continued study.

A similar procedure was followed for GaAsSb, where the optimal temperature in the range between 400°C and 600°C was found. Then the As/Ga ratio was optimised between 9 and 27. Due to lack of time (and promising results) a decision was made to abandon the

GaAsSb optimisation, and focus solely on InAsSb. Therefore, no optimisation of Sb/Ga ratio was performed.

After the initial experiments, an effort was made to try to increase the yield of wires growing in [001] from Au particles. Therefore, several growth runs were done to try to grow InAs stems, upon which InAsSb wires could be grown. This was because InAs is a material that is easier to grow than InAsSb, and the stems could then act as nucleation points for further growth. For the stems, the growth temperature chosen was the same as the best InAsSb sample found, and the As/In ratio was varied between 17 and 6871, to find the optimal growth conditions for that temperature. A few growth runs then aimed to grow InAsSb wires on top of [001] oriented InAs stems. Here, the parameters that produced the best InAs stems were used for the growth of the stems, before switching over to parameters that gave good InAsSb growth. Since the system in the InAsSb growth phase is different when using stems (the machine has already had gases flowing in, the particles have been in high temperature for long, etc.), parameters in the vicinity of the best InAsSb parameters had to be tested.

The reproducibility of the good growth runs was also tested. As it turns out, due to machine drift, where the temperature and TMSb source changed over time, the reproducibility of the runs proved to be bad, and results from earlier experiments could not easily be reproduced later on. Therefore, a few runs were dedicated to change values in the growth according to findings of other members of the group, who had similar problems, and see if this could reproduce results found earlier.

The final growth runs were used to try out a few changes to the parameters, which could give more insight into the system. Therefore, a run with only annealing and no nanowire growth was performed, as well as regular growth runs but without the annealing step. The run with only annealing could give information about the early stages of growth, while the runs without the annealing step could show how the annealing step affects the growth.

After all the growth runs were completed, TEM, as well as EDX, analysis was performed on one of the good samples, to make sure that the growth direction is the one assumed, and to reveal the crystal structure, composition and presence of ordering. This analysis was done in the JEM-3000F TEM equipped with an Oxford XEDS system.

4 Results

In this section, the results from the growth series will be presented. The data is presented in such a way as to highlight the samples that gave a high yield of wires oriented in the [001] growth direction, since this was the main goal of the growth optimisation. Samples that are extraordinary in other ways will however also be mentioned and discussed more in depth in Section 5. Certain samples will be named after the figure they first appear in. Some samples that do not provide much additional information have been left out for clarity.

Before showing micrographs of the actual samples, a brief discussion of the general morphology and growth direction of the wires found will be presented.

4.1 Types of wires observed

During the growth runs, many different types of wires grew for different parameters. To facilitate the presentation of the results from the actual growth runs, these wires will be discussed briefly now.

Figure 4.1 shows the most reoccurring types of wires observed throughout all the samples. (a) shows the appearance of the wires when viewing them from the top of the substrate, while (b) shows a side view, along one of the sides. The wires are numbered in both subfigures, to clarify that the same wires are shown from different angles. 1 is a regular vertical wire, growing in the [001] direction. These are the wires that are sought after. When viewing the sample without tilt, these wires appear as bright spots on the substrate, with shape depending on their cross section. This will be discussed more in Section 5.2.1.

2 and 3 are both planar wires, growing on the surface in the <110> directions along the side facets of the substrate. Wire number 2 is thin and often has some widening and surface growth at the base. Wire number 3 is growing perpendicular to 2. These "christmas tree"-like wires show significant tapering, and will, together with wire 2, be discussed further in Section 5.3. Typically, growth of one of these two types of wires is preferred over the other.

Inclined wires growing in one of the <111> directions, 35.3° from the surface, are also common. The distinction between wire 4 and 5 is that one of them is growing in [111]A and the other is growing in [111]B, depending on the orientation. This results in a difference in yield between the two types of wires. For most nanowire growth, [111]B is the preferred growth direction, as has been discussed in Section 2.11. It is highly likely to be the case in our system as well, but has not been investigated. Wire number 6 is a higher order inclined wire, that grows with a larger angle to the surface than the <111> wires. These wires appear shorter and with more contrast when viewed from above. The last wire, number 7, is a representation of a curly wire, a wire that kinks and changes growth directions many times during growth.

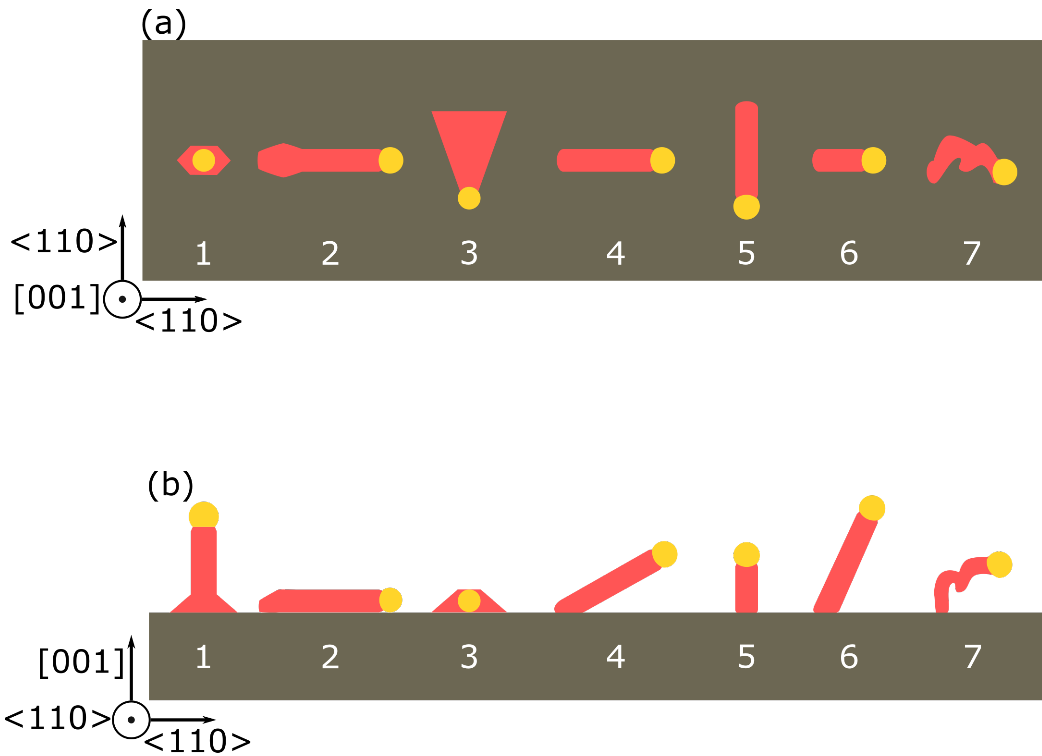

Figure 4.1: Most of the different types of wires observed are shown. (a) shows a top view, while (b) shows a side view along one of the cleavage edges of the substrate. The different wires are 1. Vertical [001], 2. Thin planar <110>, 3. Tapered planar <110>, 4.,5. Inclined <111>, 6. Higher order inclined, 7. Curly.

4.2 InAsSb

In this section, the InAsSb samples will be presented and briefly discussed.

4.2.1 Au seeded InAsSb

Figure 4.2 shows how the morphology of the InAsSb wires grown from Au particles changes with growth temperature. At low temperatures, Figure 4.2(a), most wires are thin and planar (low contrast in the background), while most of those that actually take off from the surface are inclined, with a few curly as well (both of these types have higher contrast). For intermediate temperatures, Figure 4.2(b), however, there are wires growing in the wanted [001] direction, indicated by bright spots to the right in the micrograph, along with planar wires (low contrast) and inclined wires growing in <111>. The [001] wires are lost as the temperature approaches higher values, and only planar and inclined wires are observed in Figure 4.2(c). For high temperatures, Figure 4.2(d), no nucleation is observed. 375°C was chosen as an appropriate temperature for the optimisation of the other parameters. The sample shown in Figure 4.2(b) will from here on be referred to as Sample 4.2(b).

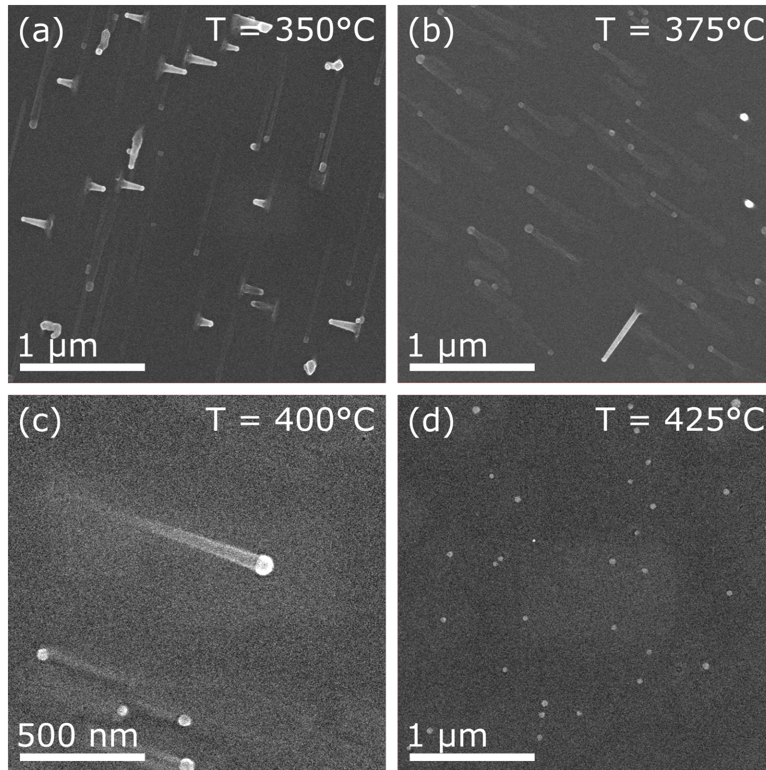

Figure 4.2: Top-view SEM images of Au seeded InAsSb nanowires grown at (a) 350°C (b) 375°C (c) 400°C (d) 425°C. For all samples shown, the values As/In = 137 and Sb/In = 24 were used.

The As series for InAsSb wires grown from Au particles is shown in Figure 4.3. For low As/In ratios, Figure 4.3(a) the wires start to nucleate, but remain on the surface and do not grow in wire-like structures. Increasing the As/In ratio, as shown in Figure 4.3(b), makes most wires grow out of the surface in an inclined manner. This sample will be referred to as Sample 4.3(b), and will be discussed further in Section 5.4, since the wires seem to be of the higher order type. Increasing the As/In ratio further gives us Sample 4.2(b) again, shown in Figure 4.3(c). For higher As/In ratios, the yield of [001] wires decreases until only planar wires grow in Figure 4.3(d) and ultimately no growth is observed in Figure 4.3(e). As/In values both higher and lower in the vicinity of Sample 4.2(b) were tested (ratios of both 103 and 172), but only resulted in a lower yield of vertical wires. A very low As/In ratio of 7 was also tested, which resulted in swollen particles, a few 100 nm in diameter, and some curly growth. The As/In ratio of 137 was chosen for the optimisation of Sb/In ratio.

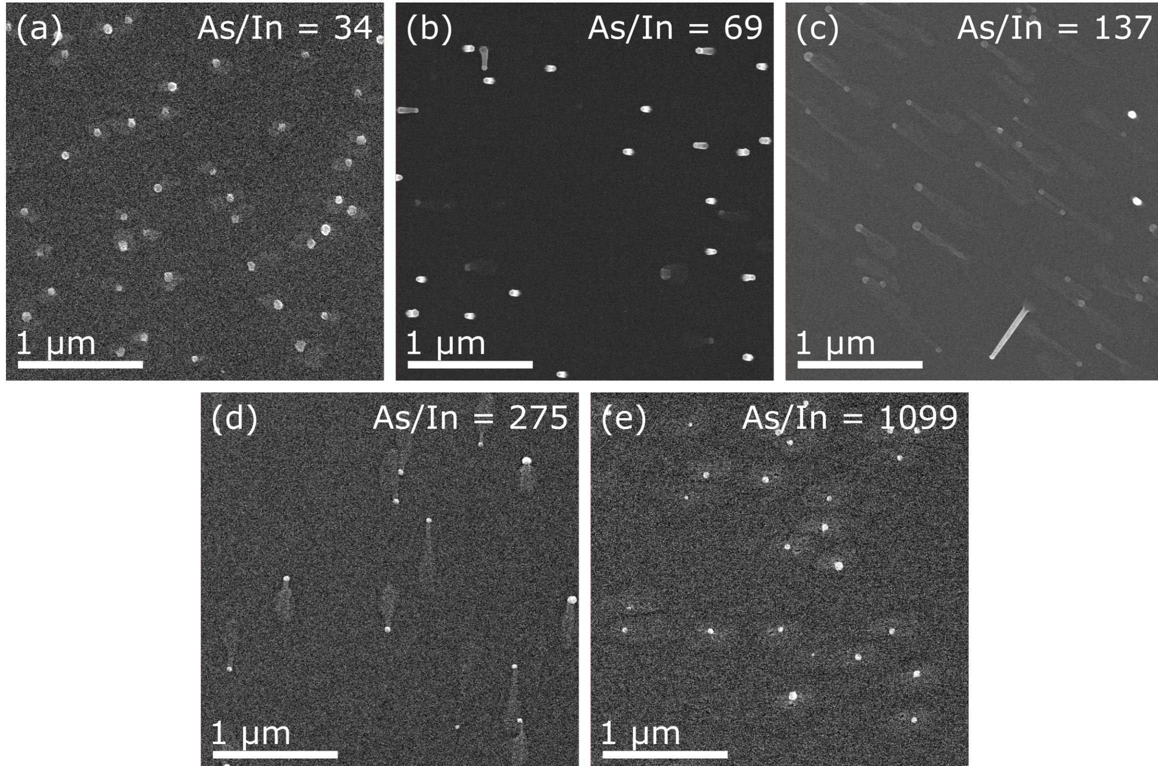

Figure 4.3: Top-view SEM images of Au seeded InAsSb nanowires grown with As/In ratios of (a) 34 (b) 69 (c) 137 (d) 275 (e) 1099. For all samples shown, the values T = 375°C and Sb/In = 24 were used.

Results of the growth of InAsSb nanowires as a function of the Sb/In ratio are shown in Figure 4.4. As can be seen, the amount of Sb does not seem to hinder the appearance of [001] oriented wires much in the small window tested, since they are present in subfigures (a)-(d). Sb/In ratios both below and above that of the Sample 4.2(b), shown in Figure 4.4(c), seem to decrease the yield, however. For too high InSb V/III, Figure 4.3(e), most of the wires that take off from the surface are curly or inclined <111> wires. The Sb/In ratio of 24 produced the best results.

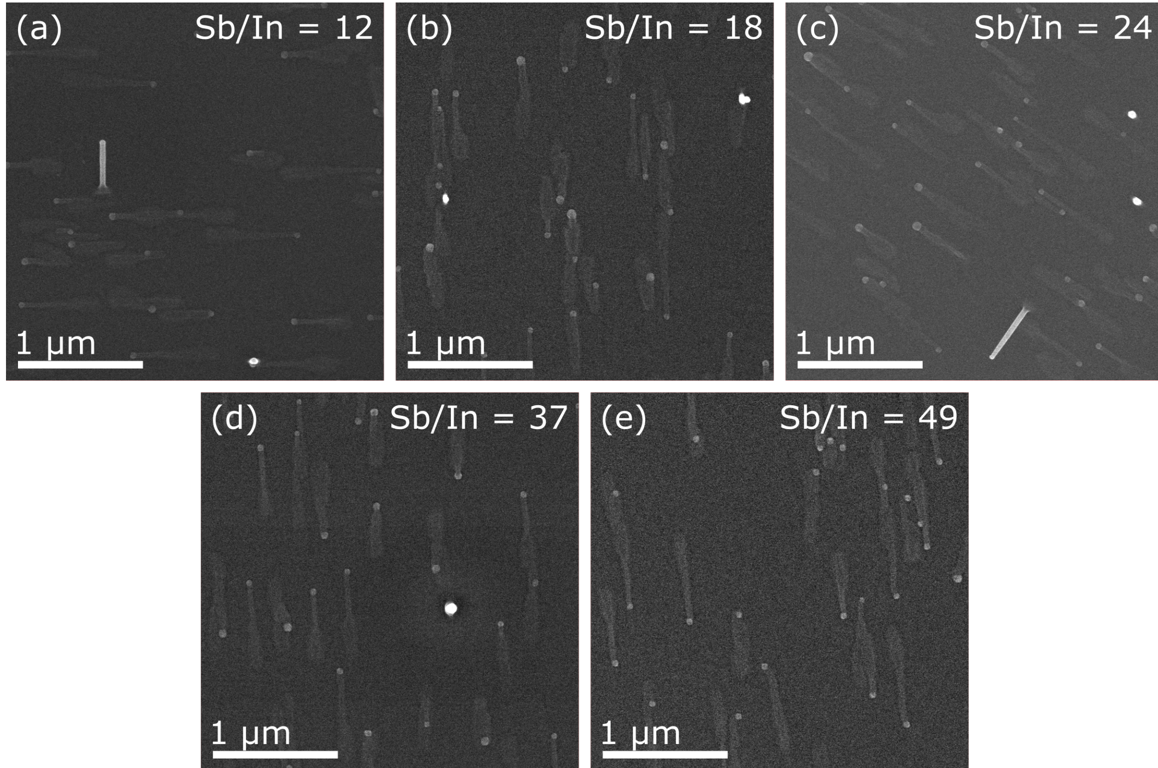

Figure 4.4: Top-view SEM images of Au seeded InAsSb nanowires grown with Sb/In ratios of (a) 12 (b) 18 (c) 24 (d) 37 (e) 49. For all samples shown, the values T = 375°C and As/In = 137 were used.

It should be noted that due to the fact that substrates with all the three particle types were loaded into the chamber together for every growth run, the optimisation process really only referred to the samples that produced the best results, i.e. the Au samples. The value chosen as the "best" of a certain parameter for Au in a series did not necessarily produce the best result for AgAu and Ag. But since Au produced the best results overall, this was a natural route to take.

4.2.2 AgAu seeded InAsSb

The temperature series in Figure 4.5 shows the InAsSb wires grown from AgAu particles for different temperatures. For low temperatures, Figure 4.5(a), many curly, as well as thin planar, wires grow. For intermediate temperatures, Figure 4.5(b), there are many inclined, curly and tapered planar wires, and also a few that seem to be vertical. The planar wires have therefore transitioned to the perpendicular tapered kind. Increasing the temperature further, as shown in Figure 4.5(c), the wires do not take off and only produce tapered planar wires on the surface. For high enough temperatures, Figure 4.5(d), no nucleation is seen, although the pits around the particles indicate that the wires might have grown, but at the same speed as the layer growth.

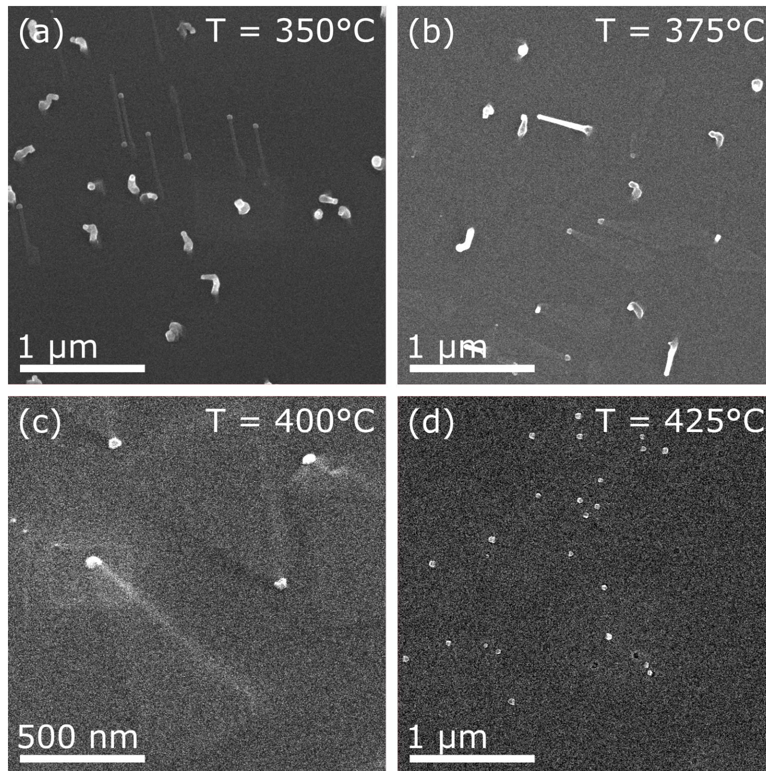

Figure 4.5: Top-view SEM images of AgAu seeded InAsSb nanowires grown at (a) 350°C (b) 375°C (c) 400°C (d) 425°C. For all samples shown, the values As/In = 137 and Sb/In = 24 were used.

Figure 4.6 shows how the growth of InAsSb wires from AgAu particles varies with As/In ratio. For low As/In ratio significant particle splitting is observed (Figure 4.6(a)). For higher As/In, Figure 4.6(b), (c), the usual, seemingly random growth directions are observed. More wires that grow in [001] are observed as the As/In is increased in Figure 4.6(d), although the yield is still very low. For the highest As/In, Figure 4.6 (e), no nucleation is observed.

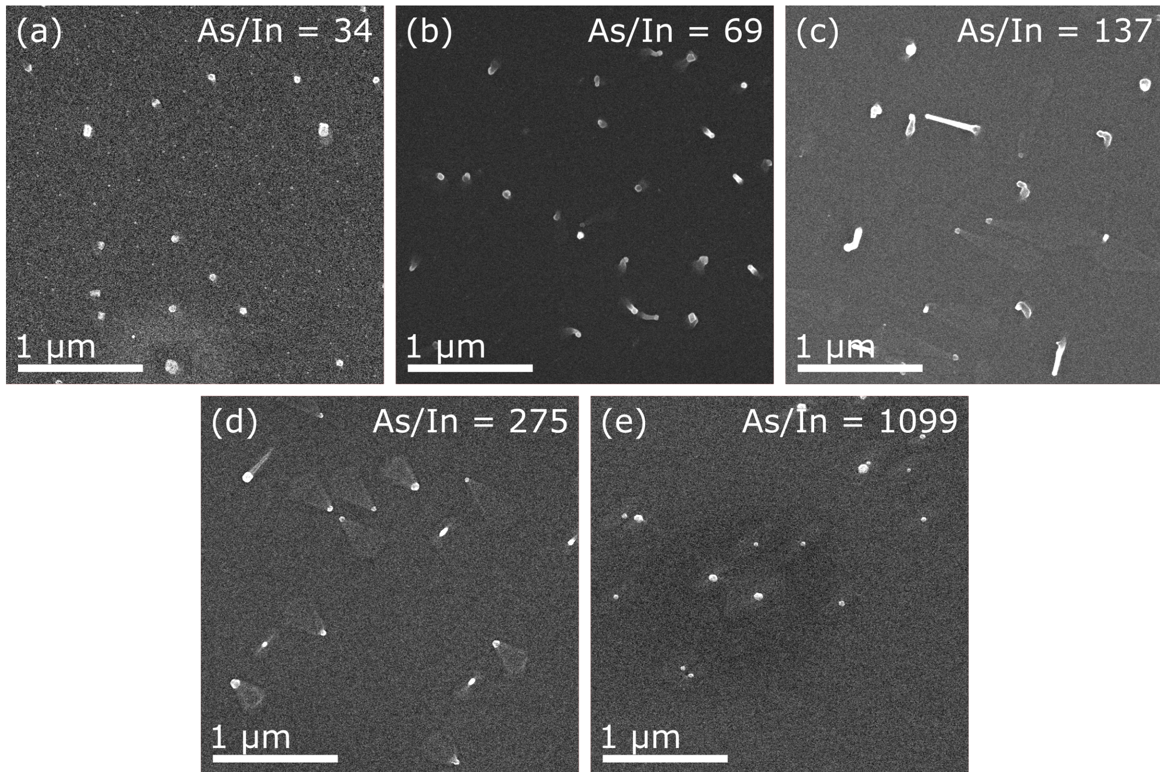

Figure 4.6: Top-view SEM images of AgAu seeded InAsSb nanowires grown with As/In ratios of (a) 34 (b) 69 (c) 137 (d) 275 (e) 1099. For all samples shown, the values T = 375°C and Sb/In = 24 were used.

In Figure 4.7, the growth series showing the Sb/In ratio effect on the growth of InAsSb wires grown from AgAu particles is presented. The general appearance of all the samples is the same, with planar, inclined, curly and a very low yield of seemingly [001] oriented nanowires. For higher Sb/In ratios, as shown in Figure 4.7 (d),(e), however, more particle splitting is observed, similar to what is observed for lower As/In ratios (Figure 4.6(a)).

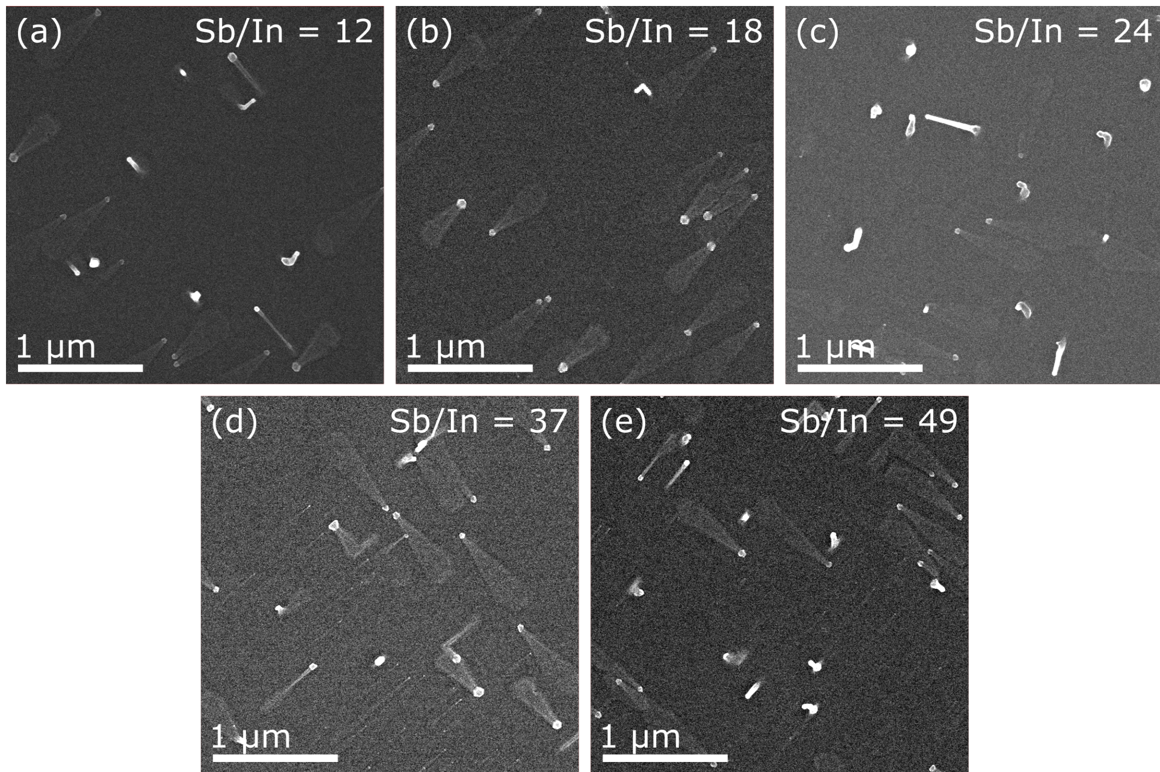

Figure 4.7: Top-view SEM images of AgAu seeded InAsSb nanowires grown with Sb/In ratios of (a) 12 (b) 18 (c) 24 (d) 37 (e) 49. For all samples shown, the values T = 375°C and As/In = 137 were used.

4.2.3 Ag seeded InAsSb

Figure 4.8 shows the temperature series for Ag seeded InAsSb. For all temperatures, the particles remained or formed rod-like structures on the surface. It was concluded that the rods were not nanowires, since no particle is present in either end and there are no signs of nucleation on the surface.

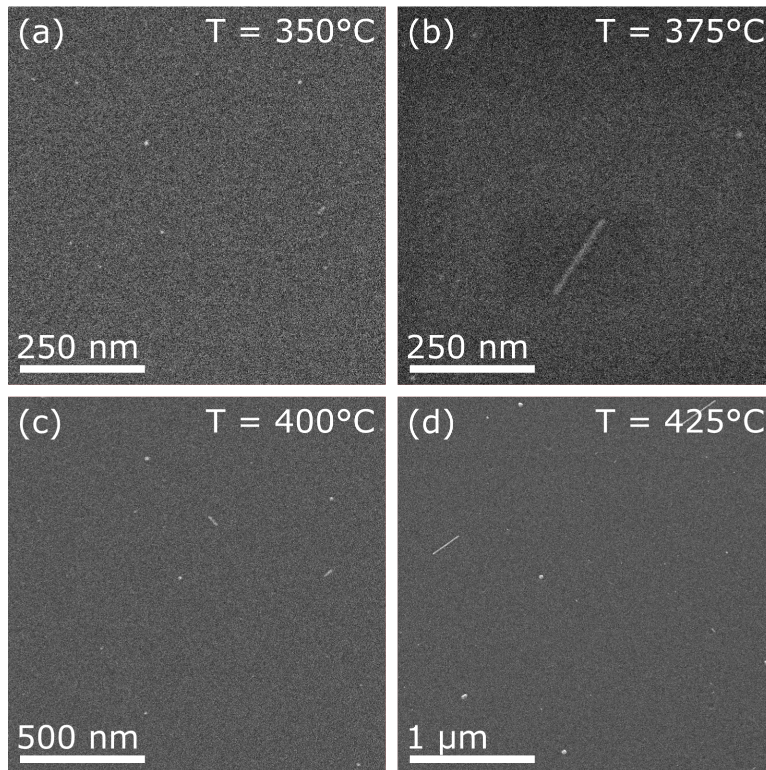

Figure 4.8: Top-view SEM images of attempted Ag seeded InAsSb nanowires grown at (a) 350°C (b) 375°C (c) 400°C (d) 425°C. For all samples shown, the values As/In = 137 and Sb/In = 24 were used.

Figure 4.9 shows the As/In series for Ag seeded InAsSb. For low As/In ratios, Figure 4.9(a), the swollen particles seem to have initiated some nucleation, since there seems to be material deposited on the surface around them. For higher As/In ratios, the particles again take the rod-like shape.

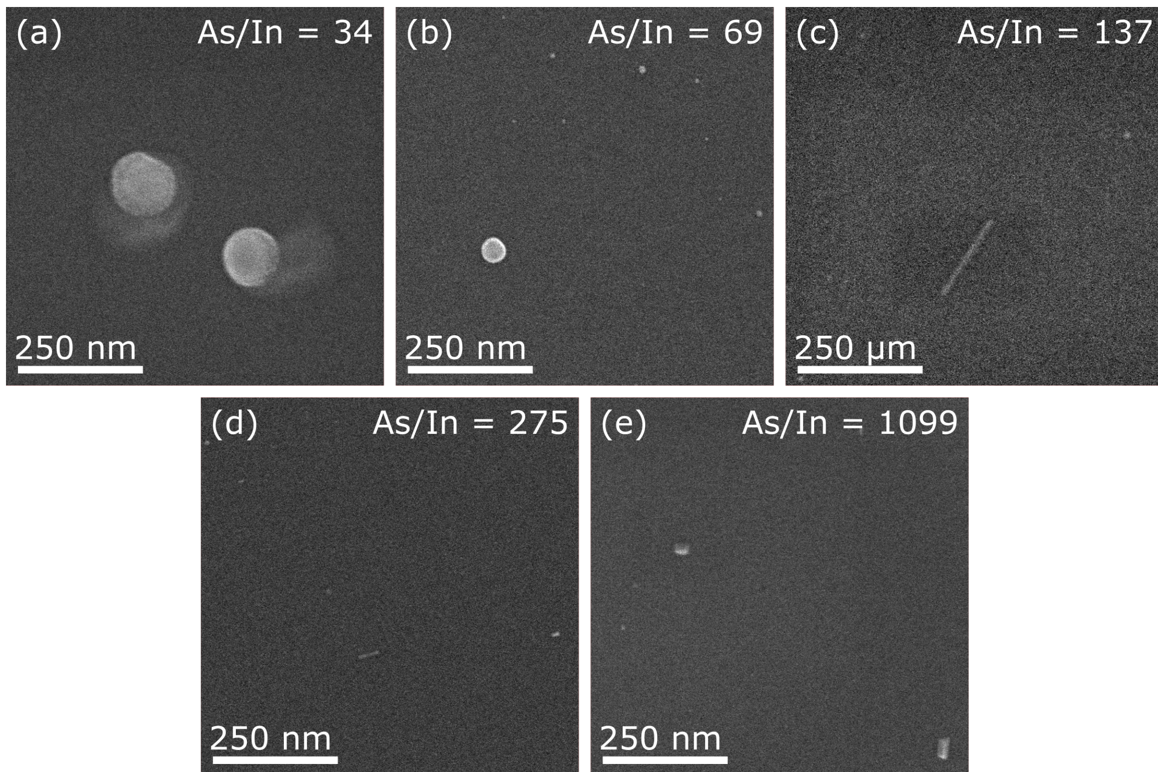

Figure 4.9: Top-view SEM images of Ag seeded InAsSb nanowires grown with As/In ratios of (a) 34 (b) 69 (c) 137 (d) 275 (e) 1099. For all samples shown, the values T = 375°C and Sb/In = 24 were used.

Figure 4.10 shows the Sb/In series for Ag seeded InAsSb. The Sb/In ratio does not seem to influence whether or not the particles form rods, for the set As/In ratio and temperature used.

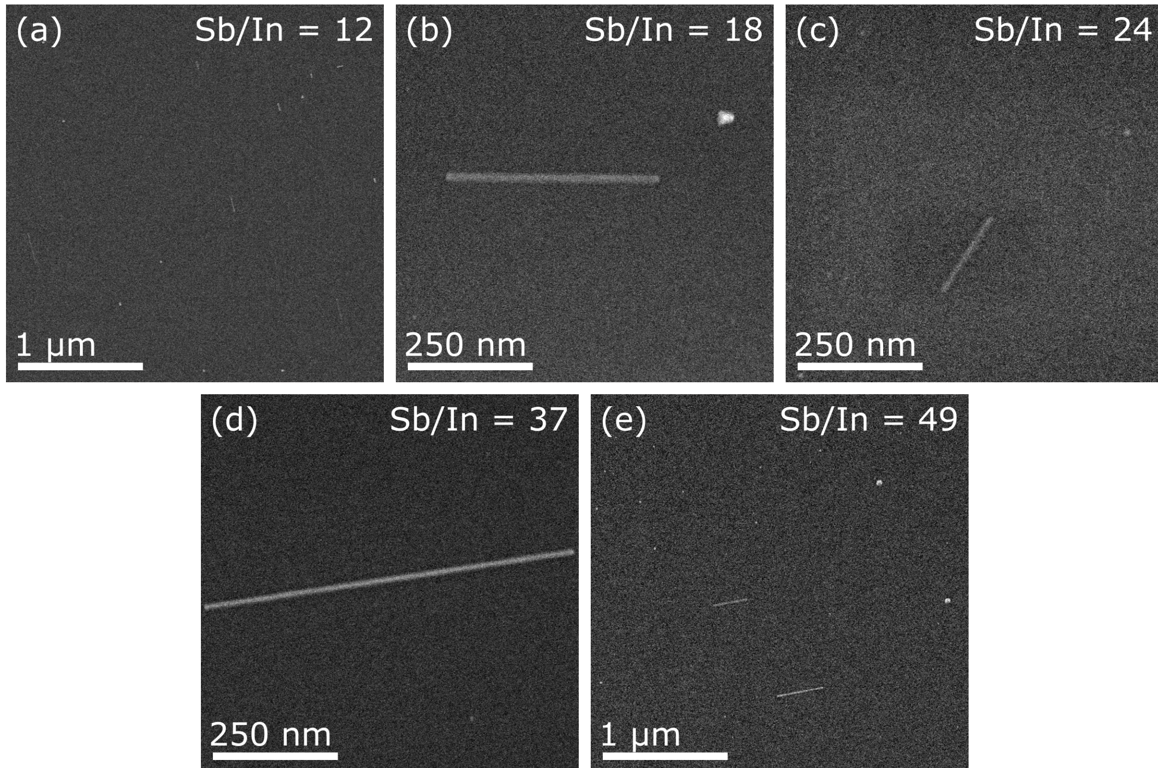

Figure 4.10: Top-view SEM images of Ag seeded InAsSb nanowires grown with Sb/In ratios of (a) 12 (b) 18 (c) 24 (d) 37 (e) 49. For all samples shown, the values T = 375°C and As/In = 137 were used.

4.3 GaAsSb

The following section will present the results from the GaAsSb growth sessions.

4.3.1 Au seeded GaAsSb

Figure 4.11 shows how the GaAsSb wires grown from Au particles change with temperature. For low temperatures, Figure 4.11(a), the yield is high, with different types of wires nucleating and growing mainly in one of the <111> directions. Particle splitting seems to be present, since the diameter of most particles/wires seems to be small. For intermediate temperatures, Figure 4.11(b), the wires grown are more homogeneous in size, shape and direction. Most nucleate in one of the <111> directions, and some of them kink later on. The diameter seems to correlate well to the particle diameter, with no significant tapering. For higher temperatures, Figure 4.11(c), the wires seem to grow planarly, and occasionally kink to grow in one of the <111> directions. All wires are tapered, with a wide base, and the yield is lower than for the other temperatures. For the highest temperature, Figure 4.11(d), no nucleation was observed. 450 °C was chosen as an appropriate temperature for the subsequent growths, since the wires were homogeneous and took off from the surface, and the yield was high.

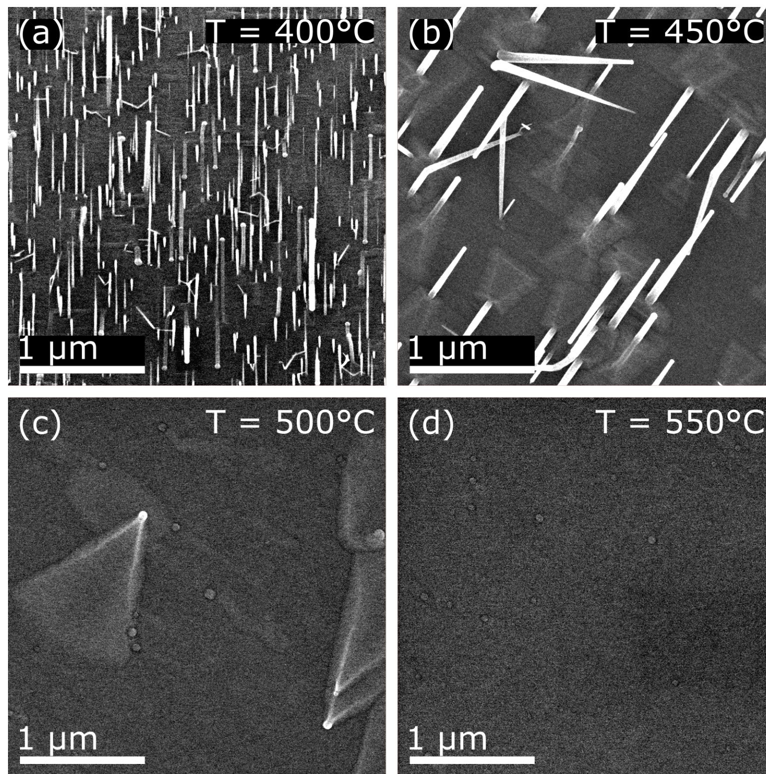

Figure 4.11: Top-view SEM images of Au seeded GaAsSb nanowires grown at (a) 400°C (b) 450°C (c) 500°C (d) 550°C. For all samples shown, the values As/Ga = 13 and Sb/Ga = 2 were used.

For low As/Ga ratios, as seen in Figure 4.12 (a), (b), the Au seeded GaAsSb wires are thin and often kink, compared to the wires grown under a higher As/Ga in Figure 4.12(c). In both cases, the wires prefer to grow in one of the <111> directions. For the highest of the As/Ga ratios, Figure 4.12(d), tapering is observed in the wires, and strange facets seem to grow at the base of the longer and thicker wires. The wires still grow preferentially in one of the <111> directions.

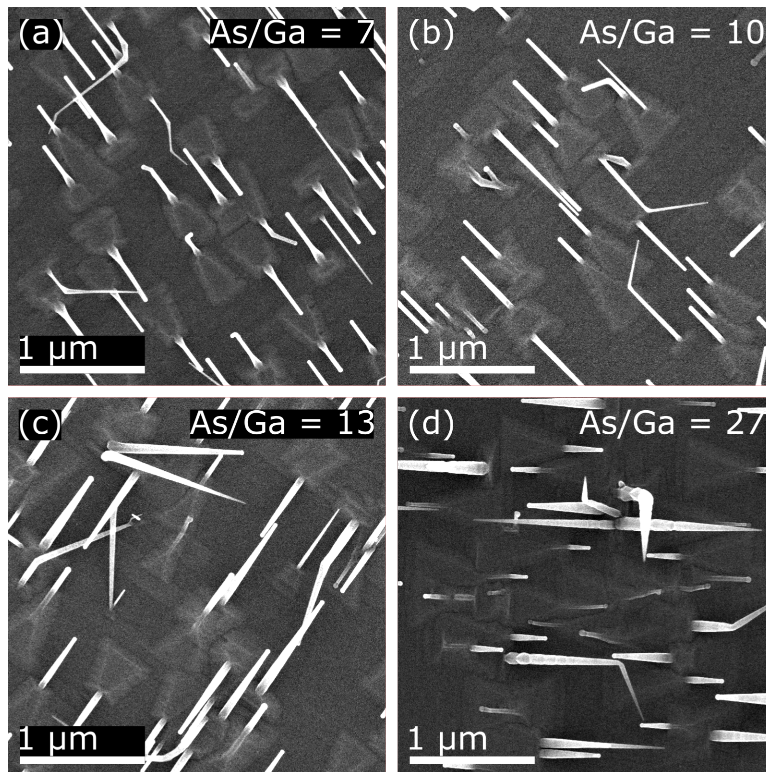

Figure 4.12: Top-view SEM images of Au seeded GaAsSb nanowires grown with As/Ga ratios of (a) 7 (b) 10 (c) 13 (d) 27. For all samples shown, the values T = 450°C and Sb/Ga = 2 were used.

4.3.2 AgAu seeded GaAsSb

The temperature series for AgAu seeded GaAsSb wires is shown in Figure 4.13. For low temperatures, Figure 4.13(a), significant particle splitting is observed, and most wires grown are short and thin curly wires. Some big particles nucleate, however, preferentially in one of the <111> directions, and a few shorter ones in the perpendicular <111> direction or some type of higher order direction (higher contrast in Figure 4.13). Going up in temperature, Figure 4.13(b), gives a higher yield of both of these types of wires. Going up to even higher temperatures, as shown in Figure 4.13(c), the morphology of the wires changes drastically, going from regular, thin wires with no significant tapering to shark teeth-like wires. These wires seem to be thin in one of the radial directions, while being significantly tapered in the other, making them appear as thin triangular flakes growing in one of the <111> directions. This was however not verified. For the highest temperatures, Figure 4.13(d), no growth is observed.

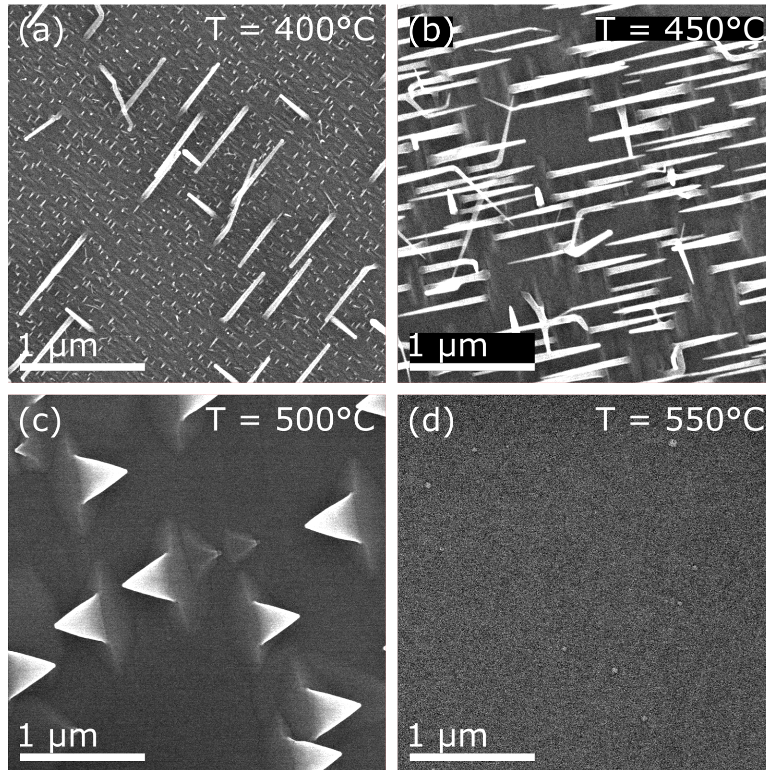

Figure 4.13: Top-view SEM images of AgAu seeded GaAsSb nanowires grown at (a) 400°C (b) 450°C (c) 500°C (d) 550°C. For all samples shown, the values As/Ga = 13 and Sb/Ga = 2 were used.

Figure 4.14 shows the effect of different As/Ga ratios on AgAu seeded GaAsSb nanowires. For low As/Ga ratios, Figure 4.14(a), the yield is low, and many wires are kinked from the preferred <111> nucleation direction. The yield is increased for intermediate As/Ga ratios, Figure 4.14(b), and some wires now also grow in the other <111> direction (or a higher order direction, as is implied by the contrast). This does not change much for even higher As/Ga ratios, Figure 4.14(c). However, strange facets are observed at the base of many of the wires grown under higher As/Ga ratios, Figure 4.14(d).

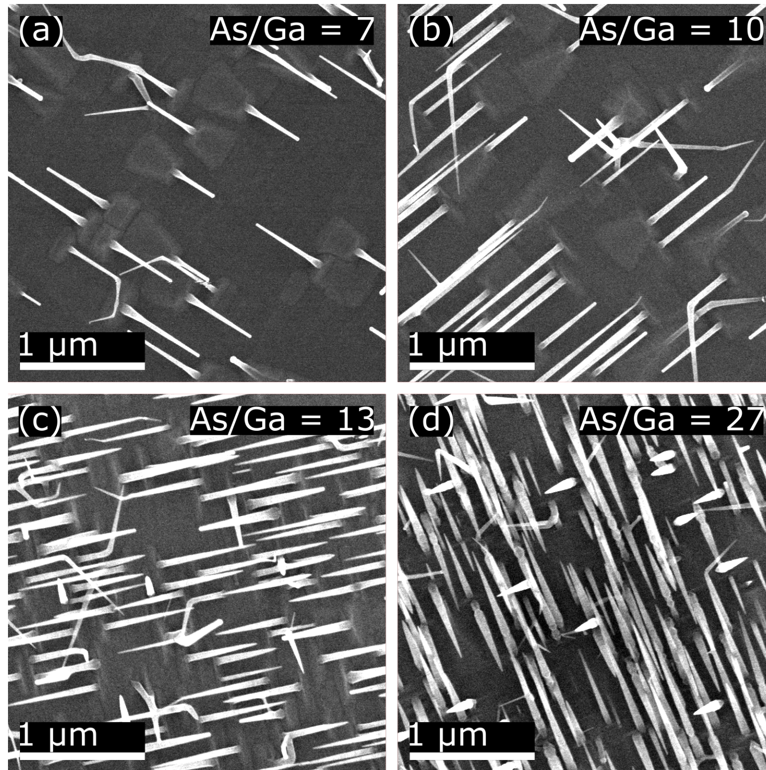

Figure 4.14: Top-view SEM images of AgAu seeded GaAsSb nanowires grown with As/Ga ratios of (a) 7 (b) 10 (c) 13 (d) 27. For all samples shown, the values T = 450°C and Sb/Ga = 2 were used.

4.3.3 Ag seeded GaAsSb

GaAsSb wires grown from Ag seed particles for different temperatures are shown in Figure 4.15. For low temperatures, Figure 4.15(a), the particle splitting is significant, and most of the wires that nucleate are either short and thin or curly. The short nanowires seem to prefer growth in one of the <111> directions. This preferred direction is kept for higher temperatures, Figure 4.15(b), where a high yield of slightly tapered wires is obtained. For even higher temperatures, Figure 4.15(c), the yield is very low, but the wires still grow in the same <111> direction, with a much higher degree of tapering, and no growth is observed if the temperature is increased even further, as shown in Figure 4.15(d).

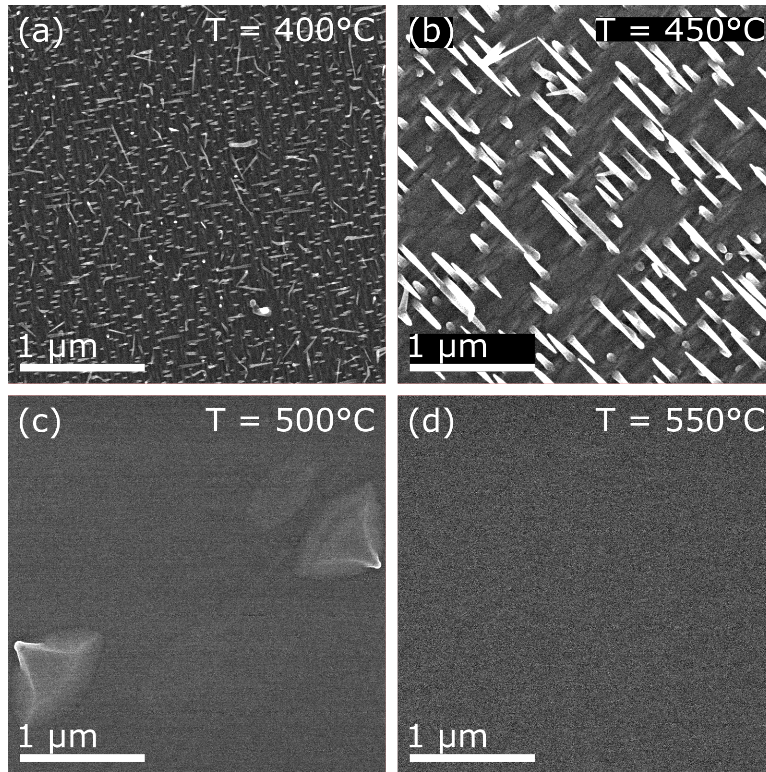

Figure 4.15: Top-view SEM images of Ag seeded GaAsSb nanowires grown at (a) 400°C (b) 450°C (c) 500°C (d) 550°C. For all samples shown, the values As/Ga = 13 and Sb/Ga = 2 were used.

GaAsSb nanowires grown with varying As/Ga ratios from Ag particles are shown in Figure 4.16. A very low yield of wires, with no apparent preferred growth direction, is shown in Figure 4.16 (a). Increasing the As/Ga ratio first seems to remove all growth, as shown in Figure 4.16(b), but then promotes a high yield of <111> orientated wires, Figure 4.16(c). Even higher As/Ga ratios, Figure 4.16(d), stops the growth again. It seems that the growth window for the high yield sample is narrow.

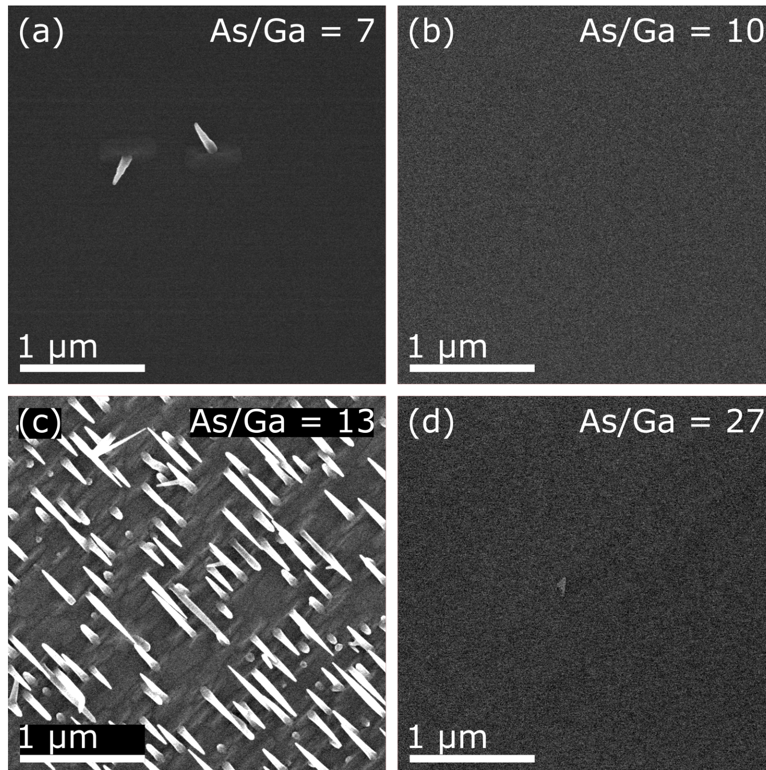

Figure 4.16: Top-view SEM images of Ag seeded GaAsSb nanowires grown with As/Ga ratios of (a) 7 (b) 10 (c) 13 (d) 27. For all samples shown, the values T = 450°C and Sb/In = 2 were used.

4.4 InAs nanowires

Figure 4.17 shows how the growth of Au seeded InAs wires changes with As/In ratio. Going from low to high As/In ratio there is no growth for the first sample, Figure 4.17(a), a high yield of [001] wires and also inclined and planar wires in Figure 4.17(b), and only planar and inclined in Figure 4.17(c). In Figure 4.17(d) the nucleation only seems to give surface growth, and for Figure 4.17(e) no growth is observed. The sample shown in Figure 4.17(b) will be referred to as Sample 4.17(b).

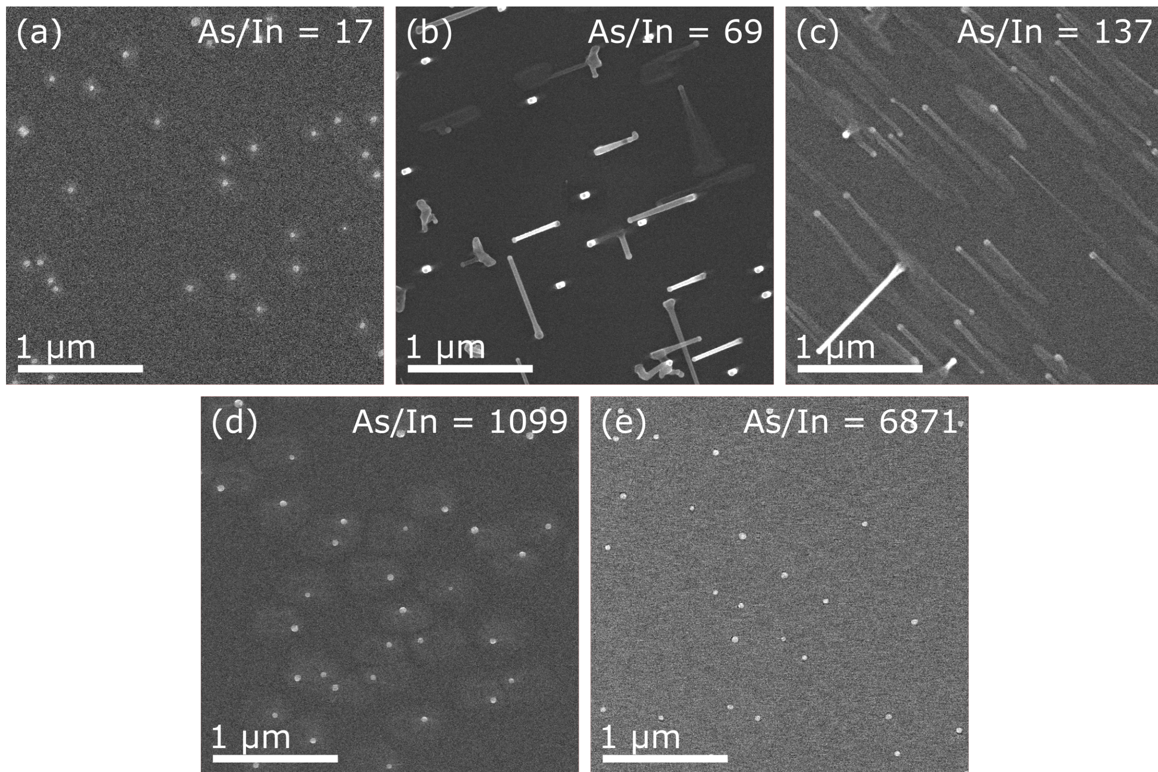

Figure 4.17: Top-view SEM images of Au seeded InAs nanowires grown with As/In ratios of (a) 17 (b) 69 (c) 137 (d) 1099 (e) 6871. For all samples shown, the temperature T = 375°C was used.

4.5 InAs stem and InAsSb wire

The results from the InAs stem + InAsSb nanowire growth runs are presented in Figure 4.18. It was during these growth runs that we discovered a few things that could be wrong with the reproducibility due to machine drift, so the parameters used for the runs are quite similar.

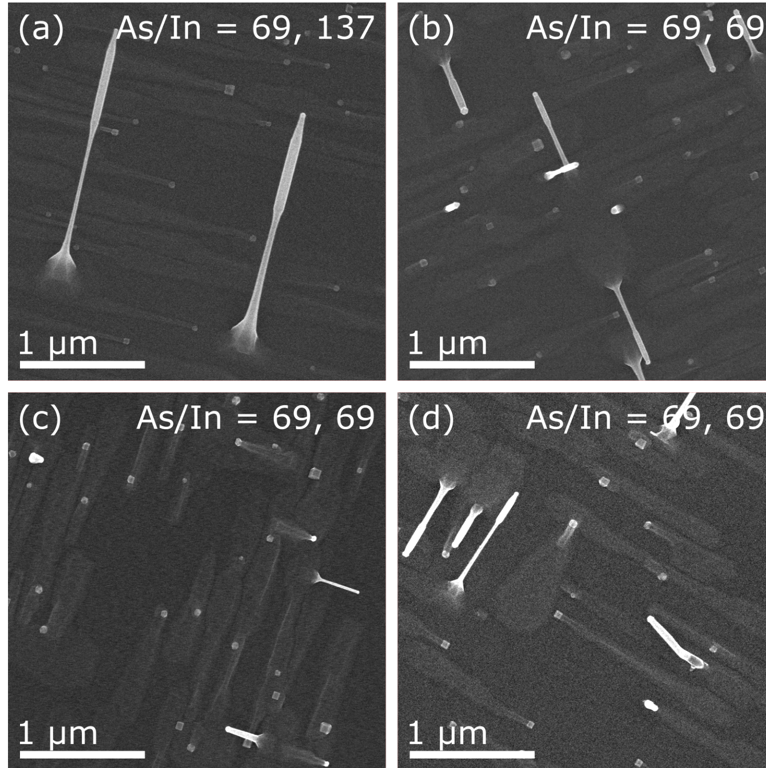

Figure 4.18: Samples of Au seeded InAsSb wires grown on InAs stems. Both sections of the wires were made in the same run. The values of As/In shown at the top represent the value used for the InAs stem and the InAsSb wire, respectively. T = 375°C and Sb/In ratio = 24 were used for all runs (with the Sb turned off for the stem growth, of course).

In Figure 4.18(a), the widening of the wire as the growth material used is switched from InAs to InAsSb is clear. However, most wires grow planarly and only a few of them grow as inclined wires. Very few vertical wires were found and they often kinked at the heterojunction between InAs and InAsSb. The low yield of vertically growing wires was unexpected, since the exact same growth conditions were used to get Sample 4.17(b), which had a really high yield of InAs stem-wires.

In Figure 4.18(b), a similar growth run was performed, but with a lower As/In ratio for the InAsSb part. The wires are shorter, but the results are similar. After this run, it was speculated whether the chamber actually got clean from the etch and cover process

employed, since the stems not growing vertically could be related to residual surfactant Sb in the chamber. So from this point on, the etch and cover was increased from 10 + 30 minutes to 30 + 60 minutes.

In Figure 4.18(c), the wires grown after a more substantial cleaning (and accidentally with slightly higher temperature) are shown. Otherwise the parameters are the same as Figure 4.18(b). The samples are very similar in their poor results, and the change in yield of inclined wires is probably due to the higher temperature. After this run it was discovered that the machine had drifted some in its temperature calibration over the last few weeks, and the set temperature therefore had to be lowered.

In Figure 4.18(d) wires grown after the better cleaning and under a more appropriate growth temperature, are shown. These look very similar to Figure 4.18(b), so it was concluded that the longer etch and cover did not do much for the reproducibility, and therefore also that the chamber got sufficiently clean during the shorter etch and cover (or, less likely, not clean enough after the long etch and cover). The long etch and cover was still kept for subsequent runs, just to be sure that the reactor was clean.

4.6 Reproduce the best sample

After discovering that the actual values of the temperature had drifted since the first growth runs, a few attempts were made to recreate Sample 4.2(b) (T = 375 °C, As/In ratio = 137 and Sb/In ratio = 24). The results are shown in Figure 4.19.

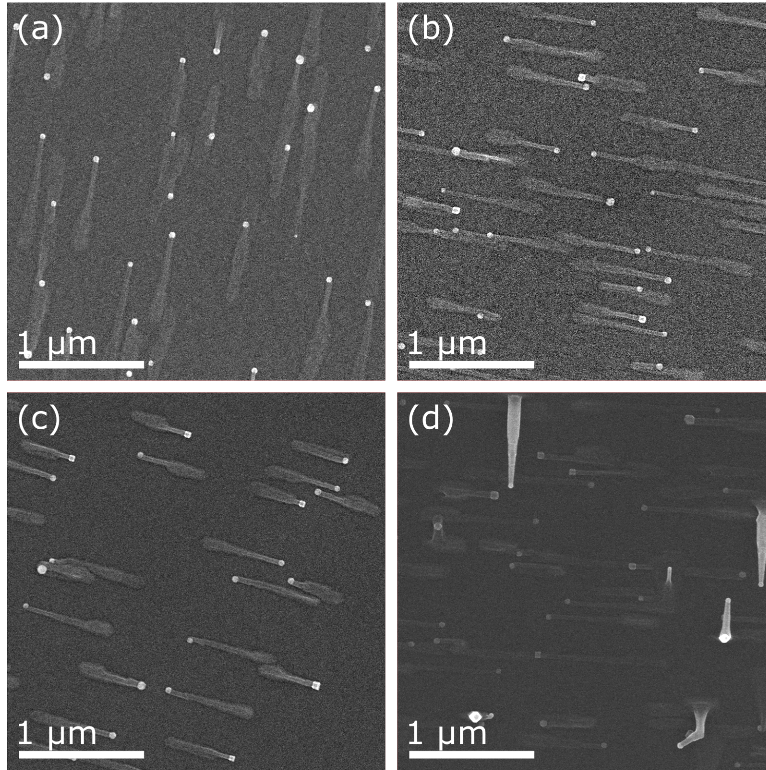

Figure 4.19: Different attempts to recreate Sample 4.2(b) are shown in (a)-(d). The actual values used are described in the text.

Figure 4.19(a) shows a sample where the exact same parameters were used to try to recreate Sample 4.2(b). Evidently, most wires found grew planarly, and no vertical wires were seen. Figure 4.19(b) shows a sample where the drift in temperature was corrected for. This sample did not show any vertical wires either; just planar ones. Around this time, problems with the stability of the Sb source were found. Therefore, the sample shown in Figure 4.19(c) has both a corrected temperature and a higher TMSb flow, giving a final Sb/In ratio of 34. Even so, the sample contained no vertical wires, only planar.

In our group it was discovered how to change the flows to reproduce old growth runs, so the same formula was tested in the sample shown in Figure 4.19(d). This sample was temperature corrected, with a higher flow of TMIn (18), As/In ratio of 137 and Sb/In ratio of 34. This time there were both vertical, inclined and planar wires. The most interesting part of the vertical wires was that the cross section differed from what was observed before, so the actual growth conditions must have changed. This sample will be referred to as Sample 4.19(d), and the vertical wires are discussed further in Section 5.2.1.

4.7 Annealing tests

Even though vertical growth was achieved in Section 4.6 for Sample 4.19(d), the yield was still low. One parameter that had not been explored was the annealing step. One run of only the annealing step was performed. These samples are shown in Figure 4.20.

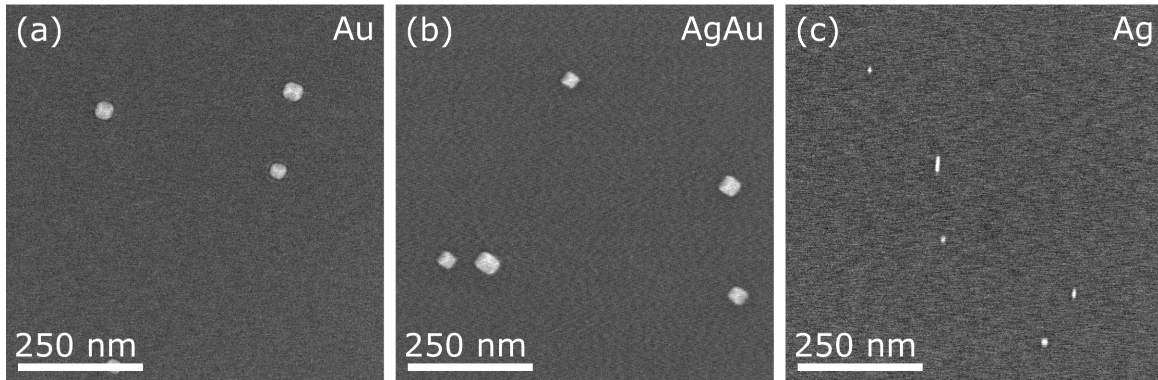

Figure 4.20: Top-view SEM micrographs of the different particle types, indicated in the top right corner, on InAs substrates after the annealing step only.

There are significant differences between the behaviour of the different particle types. The Au particles in Figure 4.20(a) look slightly elongated, with some clear facets (discussed further in Section 5.2.1). The AgAu particles, Figure 4.20(b), had a more square-like shape after annealing, while the Ag particles, Figure 4.20(c), took the rod-like shape observed in earlier experiments. The Ag particles are also very small, which suggests substantial particle splitting.

A few runs were also performed where the annealing step was completely skipped. Otherwise the parameters were the same as Sample 4.2(b) (T = 375 °C, As/In ratio = 137 and Sb/In ratio = 24), but with temperature correction. The results from these experiments are shown in Figure 4.21.

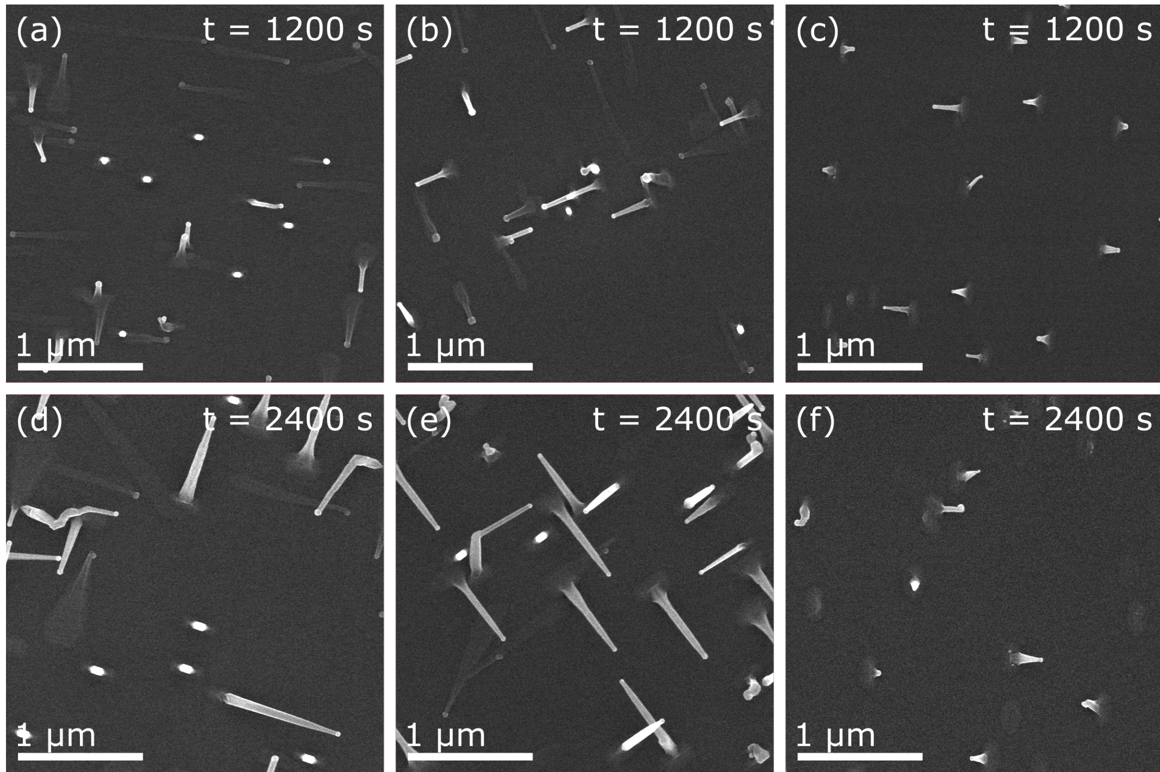

Figure 4.21: Top-view SEM micrographs of InAsSb wires grown without the annealing step. In the top right corner, the growth time is indicated. (a) and (d) were grown from Au particles, (b) and (e) from AgAu particles, and (c) and (f) from Ag particles.

The top row shows the samples grown with regular growth time, while the bottom row shows the samples grown with double growth time, i.e. 2400 s. In Figure 4.21(a), InAsSb wires are grown from Au particles. As can be seen, there exists curly, planar (both types), inclined (both types) and vertical wires. The yield of vertical wires is high, with lengths of about 300 nm, which was revealed by tilted SEM images (not shown here). In Figure 4.21(d), where the double growth time was used, however, the vertical wires grew to about 600 nm. These wires also had a more defined cross section. These two samples were in general very similar, except of course the length of the wires.

In Figure 4.21(b) and (e), the wires grown from AgAu particles are shown. Both of these samples had curly, planar (both types), inclined (both types) and vertical wires. Similarly to the Au samples, as the growth time was increased, the wires grew longer, but otherwise remained the same. The yield of vertical wires was however lower than for the samples grown with Au particles.

Figure 4.21(c) and (f) show the wires grown from Ag particles. These samples had mainly one of the inclined nanowire-types, as well as curly wires. Curiously, the wire length did

not seem to change with growth time, as the samples in Figure 4.21(c) and (f) are similar in appearance. These were the first samples to give any interesting growth of InAsSb wires from Ag, so it seems like the Ag particles can not handle the annealing step very well.

Due to lack of time, only the sample shown in Figure 4.21(d) was chosen for further investigation. This was due to the high yield of good looking wires growing in the [001] direction. This sample will be referred to as Sample 4.21(d). On this sample TEM was performed, to investigate the composition of the wires (and particles), crystal structure and presence of ordering. It turned out that the wires grew with a ZB structure, but that no ordering was present in the wires analysed. The composition was difficult to investigate due to overlap between the signal from In and Sb. Sample 4.21(d), and its TEM and EDX analysis, is discussed more thoroughly in Section 5.2 and Section 5.6.

5 Discussion

In this section the results presented in Section 4 will be discussed more in depth. First, a summary of the growth observed for the particle types and materials, will be presented. A large part of the further discussion will be regarding the best samples of InAsSb wires that were observed. Then other interesting wire types, as well as the results from the growth runs performed after the growth series will be discussed briefly. Finally, the TEM and EDX analysis will be presented and discussed more clearly.

5.1 General growth characteristics of the particle types

5.1.1 InAsSb samples

Common characteristics for the Au samples is that each individual sample is quite restrictive in the types of wires observed, see Figures 4.2, 4.3 and 4.4. Every sample mainly shows one to three different wire types, where one type usually is the thin, planar wire indicated by "2" in Figure 4.1, and the other one or two are wire types growing out of the surface. Exceptions from this is found at high temperatures (Figure 4.2 (d)), where no nanowire growth is observed, and low/high As flows (Figure 4.3 (a)(e)), where the growth only gives small islands under the particles. In transition steps towards these values, some samples show almost exclusively the thin, planar wires. Good, high yield, growth of nanowires in the [001] direction is not found for big parameter windows, but was still found in a few samples. These are discussed in Section 5.2.

The restrictiveness of the Au samples is not observed when switching to AgAu as seed particle. These samples often contain most or all of the observed nanowire types, see Figures 4.5, 4.6 and 4.7. Whenever growth occurred, there were curly wires (7 in Figure 4.1) or wires growing in strange directions, seemingly without preference. For certain samples (Figure 4.5 (b), 4.6 (d), etc.), something similar to vertical [001] wires was observed, although they were mostly short. It is unclear whether these wires would continue to grow in the [001] direction given the chance, or if they would develop into curly wires later on. One type of wire that is quite dominant in the AgAu samples is the type "3" tapered planar wire shown in Figure 4.1. The nucleation of the planar wires is discussed further in Section 5.3.

The Ag samples have been disappointing in terms of growth; almost no samples had any real growing wires, see Figures 4.8, 4.9 and 4.10. It seems that the Ag particles instead like to line up along the cleavage edges, and form nanorods without catalysing any growth. The reason for this could be that Ag reacts more to the surfactant effect Sb has, meaning that the particles easily become flat or elongates, or that the state of the particle differs from the other particle types. It could be that the Ag particles turn liquid at a lower temperature and that the droplet become flat due to the presence of Sb. Since the particles left on the surface seem to be few as well, most particles are probably overgrown by the surface layer. The formation of the nanorods is still a mystery, however.

5.1.2 GaAsSb samples

The Au samples are found in Figures 4.11 and 4.12. The Au particles promoted mainly growth of inclined <111> nanowires, indicated by type 4 or 5 in Figure 4.1, although many wires kink later on. The symmetry is twofold, i.e. either <111> A or <111> B is preferred, so only one of the types appears on any sample. For high temperatures, Figure 4.11 (c), the growth is mainly planar, where the planar wires grow parallel to the inclined. For low temperatures, Figure 4.11 (a), some wires seem to be of type ”6” in Figure 4.1, since they have much higher contrast and appear short.

The wires catalysed by AgAu particles, shown in Figures 4.13 and 4.14, also seemed to prefer to nucleate in one of the <111> directions mainly, and most often had type 6, highly inclined wires growing in the perpendicular direction. For low temperatures, Figure 4.13 (a), there was much particle splitting, and among the wire types discussed above, there were also very small wires growing in the same directions. For high temperatures, Figure 4.13 (c), the wires kept the <111> growth, but took the appearance of triangles instead of rods. The appearance of these triangles seem to be as flakes, due to the contrast observed.

Ag catalysed GaAsSb wires had much better growth than their InAsSb counterpart; most samples showed some growth, as seen in Figures 4.15 and 4.16. The absolute best Ag sample had mainly growth in one of the <111> directions, with nice, somewhat tapered, wires, shown in Figure 4.15 (b). This directionality of the wires was kept for low temperatures, but the length diminished a lot, while for high temperatures, the wires became tapered and few. It seems like the window for good GaAs V/III ratio is small, since the growth using any other values than the best resulted in poor growth.

In terms of growth in the [001] direction, no good GaAsSb samples were found. The yield of actual wires has, however, been higher for the GaAsSb samples, and a few samples, namely the ones seen in Figure 4.13(c) and Figure 4.15(b), would be interesting to investigate further.

5.2 The Good Samples

After thoroughly analysing all produced samples in the SEM it became evident that the InAsSb samples grown from Au produced the best results, where a few individual samples showed a high yield of sufficiently long, [001] oriented wires. The first one that was found, Sample 4.2(b), was grown with the parameters T = 375 °C, InAs V/III ratio of 137 and InSb V/III ratio of 24. This sample is shown more in-depth in Figure 5.1 below.

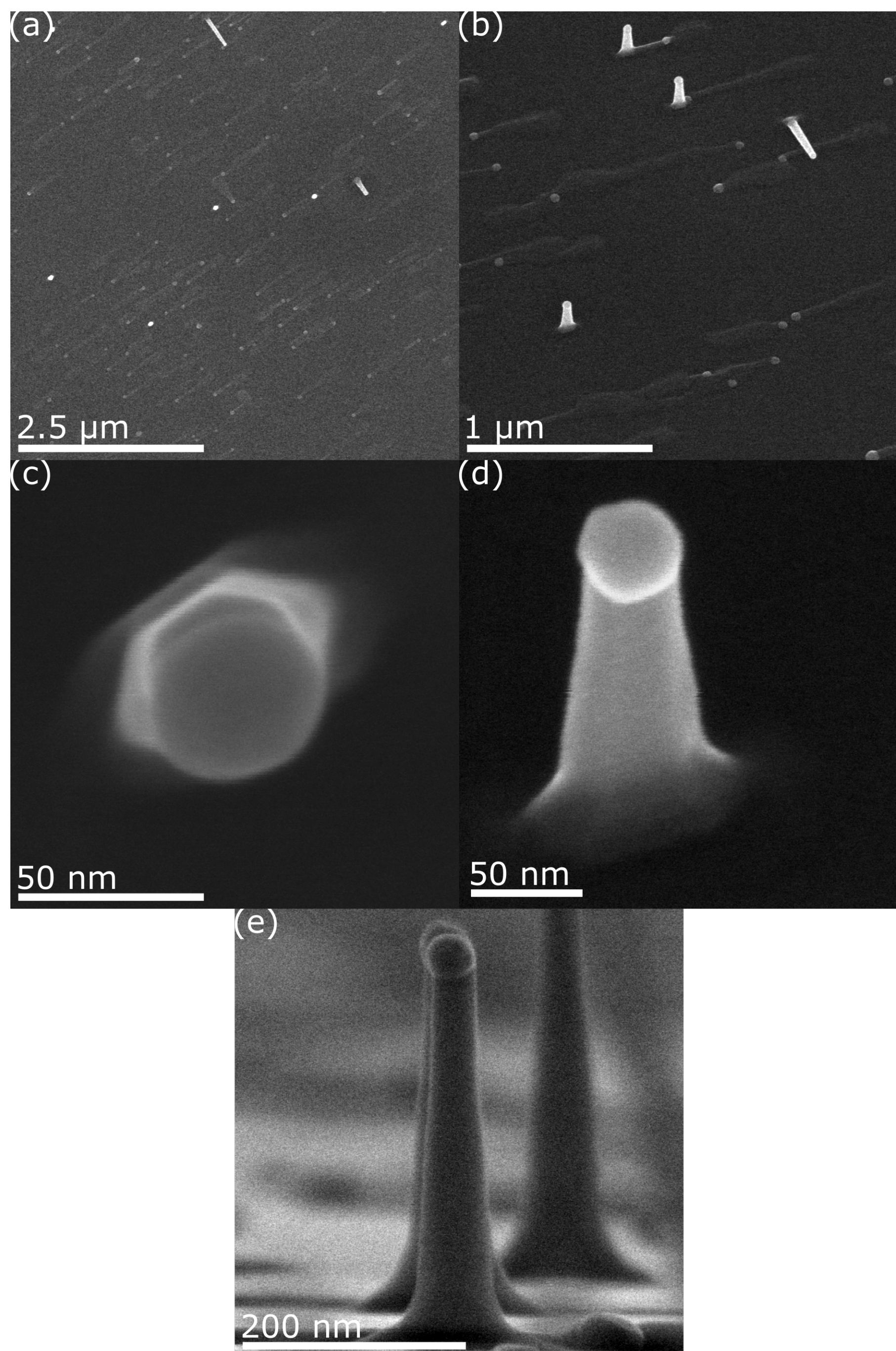

Figure 5.1: These micrographs show Sample 4.2(b). (a) shows an overview, where the different wire types can be observed. (b) shows a 30° tilted view. In (c) a zoomed in micrograph of a single wire is shown from above. (d) shows a zoomed in micrograph of a wire at a 30 ° angle, while (e) shows a couple of wires viewed from the side along one of the side facets of the substrate.

As already discussed, we can see in Figure 5.1(a) that most of the wires grow as planar, type 2 wires in Figure 4.1, while some are vertical, a few are inclined [111], and one is growing as the tapered planar type 3 wire. By analysing the growth direction of a few hundred wires on the sample, it was determined that the yield of vertically growing wires was about 10%.

Another good sample was Sample 4.19(d), where all the flows were increased and the temperature calibrated for. This sample is shown here in Figure 5.2. As was stated earlier, the most interesting thing about this sample is the cross section, which differs from all other samples where vertical wires were seen. The yield was however very low: about 1 % of the wires were vertical. These wires are discussed further in Section 5.2.1.

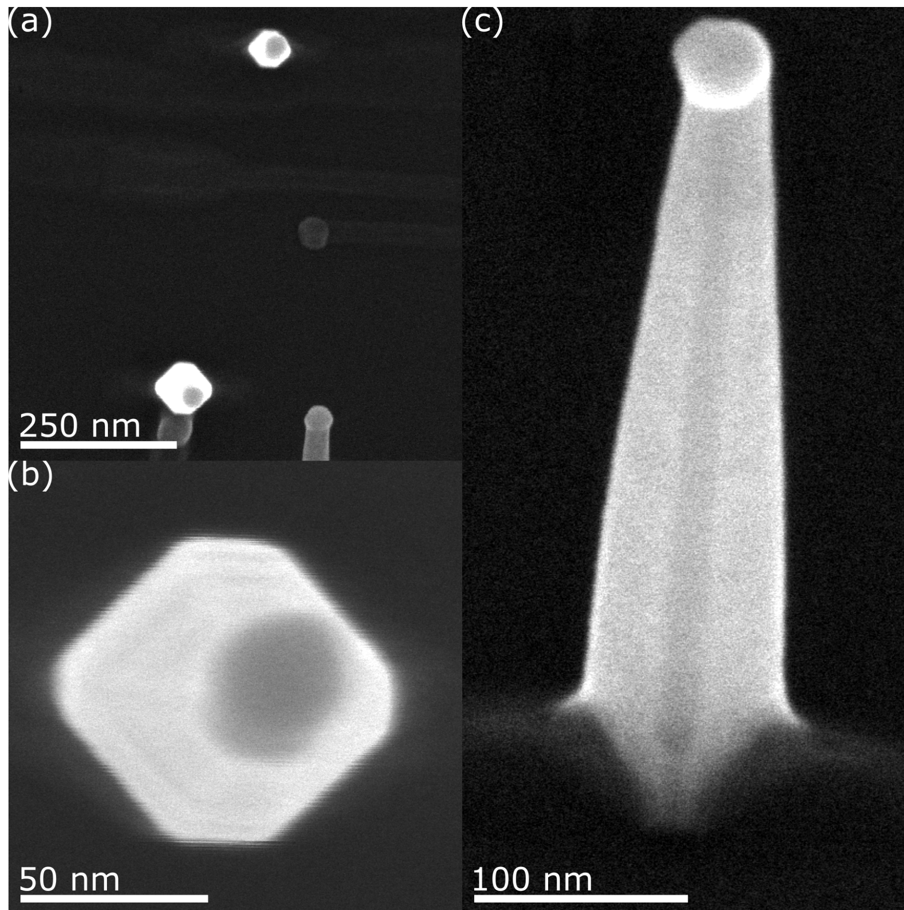

Figure 5.2: The SEM micrographs show Sample 4.19(d), where the growth temperature was calibrated and all flows were increased. (a) shows a top view of two vertical wires, while (b) is a zoomed in image. (c) shows a tilted 30° image of a wire.

Finally, the sample with the highest yield of long wires that grew in the [001] direction is Sample 4.21(d), grown from Au particles without annealing and with double growth time. This sample is shown in Figure 5.3. The wires in this sample had the same common cross section as most other vertical wires found, and the yield was estimated to be about 16 %. The wires from this sample was ultimately analysed by TEM and EDX, and will be discussed further in Section 5.6.

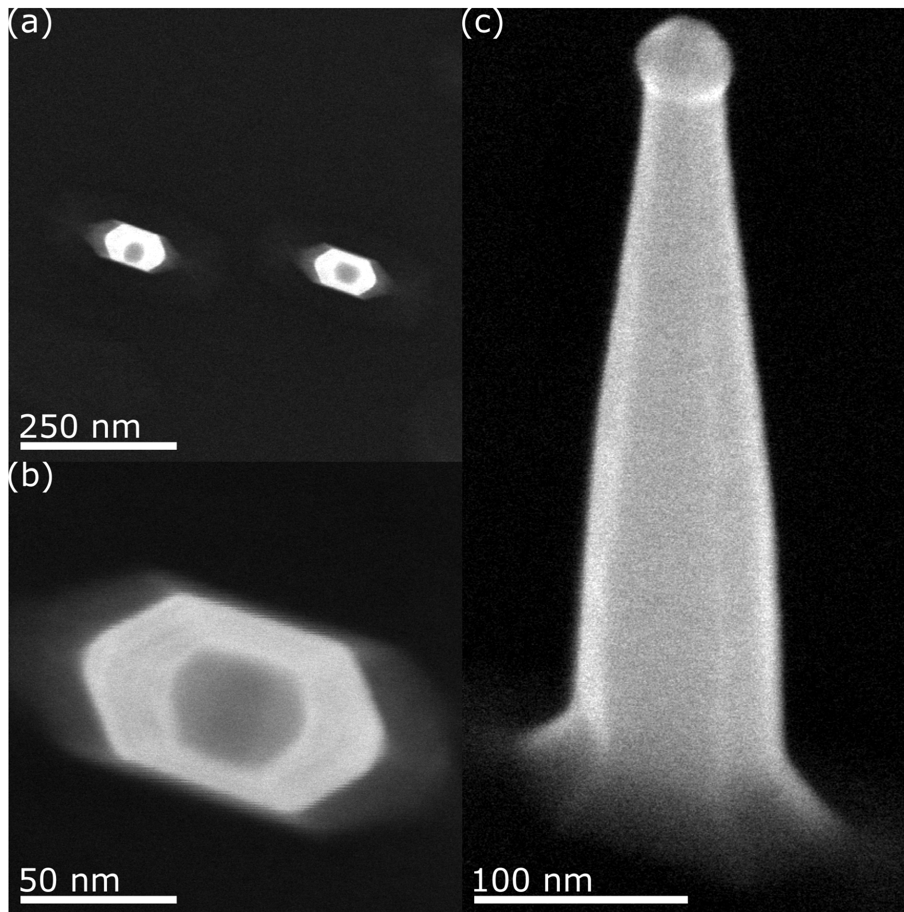

Figure 5.3: The SEM micrographs show Sample 4.21(d), where the growth temperature was calibrated and no annealing step was performed. (a) shows a top view of two vertical wires, while (b) is a zoomed in image. (c) shows a tilted 30° image of a wire.

5.2.1 [001] Nanowire Morphology

The cross section of vertical nanowires grown on (001) oriented substrates is expected to be square-like [9]. However, as the nanowires were analysed in the SEM, a different cross section was discovered. The square like shape was not immediately found in any of the (001) oriented nanowires grown from Au seed particles. What was found, however, was a type of elongated hexagonal shape, as seen in Figure 5.1(c) for Sample 4.2(b) and an

octagonal shape as seen in Figure 5.2(b) for Sample 4.19(d). The hexagonal shape will be discussed firstly. The angles at the endpoints in the elongated directions were measured for several wires, and are thought to be 90°. The exact angle is difficult to know due to resolution limits, but it seems like a safe assumption. Elongated hexagons were fitted to the nanowires to see the match. A micrograph with fitted hexagons is shown in Figure 5.4. A wire without the hexagons is shown in Figure 5.1(c).

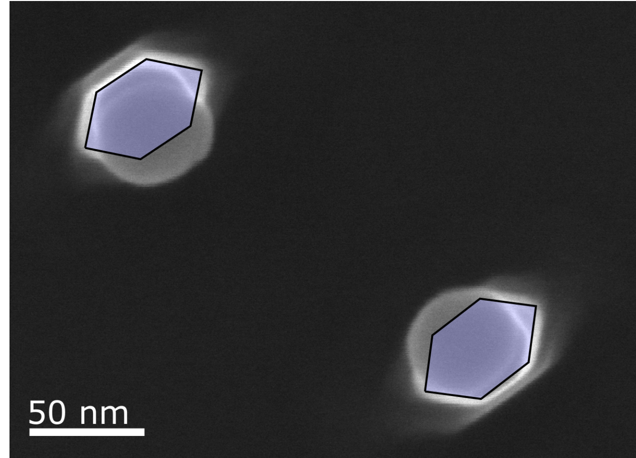

Figure 5.4: Nanowires growing in [001], with elongated hexagons fitted to match their cross section.

By comparing the orientation of the nanowires to the cleavage edges of the substrate, the facets of the hexagons could be revealed. Figure 5.5 shows one of the fitted hexagons with added angles and miller indices for the crystal planes building up the shape.

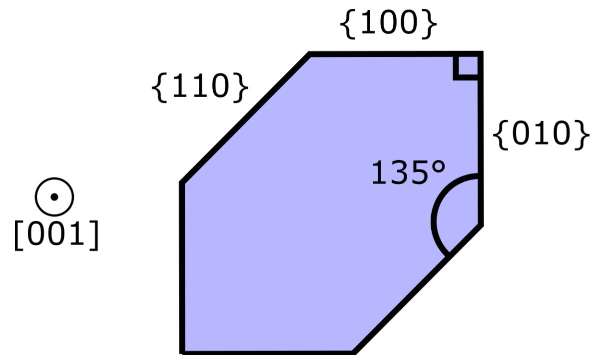

Figure 5.5: A schematic of the hexagonal cross section of a nanowire, with added miller indices for the facets.

The SEM was used to view the wires from another angle, along one of the side facets. This is shown in Figure 5.1(e). What can be noticed is that the wires seem to be slightly tapered, and that the bases of the wires are wide. This could mean that the actual cross

section of the wires is more square-like, but with significant tapering at the base, as suggested by the wires shown in Figure 5.1(e).

During the efforts to reproduce Sample 4.2(b), another type of vertical nanowire was found. This was Sample 4.19(d) where the flows were increased and the temperature was calibrated, shown in Figure 5.2. The cross section of these wires is shown below in Figure 5.6.

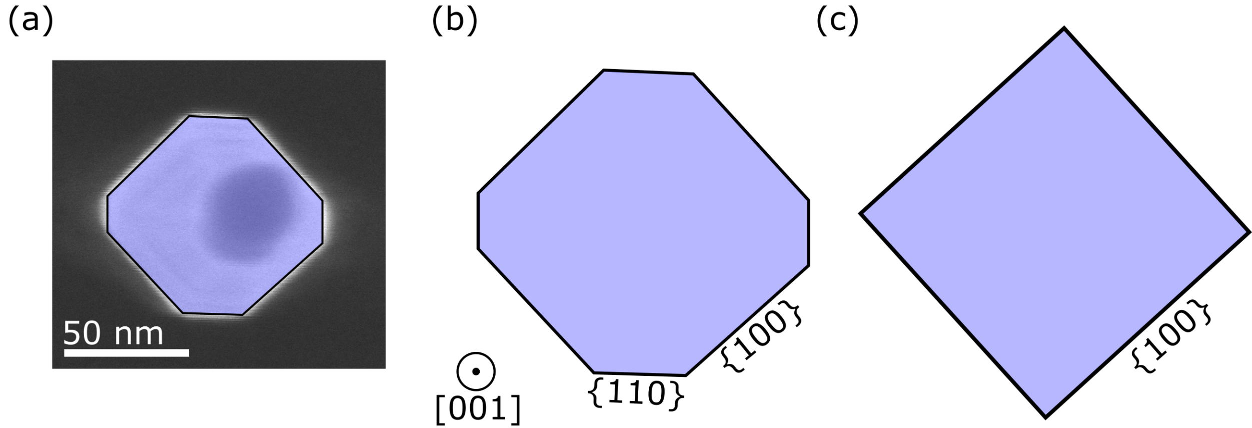

Figure 5.6: The more square-like or octagonal cross section of the wires from Sample 4.19(d). (a) shows a top-view SEM micrograph, with an added octagonal shape fitted to show the cross section. (b) shows the octagon with added miller indices to show the facets, while (c) shows the expected shape if the growth would continue.

In Figure 5.6(b) an octagon can be seen, representing the cross section of the wire imaged in Figure 5.6(a). The miller indices were added since the facets of the wire could be compared and related to the cleavage edges of the samples. If this octagon is compared to the hexagonal shape shown in Figure 5.5, we can see that other facets are stable now; the longer facets for the hexagon were of {110}, while the longer facets for the octagon are {100}. This means that in this new cross section, the {110} facets grow the fastest, and if growth would continue, the cross section shown in Figure 5.6(c) is expected, where the {110} facets have completely grown away. This is more similar to what other groups have found for wires growing in the [001] direction on (001) oriented substrates. The side facets of the wires can be seen clearly for Sample 4.21(d) (which also has the hexagonal cross section) in Figure 5.3(c) and for Sample 4.19(d) in Figure 5.2(c). For Sample 4.21(d) (Figure 5.3(c)) one of the side facets is very wide at the base, but seems to become thinner towards the particle. This is the {110} facet. This is however not seen for Sample 4.19(d) (Figure 5.2(c)), where the {110} facet instead seems to remain similar in width along the wire.

5.2.2 Growth initiation

The formation of the hexagonal shape of the vertical wires in most samples could be related to the growth initiation. The initiation of growth could be helped due to etching of

the substrate by the particle, as discussed in Section 2.12. As the sample is annealed, and as material is flown in during early stages of growth, certain facets will be etched quicker than others. This depends on their respective surface energies, where facets with higher surface energies are etched (or grown during growth) quicker than surfaces with lower energies [40]. In Section 2.12, we stated that it was the {111} facets that were etched, which seems possible in our case as well by comparing the orientation of the hexagons to the cleavage edges. The equilibrium crystal shape of InAs crystals suggests that the In terminated (111)A facets have higher surface energies than the As terminated (111)B facets, and will therefore etch the fastest [41]. We assume here that this is still the case when Au is present. This means that a trench with larger (111)B facets and smaller (111)A facets could form.

It has also been shown that annealing can enable the particles to form longer trenches on (001) [24]. One could also think that a similar trench formation occurs as the substrates are heated to the growth temperature and as the particle is loaded with material. From this the formation of the hexagonal lower part of the wires can be imagined to form, before the wires change to a more square-like cross section. A schematic of a trench with marked facets is shown in Figure 5.7(a).

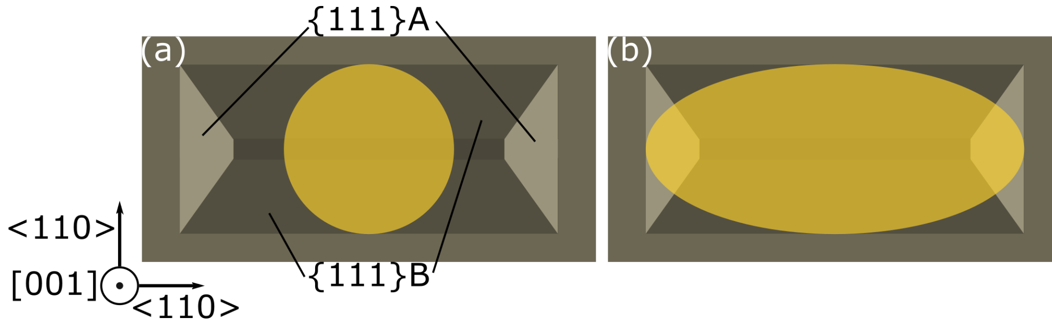

Figure 5.7: A schematic showing a possible explanation of the formation of the elongated base of the [001] wires, through the formation of a trench. In (a) the suggested facets of the trench are marked. It is unclear whether the particle diffuses in the trench or if it stretches out, as shown in (b) during the annealing process, but it seems that (b) is the most probable case.

Now, the question is whether the trenches form as particles diffuse on the surface along certain directions, absorbing material, or if the particles actually are elongated as shown in Figure 5.7(b). If the particles were to form trenches by diffusion, many particles would probably end up at the end of their trench, and not diffuse back. Since the vertical wires shown in Figure 5.1 seem to be symmetrical, where the base is spread out equally around the centre of the wire, it seems most likely that the particle originates from the middle of the trench. Therefore, the most probable explanation for the formation of the hexagonal base, is that the particle flattens and spreads along a favourable direction on the substrate, forming a trench, as shown in Figure 5.7 (b). From there the particle might take a more spherical shape as the growth proceeds in the [001] direction, but during that transition, the wire will still grow. This could give a more tapered cross section at the

base. This procedure is schematically shown in Figure 5.8. The widening of the wires could also be due to lateral overgrowth later in the growth process.

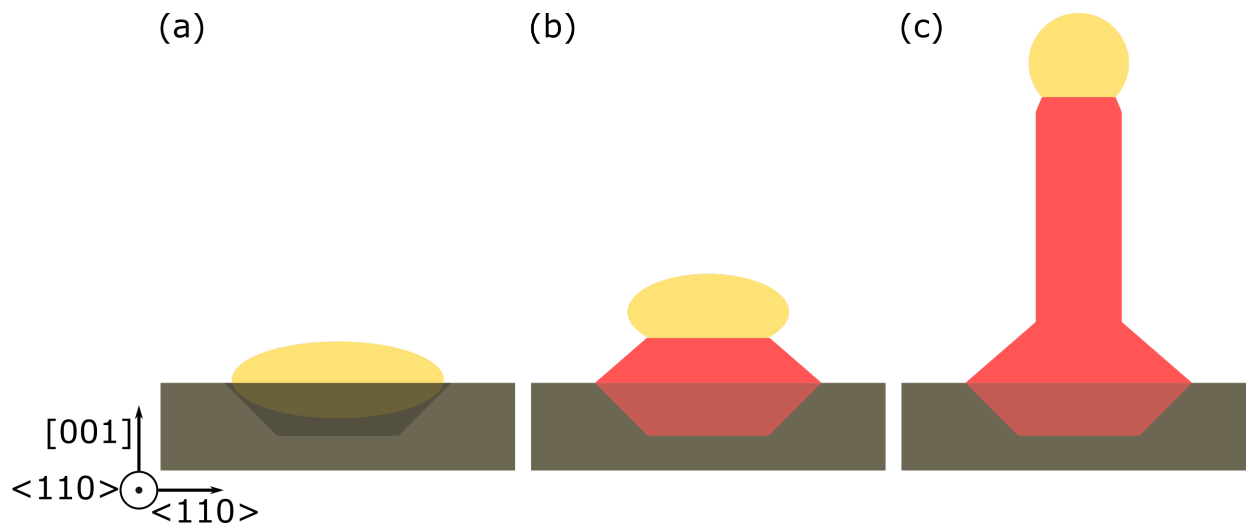

Figure 5.8: A schematic showing how growth in the trenches possibly formed by the particles could proceed. (a) shows the particle in the trench, as viewed along one of the side facets of the substrate. (b) shows the wire when it has grown a bit, and the particle has proceeded to change into a more spherical shape. In (c) the wire is fully grown, and the particle has the shape of a spherical cap.

To verify the theories surrounding the initial stages of growth, the annealing experiment was performed, where the particles were removed from the reactor after the annealing step, as shown in Figure 4.20. As the Au particles were analysed, a slight elongation of the particles along one of the cleavage edges was discovered, giving them a more rectangular shape. The particles before and after annealing are shown in Figure 5.9

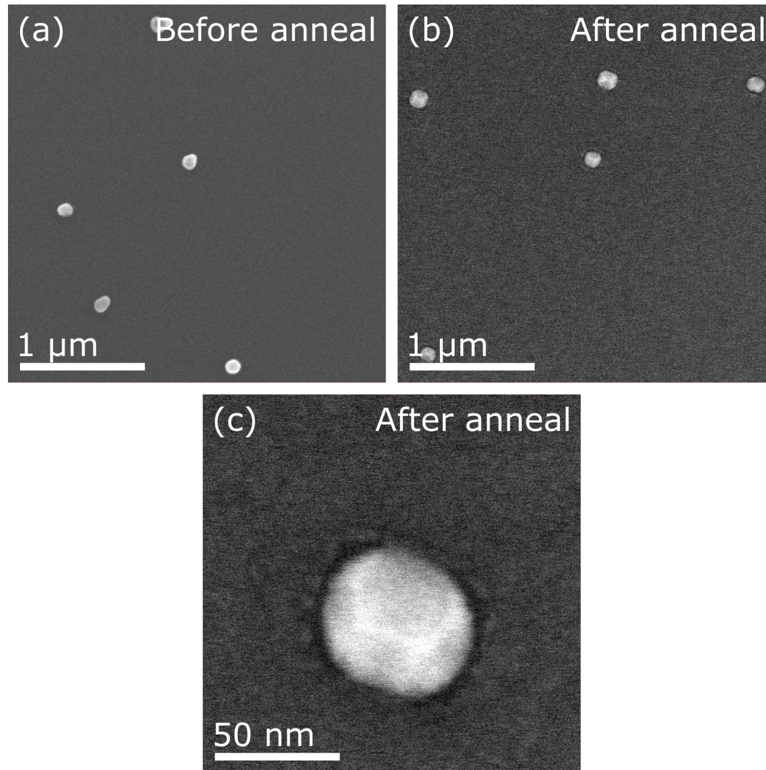

Figure 5.9: Top-view SEM micrographs of Au particles before (a) and after (b) the annealing step are shown. After the annealing, the particles look more similar and rectangular in shape. (c) shows a zoomed in image of a particle after annealing. Facets are faintly visible on the particle, and the surrounding shadow suggests that it has alloyed with the substrate.

The particles before annealing, Figure 5.9(a), were irregular in shape, while after annealing, Figure 5.9(b), most of them are slightly rectangular. If the zoomed in image, Figure 5.9(c) is studied, the faint facets of the particle can be seen. What can also be seen is the dark pits around the particle, which suggests alloying with the underlying substrate. It therefore seems that the cause of the hexagonal cross section is more likely to be due to the particle widening in trenches, rather than diffusion.

As was stated earlier, the hexagonal base of the vertical nanowires is also found in Sample 4.21(d), which was grown without the annealing step. This does not discard the theory of trenches and alloying, since the particles probably have time to alloy somewhat with the substrate at the growth temperature, before growth commences. It is however possible that the trenches formed without the annealing step are more shallow, leaving a big [001] facet at the bottom of the pit. This could be a possible explanation for the higher yield of [001] wires in Sample 4.21(d), compared to Sample 4.2(b).

A possible explanation to the octagonal (more square-like) cross section of the wires grown in Sample 4.19(d) is that the etching of both <111>A and <111>B is equally favourable for the new growth parameters. Even if the pits formed during the annealing step are rectangular, the particles have time to alloy with the substrate during the early stages of growth as well, when material starts to pump in. The pits could then change shape, allowing for a more symmetrical cross section.

5.3 The Planar wires

In most samples, there were planar wires growing along the surface. These come in two shapes; triangular wires, and regular thin wires, as was discussed in Section 4.1 and Figure 4.1. This indicates that the radial growth of the former wires is much larger than for the latter. What is often observed is that these wires lie perpendicular to each other, and both individual types have two-fold symmetry. It is commonly known that the (111)A facets in III-V semiconductor wires grow quicker than (111)B facets due to their higher surface energy. The increased growth on (111)A facets can, however, make them disappear, which is why (111)B facets are observed more often. So one reason for the occurrence of the "christmas tree"-like triangular wires could be that they have (111)A surfaces on their sides, that grow out without disappearing. The reason for the thin wires to then remain thin would be that their sides have (111)B facets, that do not grow out as much. It should be noted that thorough analysis of these wires was difficult, and not a top priority, so it is possible that some other favourable facet is the cause of the widening of the "christmas tree"-like wires. Due to the tapering, the side facets are probably not pure (111)A, but some higher order direction.

When analysing the thin planar wires in the SEM, viewed along one of the side facets, the interface between the particle and the wire was revealed. It seems that the facet is slightly sloped, and could be an (111)A facet. Since the "christmas tree" wires are perpendicular to the thin planar wires, this could mean that they nucleate on the (111)B facet. This would mean that the nucleation event happens in an inclined upwards direction, but the wire still does not take off. It therefore grows planarly, along the <110> directions instead. A proposal of how the "christmas tree"-like wires grow is shown in Figure 5.10. The nucleation on 111 facets but growth in <110> has been observed and described before, for self-seeded InAsSb wires growing on Si(001) [42].

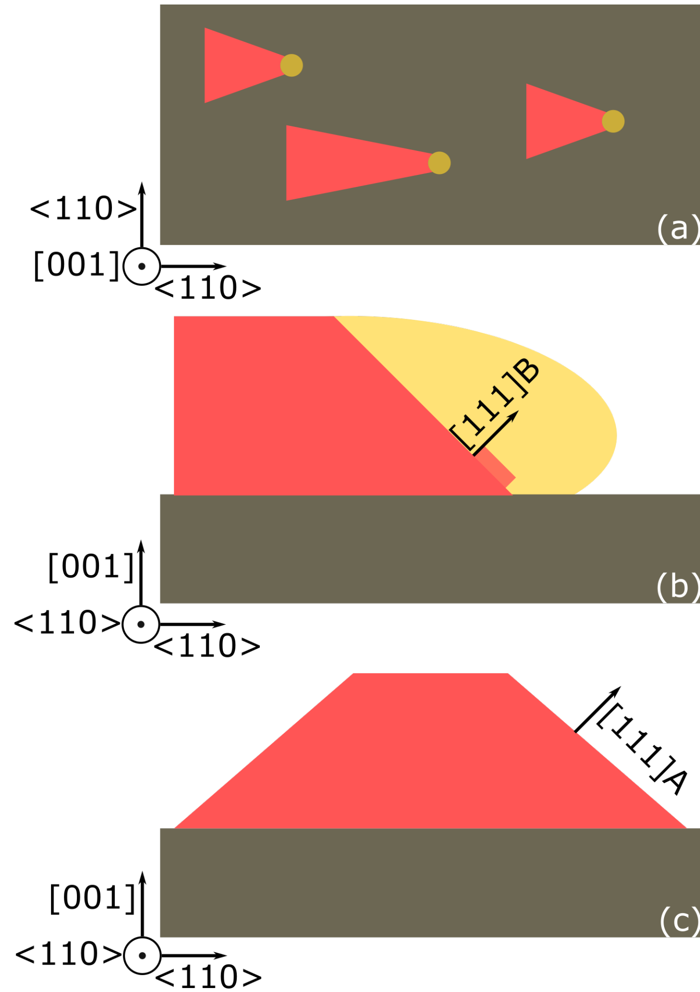

Figure 5.10: A schematic showing possible facets of the growing "Christmas tree" nanowires. (a) shows a top view of the wires, (b) shows a side view, with an added nucleation event and growth direction. (c) shows the wires along the growth direction, with the tapered growth direction marked.

The occurrence of the thin planar wires could be amounted to the occurrence of the trenches discussed in Section 5.2.1, Figure 5.7. These could potentially provide energetically favourable kink-sites for continued nucleation, and therefore promote growth on the (111)A facet instead.

5.4 High order [11x] wires

Sample 4.3(b), shown in Figure 4.3(b), was interesting due to the high yield of higher order inclined nanowires found. Figure 5.11 shows more micrographs of the sample.

Figure 5.11(a) and (b) simply show the yield, but if Figure 5.11(c) is analysed more closely, one can see a line along the wire between the edges. This would indicate that the cross section of the wire is square like. Figure 5.11(d) shows that the wires seem to nucleate in a similar way as the wires in Sample 4.2(b) shown in Figure 5.1, but kink after the initial growth of the base. From Figure 5.11(d), the angle of the wires with respect to the [001] direction could be measured. The values ranged from 14.6° to 20.2° with the average being about 16.3°. By comparing the direction of the wires to the cleavage edge of the substrate, and using some trigonometry, it was deduced that the wires likely grow in the [114] direction, which theoretically should be 19.5° from the [001] direction. Another possibility is that they grow in a strange direction due to some other effect, like twinning or that the particle changes the preferred facet to grow on during growth.

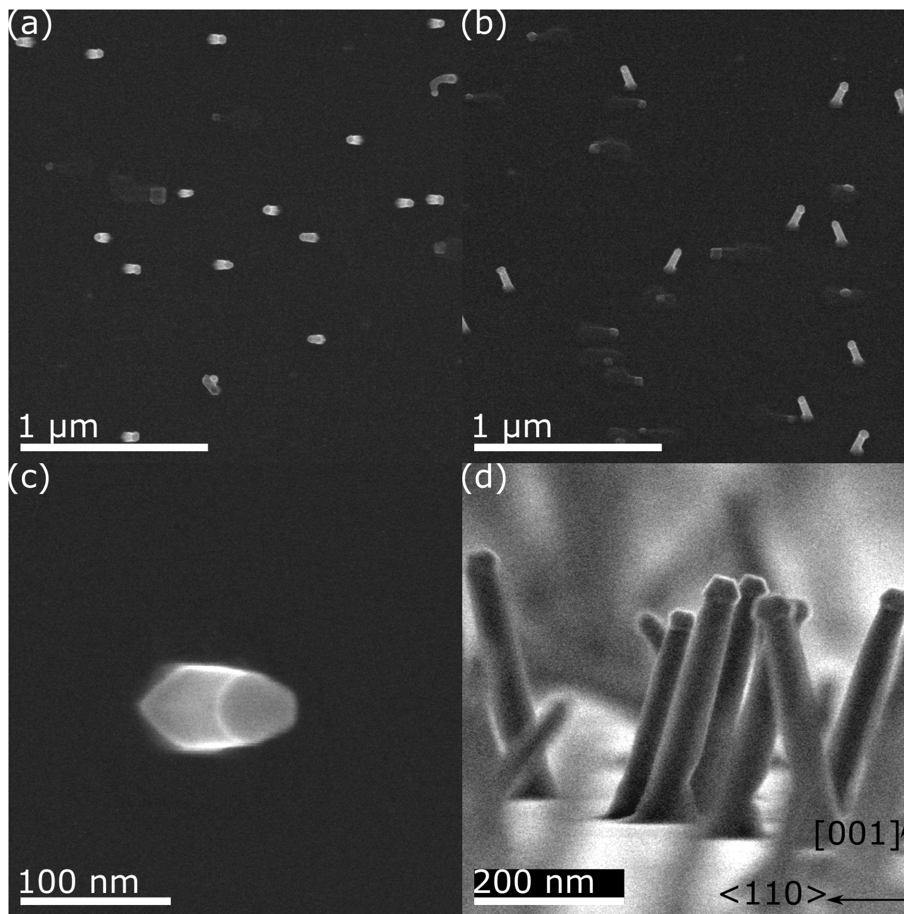

Figure 5.11: Micrographs of the [11x] higher order inclined nanowires. (a) shows an overview along [001], while (b) shows a 30° tilted view. (c) is a zoomed in micrograph of a nanowire along [001] and (d) is a micrograph recorded along one of the side facets of the substrate.

5.5 InAs samples

Figure 5.12 shows a collection of micrographs recorded on Sample 4.17(b), which had the best InAs stem wires. What can be noted is that the cross section at the base of these wires, seen in Figure 5.12(c), is similar to what was found for the InAsSb wires (Figure 5.2.1), but the hexagonal shape is more elongated and almost rectangular. The yield of vertical wires in this sample was 50%.

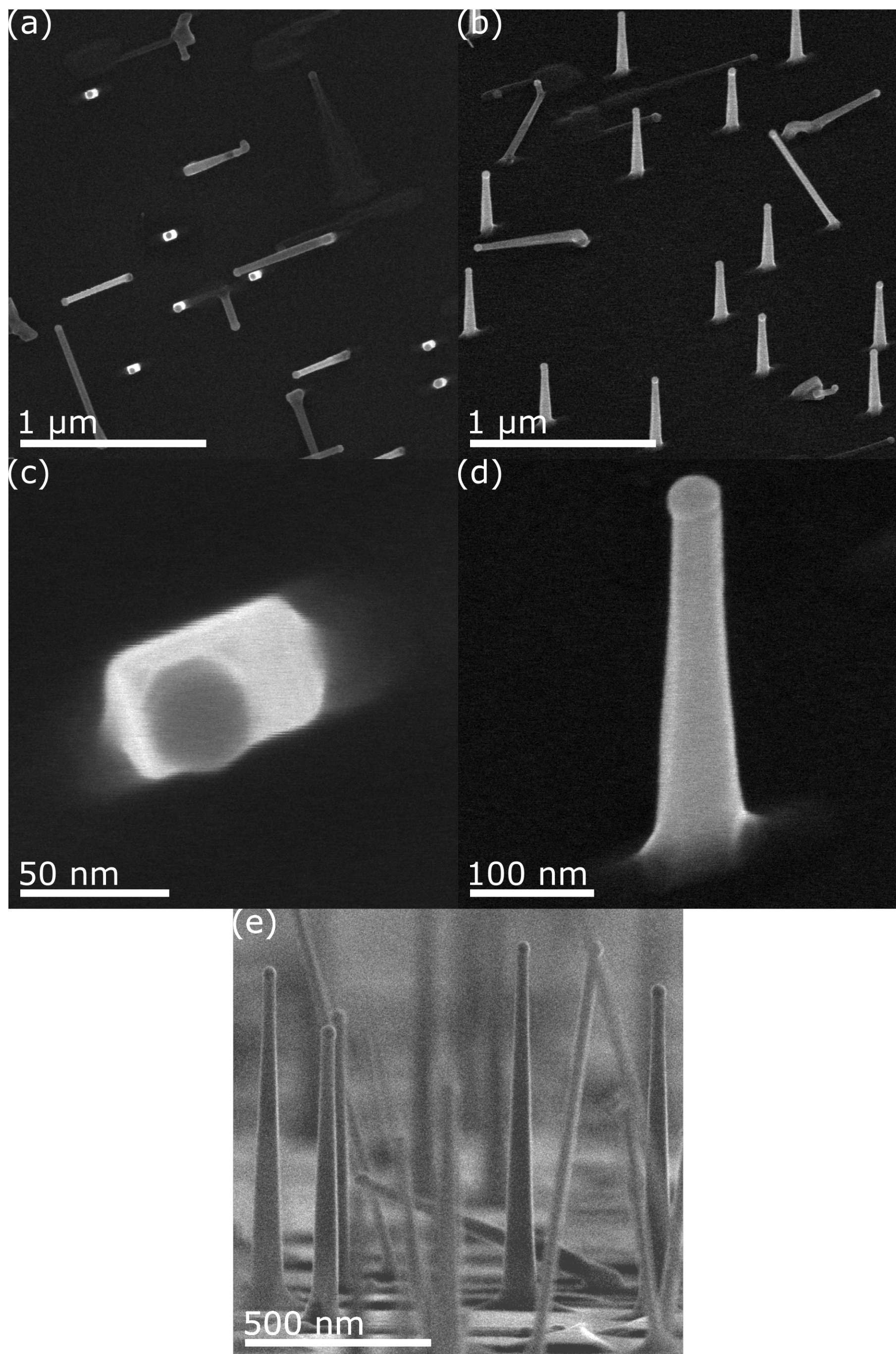

Figure 5.12: These are micrograhs recorded from Sample 4.17(b). (a) is an overview along [001], while (b) shows an image with 30° tilt. (c) shows a zoomed in micrograph of one of the wires, so that the cross sectional shape of the base can be seen. (d) is a zoomed in wire with 30° tilt, which shows the base more clearly. (e) is a micrograph of the wires when viewing along the side facets in a <110> direction.

Unfortunately, the good growth could not be reproduced, and no good InAsSb wires grown from InAs stems could be made.

5.6 TEM Analysis

Since the vertical wires grown in Sample 4.21(d) were long, numerous and with nice facets, this sample was chosen to be analysed in the TEM.

Three different wires, with their respective diffraction patterns or FFTs, are shown in Figure 5.13.

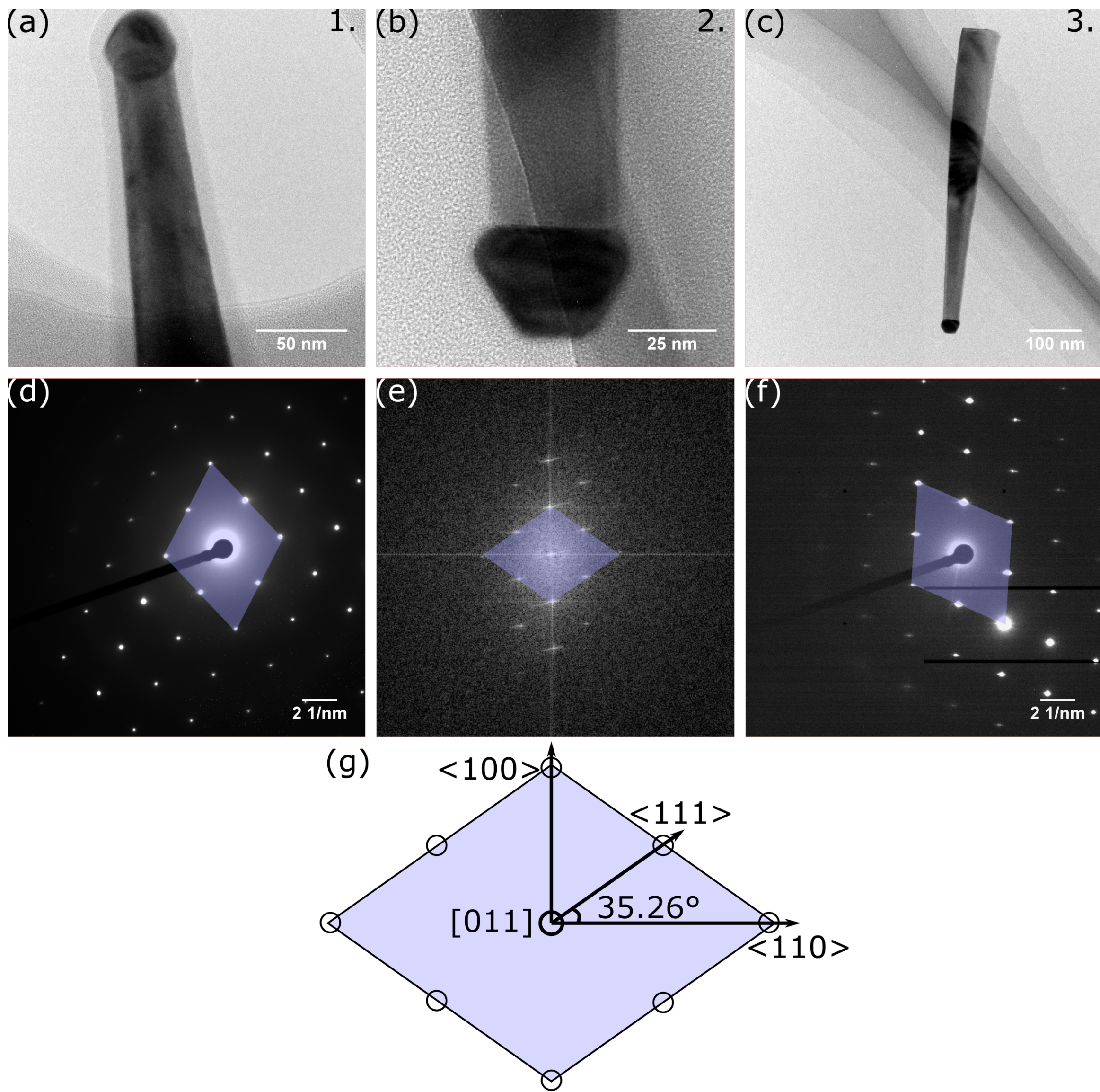

Figure 5.13: TEM images of three (numbered) nanowires from Sample 4.21(d), viewed along the [011] direction, together with representative diffraction patterns and FFT. The images are related (a)-(d), (b)-(e) and (c)-(f), where (d) and (f) are diffraction patterns, while (e) is a FFT. (g) shows the diamond shape the closest diffraction spots create. The diamond was overlaid on the diffraction patterns and FFT to determine the growth direction of the wires.

The diffraction pattern of wire 2 was not recorded due to lack of time during the TEM session. As can be seen in Figure 5.13(a)-(c), wires 1 and 2 have a stacking fault free, ZB crystal structure. Wire 3 has a single stacking fault formed diagonally to the growth di-

rection, which might be difficult to see here. The ZB crystal structure is seen more clearly in Figure 5.14. To verify the growth direction, the diffraction patterns and FFTs shown in Figure 5.13(d)-(f) were studied. By relating the direction of the wires to the patterns, as well as the angles between the spots, the growth direction could be determined. The diamond, which is formed by the spots closest to the central spot in the patterns, that was used for the determination of the growth directions, is shown in Figure 5.13(g). This showed that wire 1 grew in [110], wire 2 grew in [001] and wire 3 grew in [111]. Since the diffraction patterns did not show any additional spots, it was concluded that ordering was not present in wire 1 or wire 3. This was somewhat expected, since these wires do not grow in the [001] direction, which is expected to promote ordering the most. However, the FFT of wire 2 showed no signs of ordering either, even though wire 2 grows in the [001] direction expected to promote ordering.

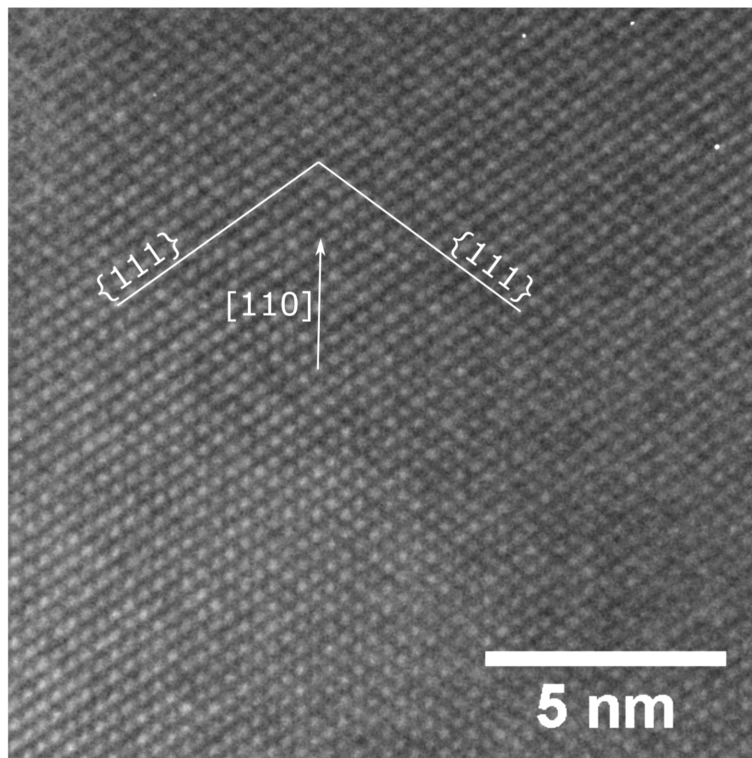

Figure 5.14: High resolution TEM image of part of wire 1 from Sample 4.21(d), viewed along the [110] direction. The ZB crystal structure is clearly seen. Shown is also the close packed crystal planes, as well as the growth direction of the nanowire.

EDX maps were made on wire 3 to see the composition in and below the particle. One problem encountered was that the energy of the x-rays generated by In and Sb overlap, so it was very difficult to distinguish between the two signals. The analysis showed a composition of 53.78 at% In, 41.99 at% As, 2.37 at% Sb and 1.87 at% Au in the wire below the particle. Since the ratio of In:(As+Sb) was not 1:1, as it should be in a III-V

semiconductor, it was concluded that the data could not be trusted. The amount of Sb in the wire is probably higher, but can not be seen due to the overlap between In and Sb.

Unfortunately, no diffraction pattern was recorded for wire 2, which grew in the [001] direction. Since FFTs are associated with a lot of noise and are only made from an image already recorded, they might not show ordering effects as clearly. However, the FFT should contain the same information as a diffraction pattern, since it is made from an image that has all the information. An intensity linescan was made to see if there were any hidden extra spots in the FFT. This proved that no spots were present and that it is safe to assume that the wire had no ordering.

If we assume that the EDX data obtained for wire 3 was not completely off, and we say that the incorporation in wire 2 is the same, we can assume that we have less than 10 at% of Sb in wire 2. Compared to the amount of As, this is very low. Therefore, if ordering would exist, the Sb layers would not be as frequent as every other layer. This would rather be something like every fifth layer. If a frequency of every fifth layer was present, the diffraction spots would be very close together (since long distances in real space becomes short distances in reciprocal space), but it is possible that the intensity of these spots would be low. Even so, it would probably be detectable, so it is more probable that the alloy is random in the wires. Of course, to get the ordering we wanted to find, the Sb content would need to be closer to the As content, so the possibilities to incorporate more Sb into the wires should be investigated.

Since no EDX map was taken of a [001] wire, and due to the difficulties with signal overlap, the real amount of Sb in these wires is unknown. One speculation is that the Sb content can determine which direction the wires will grow in, so it might be impossible to grow wires with much Sb in [001]. Or rather, it might be possible that the wires grown in [001] actually have a higher amount of Sb incorporated, than was estimated for wire 3, which grew in [111]. This would be interesting to investigate further.

6 Conclusions

In this project, InAsSb nanowires were successfully grown in the [001] direction on InAs (001) substrates from Au (and AgAu, but not verified by TEM) particles. For the samples where growth was achieved, the yield varied much, but was the greatest for Sample 4.21(d), where a yield of 16 % was found. When wires from Sample 4.21(d) were analysed in the TEM, the composition proved difficult to determine, although it at least seemed like Sb was present in the wires. A better measurement would be interesting, to determine if the growth directions could be related to the amount of Sb incorporated in the wires or present in the particle. It would also be good to analyse more than one wire growing in each direction, to see the spread in composition.

Although no ordering was observed for any wires from Sample 4.21(d), the possibilities of ordering to arise can not be ruled out. It is possible that ordering can be found for wires with higher Sb content. And since the cross sections of Samples 4.2(b) and 4.19(d) were very different, which suggests that the growth parameters were indeed different, there seems to be much room for exploration and discovery in the growth parameters, that could lead to, for example, higher Sb incorporation. One could also try different techniques like pre-patterning or Molecular Beam Epitaxy to direct the growth more and get more wires to take off in the [001] direction, since this could allow the parameters to be even more varied. This could also solve the problem of relatively low yield of wires.

Other interesting phenomena like the [114] and GaAsSb shark-teeth wires were also seen in the project, and would be interesting to analyse further. It was also good to see how the annealing affected the Ag particles on InAs, where the only samples where wires actually grew were the samples where the annealing step was skipped. A more thorough investigation of the Ag particles is needed before they can be useful, but the possibility of a parameter window where Ag produces better results than Au can not be discarded.

What concerns future applications for these nanowires, there is still a long way to go before integration into electronic devices can be easily made. Probably some sort of heterostructure needs to be grown, where two or more semiconductor materials need to be grown on top of each other in a single wire, and this is difficult to achieve. The yield and Sb incorporation also need to be increased. But instead of seeing the problems and challenges needed to be overcome to make the growth perfect, it can instead be viewed as a tool for others in their experiments. Since it was shown in this report that growth of InAsSb nanowires can be achieved in [001], other groups can now use this in further experiments to explore the growth direction. Important steps have also been made in the exploration of alternative seed particles. Therefore, I think that my findings will contribute to the nanowire, and possibly IC, community.

7 References

[1] R. S. Wagner and W. C. Ellis, "VAPOR-LIQUID-SOLID MECHANISM OF SINGLE CRYSTAL GROWTH," *Applied Physics Letters*, vol. 4, no. 5, pp. 89–90, mar 1964. [Online]. Available: https://doi.org/10.1063/1.1753975http://aip.scitation.org/doi/10.1063/1.1753975

[2] B. Mattias Borg and L.-E. Wernersson, "Synthesis and properties of antimonide nanowires," *Nanotechnology*, vol. 24, no. 20, p. 202001, may 2013. [Online]. Available: http://stacks.iop.org/0957-4484/24/i=20/a=202001?key=crossref.eea6c3ca7a8c9f9bf73dac16bdd681de

[3] A. Aardvark, N. Mason, and P. Walker, "The growth of antimonides by MOVPE," *Progress in Crystal Growth and Characterization of Materials*, vol. 35, no. 2-4, pp. 207–241, jan 1997. [Online]. Available: http://www.sciencedirect.com/science/article/pii/S0960897498000047

[4] E. A. Anyebe, M. K. Rajpalke, T. D. Veal, C. J. Jin, Z. M. Wang, and Q. D. Zhuang, "Surfactant effect of antimony addition to the morphology of self-catalyzed $InAs_{1-x}Sb_x$ nanowires," *Nano Research*, vol. 8, no. 4, pp. 1309–1319, apr 2015. [Online]. Available: http://link.springer.com/10.1007/s12274-014-0621-x

[5] B. M. Borg, K. A. Dick, J. Eymery, and L.-E. Wernersson, "Enhanced Sb incorporation in InAsSb nanowires grown by metalorganic vapor phase epitaxy," *Applied Physics Letters*, vol. 98, no. 11, p. 113104, mar 2011. [Online]. Available: http://aip.scitation.org/doi/10.1063/1.3566980

[6] A. Norman, T. Seong, B. Philips, G. Booker, and S. Mahajan, "Nature and origin of atomic ordering in iii-v semiconductor alloys," in *CONFERENCE SERIES-INSTITUTE OF PHYSICS*, vol. 134. IOP PUBLISHING LTD, 1993, pp. 279–279.

[7] D. Ercolani, M. Gemmi, L. Nasi, F. Rossi, M. Pea, A. Li, G. Salviati, F. Beltram, and L. Sorba, "Growth of InAs/InAsSb heterostructured nanowires," *Nanotechnology*, vol. 23, no. 11, p. 115606, mar 2012. [Online]. Available: http://stacks.iop.org/0957-4484/23/i=11/a=115606?key=crossref.1de2478d1d50b2c7e5285d6c5b498f8e

[8] S. A. Fortuna and X. Li, "Metal-catalyzed semiconductor nanowires: A review on the control of growth directions," *Semiconductor Science and Technology*, vol. 25, no. 2, 2010. [Online]. Available: http://stacks.iop.org/0268-1242/25/i=2/a=024005?key=crossref.7170231c5020563528883a730144336f

[9] C. Lindberg, A. Whiticar, K. A. Dick, N. Sköld, J. Nygård, and J. Bolinsson, "Silver as Seed-Particle Material for GaAs Nanowires—Dictating Crystal Phase and Growth Direction by Substrate Orientation," *Nano Letters*, vol. 16, no. 4, pp. 2181–2188, apr 2016. [Online]. Available: http://pubs.acs.org/doi/10.1021/acs.nanolett.5b04218

[10] A. Mikkelsen, N. Sköld, L. Ouattara, and E. Lundgren, "Nanowire growth and dopants studied by cross-sectional scanning tunnelling microscopy," *Nanotechnology*, vol. 17, no. 11, pp. S362–S368, jun 2006. [Online]. Available: http://stacks.iop.org/0957-4484/17/i=11/a=S22?key=crossref.af0dcf345d3fb2225beb4f44a7845297

[11] K. A. Dick, "A review of nanowire growth promoted by alloys and non-alloying elements with emphasis on Au-assisted III–V nanowires," *Progress in Crystal Growth and Characterization of Materials*, vol. 54, no. 3-4, pp. 138–173, sep 2008. [Online]. Available: http://linkinghub.elsevier.com/retrieve/pii/S0960897408000181

[12] N. Baber, H. G. Grimmeiss, M. Kleverman, P. Omling, and M. Z. Iqbal, "Characterization of silver-related deep levels in silicon," *Journal of Applied Physics*, vol. 62, no. 7, pp. 2853–2857, oct 1987. [Online]. Available: http://aip.scitation.org/doi/10.1063/1.339425

[13] L. Smart and E. Moore, *Solid State Chemistry: An Introduction, Fourth Edition*. CRC Press, 2016. [Online]. Available: https://books.google.se/books?id=ViLOBQAAQBAJ

[14] U. Pohl, *Epitaxy of Semiconductors: Introduction to Physical Principles*, ser. Graduate Texts in Physics. Springer Berlin Heidelberg, 2013. [Online]. Available: https://books.google.se/books?id=DShEAAAAQBAJ

[15] G. B. Stringfellow, *Organometallic vapor-phase epitaxy: theory and practice*. Elsevier, 1999.

[16] N. Akopian, G. Patriarche, L. Liu, J.-C. Harmand, and V. Zwiller, "Crystal Phase Quantum Dots," *Nano Letters*, vol. 10, no. 4, pp. 1198–1201, apr 2010. [Online]. Available: http://pubs.acs.org/doi/abs/10.1021/nl903534n

[17] L. Namazi, M. Nilsson, S. Lehmann, C. Thelander, and K. A. Dick, "Selective GaSb radial growth on crystal phase engineered InAs nanowires," *Nanoscale*, vol. 7, no. 23, pp. 10 472–10 481, 2015. [Online]. Available: http://xlink.rsc.org/?DOI=C5NR01165E

[18] M. Dahl, L. Namazi, R. R. Zamani, and K. A. Dick, "Sb Incorporation in Wurtzite and Zinc Blende $InAs_{1-x}Sb_x$ Branches on InAs Template Nanowires," *Small*, vol. 14, no. 11, p. 1703785, mar 2018. [Online]. Available: http://doi.wiley.com/10.1002/smll.201703785

[19] F. Glas, J.-C. Harmand, and G. Patriarche, "Why Does Wurtzite Form in Nanowires of III-V Zinc Blende Semiconductors?" *Physical Review Letters*, vol. 99, no. 14, p. 146101, oct 2007. [Online]. Available: https://link.aps.org/doi/10.1103/PhysRevLett.99.146101

[20] S. Gorji Ghalamestani, S. Lehmann, and K. A. Dick, "Can antimonide-based nanowires form wurtzite crystal structure?" *Nanoscale*, vol. 8, no. 5, pp. 2778–2786, 2016. [Online]. Available: http://xlink.rsc.org/?DOI=C5NR07362F

[21] S. P. Svensson, W. L. Sarney, H. Hier, Y. Lin, D. Wang, D. Donetsky, L. Shterengas, G. Kipshidze, and G. Belenky, "Band gap of $InAs_{1-x}Sb_x$ with native lattice constant," *Physical Review B*, vol. 86, no. 24, p. 245205, dec 2012. [Online]. Available: http://link.aps.org/doi/10.1103/PhysRevB.86.245205

[22] S. Namjoo, A. S. H. Rozatian, I. Jabbari, and P. Puschnig, "Optical study of narrow band gap $InAs_{1-x}Sb_x$ (x = 0, 0.25, 0.5, 0.75, 1) alloys,"

Physical Review B, vol. 91, no. 20, p. 205205, may 2015. [Online]. Available: https://link.aps.org/doi/10.1103/PhysRevB.91.205205

[23] V. Dubrovskii, *Nucleation Theory and Growth of Nanostructures*, ser. NanoScience and Technology. Springer Berlin Heidelberg, 2013. [Online]. Available: https://books.google.se/books?id=x2glBAAAQBAJ

[24] A. M. Whiticar, E. K. Mårtensson, J. Nygård, K. A. Dick, and J. Bolinsson, "Annealing of Au, Ag and Au–Ag alloy nanoparticle arrays on GaAs (100) and (111)B," *Nanotechnology*, vol. 28, no. 20, p. 205702, may 2017. [Online]. Available: http://stacks.iop.org/0957-4484/28/i=20/a=205702?key=crossref.2473971ba6bad6371dd7decabcee50d7

[25] L. Namazi, "From understanding to realizing novel iii-sb materials via nanowires," Ph.D. dissertation, Lund University, 2 2018, defence details Date: 2018-03-23 Time: 09:15 Place: Lecture hall Rydbergsalen, Fysicum, Professorsgatan 1, Lund University, Faculty of Engineering LTH. External reviewer(s) Name: Joyce, Hannah Title: Dr Affiliation: University of Cambridge, United Kingdom —.

[26] V. Schmidt, J. V. Wittemann, S. Senz, and U. Gösele, "Silicon Nanowires: A Review on Aspects of their Growth and their Electrical Properties," *Advanced Materials*, vol. 21, no. 25-26, pp. 2681–2702, jul 2009. [Online]. Available: http://doi.wiley.com/10.1002/adma.200803754

[27] A. I. Persson, M. W. Larsson, S. Stenström, B. J. Ohlsson, L. Samuelson, and L. R. Wallenberg, "Solid-phase diffusion mechanism for GaAs nanowire growth," *Nature Materials*, vol. 3, no. 10, pp. 677–681, oct 2004. [Online]. Available: http://www.nature.com/articles/nmat1220

[28] K. A. Dick, K. Deppert, T. Mårtensson, B. Mandl, L. Samuelson, and W. Seifert, "Failure of the Vapor-Liquid-Solid Mechanism in Au-Assisted MOVPE Growth of InAs Nanowires," *Nano Letters*, vol. 5, no. 4, pp. 761–764, apr 2005. [Online]. Available: http://pubs.acs.org/doi/abs/10.1021/nl050301c

[29] N. Solak and Materials Science International Team, MSIT®, "Ag-in binary system: Datasheet from msi eureka in springermaterials (https://materials.springer.com/msi/phase-diagram/docs/sm_msi_r_10_014857_02_full_lnkdia0)," copyright 2006 MSI, Materials Science International Services GmbH, Stuttgart. [Online]. Available: https://materials.springer.com/msi/phase-diagram/docs/sm_msi_r_10_014857_02_full_LnkDia0

[30] "Ag-as-in isothermal section of ternary phase diagram: Datasheet from "pauling file multinaries edition – 2012" in springermaterials (https://materials.springer.com/isp/phase-diagram/docs/c_0204006)," copyright 2016 Springer-Verlag Berlin Heidelberg & Material Phases Data System (MPDS), Switzerland & National Institute for Materials Science (NIMS), Japan. [Online]. Available: https://materials.springer.com/isp/phase-diagram/docs/c_0204006

[31] Y.-C. Chou, C.-Y. Wen, M. C. Reuter, D. Su, E. A. Stach, and F. M. Ross, "Controlling the Growth of Si/Ge Nanowires and Heterojunctions Using Silver–Gold Alloy Catalysts," *ACS Nano*, vol. 6, no. 7, pp. 6407–6415, jul 2012. [Online]. Available: http://pubs.acs.org/doi/10.1021/nn301978x

[32] U. Krishnamachari, M. Borgstrom, B. J. Ohlsson, N. Panev, L. Samuelson, W. Seifert, M. W. Larsson, and L. R. Wallenberg, "Defect-free InP nanowires grown in [001] direction on InP (001)," *Applied Physics Letters*, vol. 85, no. 11, pp. 2077–2079, sep 2004. [Online]. Available: http://aip.scitation.org/doi/10.1063/1.1784548

[33] J. Wang, S. R. Plissard, M. A. Verheijen, L.-F. Feiner, A. Cavalli, and E. P. A. M. Bakkers, "Reversible Switching of InP Nanowire Growth Direction by Catalyst Engineering," *Nano Letters*, vol. 13, no. 8, pp. 3802–3806, aug 2013. [Online]. Available: http://pubs.acs.org/doi/10.1021/nl401767b

[34] G. B. Stringfellow, "Atomic ordering in III/V semiconductor alloys," *Journal of Vacuum Science & Technology B: Microelectronics and Nanometer Structures*, vol. 9, no. 4, p. 2182, 1991. [Online]. Available: http://scitation.aip.org/content/avs/journal/jvstb/9/4/10.1116/1.585761

[35] S. Adachi, *III-V Ternary and Quaternary Compounds.* Cham: Springer International Publishing, 2017, pp. 1–1. [Online]. Available: https://doi.org/10.1007/978-3-319-48933-9_30

[36] R. M. Biefeld, "The metal-organic chemical vapor deposition and properties of III–V antimony-based semiconductor materials," *Materials Science and Engineering: R: Reports*, vol. 36, no. 4, pp. 105–142, mar 2002. [Online]. Available: http://linkinghub.elsevier.com/retrieve/pii/S0927796X02000025

[37] P. E. Optics, *Environmental Scanning Electron Microscopy: An Introduction to ESEM.* Philips Electron Optics, 1996. [Online]. Available: https://books.google.se/books?id=S8cvHAAACAAJ

[38] D. Stokes, *Principles and Practice of Variable Pressure / Environmental Scanning Electron Microscopy (VP-ESEM)*, ser. RMS - Royal Microscopical Society. Wiley, 2008. [Online]. Available: https://books.google.se/books?id=TgYJv5BHIQ0C

[39] D. Williams and C. Carter, *Transmission Electron Microscopy*, 01 2009, vol. 1–4.

[40] S. Lehmann, J. Wallentin, D. Jacobsson, K. Deppert, and K. A. Dick, "A General Approach for Sharp Crystal Phase Switching in InAs, GaAs, InP, and GaP Nanowires Using Only Group V Flow," *Nano Letters*, vol. 13, no. 9, pp. 4099–4105, sep 2013. [Online]. Available: http://pubs.acs.org/doi/10.1021/nl401554w

[41] E. Pehlke, N. Moll, A. Kley, and M. Scheffler, "Shape and stability of quantum dots," *Applied Physics A: Materials Science & Processing*, vol. 65, no. 6, pp. 525–534, dec 1997. [Online]. Available: http://link.springer.com/10.1007/s003390050619

[42] W. Du, X. Yang, H. Pan, X. Ji, H. Ji, S. Luo, X. Zhang, Z. Wang, and T. Yang, "Controlled-Direction Growth of Planar InAsSb Nanowires on Si Substrates without Foreign Catalysts," *Nano Letters*, vol. 16, no. 2, pp. 877–882, feb 2016. [Online]. Available: http://pubs.acs.org/doi/10.1021/acs.nanolett.5b03587